AD-A064 969 DUKE UNIV DURHAM N C ADAPTIVE SIGNAL DETECTION LAB F/G 20/1
MULTIPATH SIGNAL PROCESSING USING A VERTICAL ARRAY.(U)
JUL 77 C S LIU N00014-75-C-0191
UNCLASSIFIED TR-13 NL

1 OF 2
AD A064969

SHIPPED

1 OF 2

AD
A064969

TR-13

MULTIPATH SIGNAL PROCESSING

USING A VERTICAL ARRAY

by

Charles S. Liu
Department of Electrical Engineering

Prepared under:
Office of Naval Research (Code 222)
Contract No. N000 14-75-C-0191

79 02 23 029

"This document has been approved for public release and sale; its distribution is unlimited."

LEVEL II

12

DUKE UNIVERSITY

ADAPTIVE SIGNAL DETECTION LABORATORY

Department of Electrical Engineering
School of Engineering

9 Technical Report No. 13

6 MULTIPATH SIGNAL PROCESSING USING A VERTICAL ARRAY

14 TR-13

by

10 Charles S. Liu

12 10p.

11 July 1977

ACCESSION for
NTIS White Section
DDC Buff Section
UNANNOUNCED
JUSTIFICATION
BY
DISTRIBUTION/AVAILABILITY CODES
Dist. AVAIL. and/or SPECIAL
A

Approved: L W Nolte
L.W. Nolte
Principal Investigator

Prepared under: Office of Naval Research (Code 222)
Contract No. N00014-75-C-0191
15 ###

"This document has been approved for public release and sale; its distribution is unlimited."

DDC
RECEIVED
FEB 27 1978
D

405 708

ABSTRACT

Performance of a vertical array for estimating multipath signal parameters and for detecting multipath Gaussian signals is investigated in this report. By assuming that the multipath signal directions are known and the number of array elements is larger than the number of paths, the parameters of the signal from each individual path may be estimated so that the multipath signal cancellation problem can be minimized. The performance, in terms of signal-to-noise ratio, of the Maximum Likelihood Estimate (MLE) for the signal parameters of individual paths is shown to be independent of the relative signal phases from other paths. But, the performance does depend upon the angular separation of multipath signal directions and the length of the array. In the case where some knowledge about the signal parameters is available, the Maximum A Posteriori Probability Estimate (MAP) is also considered. The linear relationship between the MLE and MAP estimates is derived. It is interesting to point out that the MAP estimate is unique even if the number of array elements is less than the number of signal paths.

The optimum array processor, for detecting multipath Gaussian signals with known arrival angles, has a quadratic structure. In a two-path signal example, the optimal array has two beamformers pointing in the directions of two signal paths and has a term which cross-correlates both beamformers, even when the signals are independent from path to path. The cross-correlated term takes care of the leakage of signals from paths other than the beamforming direction through each beamformer. The performance evaluation of the processor is achieved by the development of a general method called "the eigenvalue method". This method may be used to find the analytical expressions for the

probability of false alarm (P_F) and the probability of detection (P_D0 for array detectors implementing a quadratic sufficient statistic. Several examples are presented to illustrate the use of the eigenvalue method.

The family of Receiver Operating Characteristic (ROC) curves for detecting multipath Gaussian signals clearly show the difference between the performance for detecting multipath Gaussian signals and that for detecting multipath known-waveform signals. The ROC curves for multipath Gaussian signals cases are not only a function of the array factor and the multipath structure, but also are non-linear on normal-normal probability paper. It is also shown that the spatial discriminating capability of array detectors improves performance at high signal-to-noise ratios. In the performance comparison between optimal array detectors and an optimal signal array element detector, we found the array not only increases the output signal-to-noise ratio by k times, where k is the number of array elements, but also improves P_D in the high P_F region.

The comparison between performance of an optimal array and a suboptimal array is also carried out to give insight regarding the trade-off between processor complexity and detection performance. In the two-path signal example, the single beamformer array which points a beam in one of the two signal directions needs 10 elements to achieve the same performance as an optimal array with only 4 elements, for SNR=1 (signal-to-noise ratio per element). Performance of a double beamformer array which has two beamformers pointing in the directions of two signal paths is evaluated for comparison. These results show that the performance difference between the double beamformer and optimal arrays is noticeable only for high signal-to-noise ratios and a small array aperture. This implies that the cross correlation structure in the optimal array is not very important if either the array aperture is

large enough to isolate signal paths or the signal-to-noise ratio is low. The performance comparisons made in this report give some insight regarding the trade-off between processor structure complexity and detection performance, which are major factors to consider in implementing array detectors.

ACKNOWLEDGEMENTS

I wish to thank Dr. L. W. Nolte for his guidance, support and encouragement. Also, I acknowledge the support of the Office of Naval Research under which this work was performed.

Special thanks are due to Dr. T. G. Birdsall for his guidance and encouragement and for providing office space at the Cooley Electronics Laboratory of the University of Michigan.

MULTIPATH SIGNAL PROCESSING USING A VERTICAL ARRAY

CONTENTS

CHAPTER I INTRODUCTION

1.1 Underwater Acoustic Transmission

The acoustic sound propagation in an ocean channel is very complicated. The modes of sound propagation depend on the sound velocity profile of the underwater channel. The detailed physics about the channel characteristics is described in Tolstoy and Clay [1] and Urick [2]. The sound velocity in the ocean depends on temperature, pressure and salinity. Several typical velocity profiles are shown in Fig. 1.1 (from Tolstoy and Clay [1]). In general, the temperature at the sea surface is higher than that in deep water. The water temperature is the factor that dominates sound speed for the first 1,000 meters in depth. Beyond that, the pressure becomes the overriding factor. The shape of the velocity profile determines the multipath structure of the sound channel. Fig. 1.2 shows the sound rays associated with a particular velocity profile. The sound transducer is located at a depth at which the velocity is minimum. The rays are calculated using a ray tracing program. By this method we may predict the ray incident angle, the transmission loss and the arrival time. Since many other environmental factors such as a random surface, a time-varying sound velocity profile, and a random medium are not considered in this method, the results obtained from this method can only be used for rough estimates. In Fig. 1.2 we see different types of propagation. Some rays which do not touch the surface or bottom are called refracted-refracted (RR) rays. Some rays

which touch the surface are called refracted-surface-reflected (RSR) rays. Some rays which touch both the surface and the bottom are called surface-reflected-bottom-reflected (SRBR) rays. The multipath signals received at the receiver depend on both the depth and the range of the receiver location. This result has been presented in a paper by Flanagan, Weinberg and Clark [3].

1.2 Review of Previous Research

Many different approaches have been used to study underwater acoustic channel characteristics in the past two decades. An important paper by Steinberg and Birdsall [4] showed that the phase of the received waveform in a fixed-system in the straits of Florida varied less than 100° during intervals of 1/2 - 1 hour and that the multipath structure of the signal had stability on the order of 5 minutes. Due to the fact that the phase is much more stable than the amplitude, the phase estimates are Fourier transformed to find the relationship between the internal waves and the fluctuation of the phase spectrum [5,6,7]. The discontinuity of the phase curve which is associated with the deep amplitude fading is attributed to the signal cancellation of multipath signals [5]. The fluctuation of signal energy results in a nonstationary confidence interval for the phase estimate. Especially during a deep fade, the phase information is lost. A key to minimizing this signal cancellation is to separate the multipaths spatially. This will be discussed in later chapters.

The multipath structure of the underwater acoustic channel was investigated by Steinberg and Birdsall [4]. In that experiment a pseudo random sequence was sent through the Straits of Florida and the

received signal was matched to the sequence to find the multiple time arrivals. The temporal separation of different arrivals showed the existence of multipaths [4]. Dyer [8] examined the signal fluctuations in the ocean for both multipath and scattering processes and showed that the multipath propagation dominates the fluctuations. Adams [9] investigated the fluctuations of the transfer function of a random multipath channel. Both mean and variance of the random transfer function were calculated for his multipath model.

In order to obtain spatial information about the channel, linear arrays have been used to process underwater acoustical data [11, 12, 13]. Jobst [10] modelled the number of multipaths as a Poisson distributed random variable. Using this model the spatial coherence and temporal coherence are estimated for a horizontal line array. It is shown that spatial coherence decreases with increasing angle from broad side, with increasing frequency, with increasing sound speed, and with increasing vertical arrival angle at the receiver. Williams and Battestin [11] used a vertical beamformer to isolate a single RSR (refracted-surface-reflected) path and to investigate the phase coherence time for single and multipath signals. Urick [12] showed the effect of multipaths on the gain of an additive vertical array. The phase coherence, in terms of the clipped correlation coefficient, falls off rapidly with horizontal range of the source. However, no amplitude stability of a single path was mentioned in their papers. There are other papers that investigate theoretical signal processing techniques for arrays. Hinich [14] used match filtering concepts to formulate a maximum likelihood estimate of source depth using a vertical array. The eigenfunctions of the underwater wave guide are used to match

the array to the received signal. Bucker [15] used a similar method to locate sound sources in shallow water.

1.3 Approach of This Report

The relationship between the error in the phase estimates and the signal-to-noise ratio is presented in Chapter II. It is useful to have either the variance of the estimate or a confidence interval along with the phase estimate so that we may judge the goodness of the estimated phase. We will show that multipath signal cancellation can contribute to the loss of signal-to-noise ratio during a deep fade and therefore we would like to investigate the signal along each path. To distinguish multipath signals spatially, a vertical array is used in Chapters III and IV. The resolved path technique is introduced in Chapter III for estimating the signal waveform of each path. Both the signal amplitude and phase are estimated simultaneously. The signal waveform is assumed fixed but unknown. The maximum likelihood estimate of the signal waveform is shown to be an unbiased linear minimum mean square error estimate. In Chapter IV, each single-path signal is assumed Gaussian with known variance. Both maximum a posteriori probability estimates of the multipath signals and the likelihood ratio test are formulated. A beamforming structure in the optimal detector will be pointed out in Chapter IV. The detection performance of optimal array detectors is evaluated in Chapter V by using an "eigenvalue method". The probability density function of the sufficient statistic is shown to be dependent on a set of eigenvalues. The general form of the probability density function is derived analytically. The probability of detection and the probability of false alarm are also obtained in closed

form. The eigenvalue method can also be applied to evaluate the detection performance of suboptimal detectors. The performances of suboptimal processors, such as a single beamformer and double beamformers, are compared with that of the optimal processor. The result of this comparison will clearly show the trade-off between the complexity of processor structure and the detection performance.

CHAPTER II

PHASE ESTIMATION PERFORMANCE OF A SINGLE HYDROPHONE

The time samples of signal phase estimates have been used for investigating the environmental factors in the underwater acoustic channel [4,5,6,7,11,12]. However, the performance of the phase estimate usually is not presented along with the estimate. Some misleading conclusions may be drawn by examining only the phase estimate, especially in a deep fading situation. A typical piece of underwater data is presented in Figure 2.1 (from Steinberg and Birdsall [4]) to show both the amplitude and phase of the received waveform simultaneously. During deep fades, when the detector output is less than -30dBμb, the phase angles have 180° or 90° jumps. The deep fades may be attributed to multipath signal cancellation. Since the signal in that experiment is a single frequency sine wave, phasor diagrams are shown in Figure 2.2. A noise free signal phasor diagram shown in Figure 2.2(a) demonstrates signal cancellation in a four-path channel. If signal component S_4 rotates 150°, then the magnitude of the resulting signal phase changes a lot. The resultant signal phasor in Figure 2.2(b) is much longer than that in Figure 2.2(a).

The fluctuation of signal energy does affect the performance of the signal phase estimate. Thomas [17] and Cederquist [18] investigated the error probability density function of the phase estimate as a function of signal-to-noise ratio.

$$p(\psi) = \exp\left(-\frac{a^2}{\sigma_n^2}\right)\Big/2\pi + \left(\frac{\sqrt{2}\,a}{\sigma_n}\right)\cos\psi \cdot \exp\left(-\frac{a^2\sin^2\psi}{\sigma_n^2}\right) \cdot \operatorname{erfc}\left(-\frac{\sqrt{2}\,a}{\sigma_n}\cos\psi\right)\Big/\sqrt{2\pi}$$

where $$\operatorname{erfc}(X) = \int_X^\infty \frac{1}{\sqrt{2\pi}} \exp\left(-\frac{u^2}{2}\right) du$$

and $\frac{a^2}{\sigma_n^2}$ is the signal-to-noise ratio.

and x is the error of the phase estimate.

The effect of signal-to-noise ratio on the phase estimate can also be demonstrated graphically in Figure 2.3. Suppose there are two signal phasors, one with amplitude a_1, the other with amplitude a_2, and both are corrupted by an additive noise phasor $\underline{n}$. The resulting phase estimate error of the phasor a_1 is ψ_1 and that of the phasor a_2 is ψ_2. In Figure 2.3, we can see that ψ_2 is larger than ψ_1. As shown in Figure 2.4, the density function peaks up as the signal-to-noise ratio increases. Cederquist [18] also calculated the limits for a 90% confidence level [19]. The curves shown in Figure 2.5 are from Cederquist [18]. We can see that at low signal-to-noise ratios such as -10dB, the 90% confidence interval covers ±160°. This implies the uncertainty of the phase estimate is very high for low signal-to-noise ratios.

In a single hydrophone case, the receiver cannot distinguish signals with different incident angles. The corresponding signal-to-noise ratio (SNR) depends on the relative phases at the hydrophone of the different multipath signals as shown in the following equation:

Single hydrophone:

$$\text{SNR} = \frac{\left|\sum_{m=1}^{M} a_m e^{j\theta_m}\right|}{\sigma_n^2}$$

where a_m is the amplitude of the mth path signal, and

θ_m is the phase of the mth path signal.

In the underwater acoustic channel, the variation of water temperature due to tides and internal waves changes the acoustic sound transmission. The phase of each path varies widely for small variations in the sound velocity profile [1]. A detector output curve shown in Figure 2.1 shows the fluctuation of the amplitude of signal plus noise. If we assume the output signal-to-noise ratio fluctuates as much as the detector output shown in Figure 2.1, then it is meaningful to draw confidence intervals of the phase estimate along with the phase output curve shown in Figure 2.1. Clearly, we will have a nonstationary confidence interval. It is a reasonable practice to consider only the portion of the phase curve in which the signal-to-noise ratio is above a certain level. Of course, this will introduce new problems in dealing with data discontinuities where the signal-to-noise ratio is not high enough.

Al alternative method of dealing with the signal cancellation problem is to isolate single paths by using a vertical array. In Chapters III and IV, methods to resolve multipaths spatially are investigated with the hope that the resolved paths will be found to be more stable and that other information on channel characteristics will be obtained.

CHAPTER III

NON-RANDOM PARAMETER ESTIMATION USING A VERTICAL ARRAY

3.1 Problem Geometry and Notations

The problem geometry of a vertical array in a multipath channel is shown in Figure 3.1. The time delay between adjacent elements associated with the mth path, τ_m, depends on the vertical incident angle ϕ_m. Since the incident angles of multipath signals are different, the time delays of multipath signals are different from path to path. The time delay associated with the mth path can be expressed as:

$$\tau_m = \frac{D \cos \phi_m}{C} \tag{3-1}$$

where D is the separation of adjacent elements,

C is the sound velocity,

ϕ_m is the vertical incident angle of the mth ray.

Throughout this report the incident angles of the multipaths are assumed known. In a practical situation, these incident angles may be obtained through a ray tracing method.

We use M to denote the number of paths, and K to denote the number of array elements. We consider a single frequency sound source in a multipath channel. The received data is Fourier transformed to obtain a phasor of a signal frequency. The phasors for a time-delayed waveform are well-known to be the original phasors multiplied by a complex phase

shift $e^{-j\omega\tau}$. When the signal is present, the received data is the summation of multipath signals and noise. The complex vector $\underline{R}$ represents the phasors received by array elements and $\underline{S}$ represents the phasors of multipath signals.

$$\underline{R} = \underline{A}\,\underline{S} + \underline{n} \tag{3-2}$$

where $\underline{R}^T = (R_1, R_2, \cdots, R_K)$

R_i : phasor of received data at the ith element.

$\underline{S}^T = (S_1, S_2, \cdots, S_M)$

S_m : phasor of signal from the mth path.

$\underline{n}^T = (n_1, n_2, \cdots, n_K)$

n_i : Gaussian noise received at the ith element.

$\underline{A} = (\underline{V}_1, \underline{V}_2, \cdots, \underline{V}_M)$ a K x M matrix

$\underline{V}_m = (1, \exp[j\omega\tau_m], \exp[j\omega\tau_m 2], \cdots, \exp[j\omega\tau(K-1)])$

is the pointing vector of the mth path.

A four path noise-free phasor diagram is shown in Figure 3.2(a) to illustrate the equation above. At the ith element, the phasor of the mth path, S_m, is equal to $a_m e^{j\theta}m$ where a_m is the amplitude and θ_m is the phase of the mth-path signal. The signal phasors received at the (i+1)th element is related to that received at the ith element by the following equation.

$$S'_m = S_m \exp[j\omega\tau_m]$$

where S_m' is the signal phasor from the mth path received at the (i+1)th element and S_m is the signal phasor from the mth path received at the ith element. The time delay τ_m contributes the phase shift $\omega\tau_m$. In Figure 3.2(b) every signal phasor in Figure 3.2(a) is rotated by $\omega\tau_m$ degrees. The resultant noise-free phasor R_{i+1} turns out to be larger than R_i. This indicates that although one element has a potential signal cancellation problem, other elements still receive some signal energy, if the vertical angular separation between paths are large enough or the array is long enough to resolve paths.

3.2 Maximum Likelihood Estimate (MLE)

When the signal waveform is fixed but unknown, the maximum likelihood estimate can be used to estimate the received multipath signals [20]. Schweppe [21] developed the "decoupled-beam" data processor for estimating signal waveforms from multiple-signal sources. The maximum likelihood estimate (MLE) used in his paper is equivalent to the Linear Minimum Mean Square Error Estimate (LMSE). The technique can be used for estimating the multipath signals. The MLE is derived in the following equations by maximizing the conditional likelihood ratio, $\Lambda(\underline{R}|\underline{S})$.

$$\Lambda(\underline{R}|\underline{S}) = \exp[-(\underline{R}-\underline{A}\ \underline{S})^{*}\underline{Q}^{-1}(\underline{R}-\underline{A}\ \underline{S}) + \underline{R}^{*}\underline{Q}^{-1}\underline{R}] \tag{3-3}$$

where

$$\underline{Q} = E[\underline{n}\ \underline{n}^{*}] = \sigma_n^{2}\underline{I} \tag{3-4}$$

$$\underline{Q}^{-1} = \frac{1}{\sigma_n^{2}}\underline{I} \tag{3-5}$$

$$\underline{S}^{T} = [S_1, S_2, \cdots, S_M]$$

and S_m is the phasor of mth path signal.

$\Lambda(\underline{R}|\underline{S})$ is also called the likelihood function. The likelihood function is maximized by minimizing the first term of the exponent in equation (3-3). Hence, the maximum likelihood estimate of the signal can be found from the following equation:

$$\underline{R} - \underline{A}\,\underline{S} = 0 \tag{3-6}$$

If the dimensionality K of vector $\underline{R}$ is larger or equal to the dimensionality M of the vector $\underline{S}$, then we may solve for the maximum likelihood estimate of the received multipath signal. In other words, if the number of array elements is no less than the number of multipaths, then it is possible to resolve every path and to find values of the MLE for signals arriving along each path. Otherwise, if the number of array elements is less than the number of paths, then the MLE estimate is indefinite. (i.e., we may have an infinite number of solutions.) In general, the Maximum Likelihood Estimate of the received multipath signals, $\hat{\underline{S}}_{MLE}$, can be expressed as:

$$\hat{\underline{S}}_{MLE} = (\underline{A}^*\underline{A})^{-1}\underline{A}^*\underline{R} \quad \text{for } K \geq M \tag{3-7}$$

Since $\underline{A}^*\underline{A}$ is a K by K matrix and the rank of matrix $\underline{A}$ is not greater than min(K,M) the inverse matrix of $\underline{A}^*\underline{A}$ does not exist if the rank of $\underline{A}^*\underline{A}$ is less than K. This implies that M cannot be less than K. If $\underline{A}$ is a square matrix, then the maximum likelihood estimate for the received multipath signals is quite simple.

$$\hat{\underline{S}}_{MLE} = \underline{A}^{-1}\underline{R} \qquad \text{for } K=M \tag{3-8}$$

The mean and the covariance matrix of $\hat{\underline{S}}_{MLE}$ can be derived for $K \geq M$.

$$E[\hat{\underline{S}}_{MLE}] = E[(\underline{A}^*\underline{A})^{-1}\underline{A}^*\underline{R}] \tag{3-9}$$

$$= (\underline{A}^*\underline{A})^{-1}\underline{A}^*\underline{A}\,\underline{S} \tag{3-10}$$

$$= \underline{S}$$

$$\text{cov}[\hat{\underline{S}}_{MLE}] = E[(\hat{\underline{S}}_{MLE}-\underline{S})(\hat{\underline{S}}_{MLE}-\underline{S})^*] \tag{3-11}$$

$$= (\underline{A}^*\underline{A})^{-1}E[\underline{n}\,\underline{n}^*] \tag{3-12}$$

$$= (\underline{A}^*\underline{A})^{-1}\sigma_n^2 \tag{3-13}$$

A K=2, M=2 example is demonstrated to show the operation of the estimator and its performance. The matrices $\underline{A}$ and $\underline{A}^{-1}$ are shown in the following equations.

$$A = \begin{bmatrix} 1 & 1 \\ e^{j\omega\tau_1} & e^{j\omega\tau_2} \end{bmatrix} \tag{3-14}$$

$$\underline{A}^{-1} = \frac{1}{e^{j\omega\tau_2} - e^{j\omega\tau_1}} \begin{bmatrix} e^{j\omega\tau_2} & -1 \\ -e^{j\omega\tau_1} & 1 \end{bmatrix} \tag{3-15}$$

Since the matrix $\underline{A}$ in this example is a square matrix, the MLE can be expressed as:

$$\underline{\hat{S}}_{MLE} = \begin{bmatrix} \hat{S}_1 \\ \hat{S}_2 \end{bmatrix} = \underline{A}^{-1}\underline{R} \tag{3-16}$$

$$= \frac{1}{e^{j\omega\tau_2} - e^{j\omega\tau_1}} \begin{bmatrix} e^{j\omega\tau_2} R_1 - R_2 \\ -e^{j\omega\tau_1} R_1 + R_2 \end{bmatrix} \tag{3-17}$$

In order to see the physical meaning of the matrix operation, consider a noise-free case. When $\underline{n}=\underline{0}$, the signal phasor received at the first element, R_1, is equal to the sum of the phasors, S_1 and S_2. Similarly, R_2 is equal to the sum of the phasors S_1' and S_2', where $S_1' = S_1 e^{j\omega\tau_1}$ and $S_2' = S_2 e^{j\omega\tau_2}$. The noise-free phasor diagrams of $\hat{S}_1$ and $\hat{S}_2$ are shown in Figure 3.3. The phasor components of R_1 and R_2 are also shown in Figure 3. We notice that the resulting phasor R_1 may be very small. In Figure 3.3(c), the phasor diagram of the maximum likelihood estimate of the signal from the first path, $\hat{S}_1$, shows the complete cancellation of the signals from the second path. Similarly, the phasor diagram of $\hat{S}_2$ shows the complete cancellation of the signals from the first path. This operation is called "infinite sidelobe rejection" by Schweppe [21].

The mean and the variance of the estimate are usually used for estimation performance measurements. It is quite easy to show that the maximum likelihood estimate is an unbiased estimate.

$$E[\underline{\hat{S}}_{MLE}] = E[(\underline{A}^*\underline{A})^{-1}\underline{A}^*\underline{R}] \tag{3-18}$$

$$= E[(\underline{A}^*\underline{A})^{-1}\underline{A}^*\underline{A}\,\underline{S} + (\underline{A}^*\underline{A})^{-1}\underline{A}^*\underline{n}] \tag{3-19}$$

$$= \underline{S} \tag{3-20}$$

The variances of $\hat{S}_1$ and $\hat{S}_2$ are also derived in the following equations.

$$\mathrm{Var}[\hat{S}_1] = E[(\hat{S}_1 - S_1)^2] \tag{3-21}$$

$$= \frac{1}{\left|e^{j\omega\tau_2} - e^{j\omega\tau_1}\right|^2}\left[\mathrm{Var}(R_1) + \mathrm{Var}(R_2)\right] \tag{3-22}$$

$$= \frac{2\sigma_n^2}{\left|e^{j\omega\tau_2} - e^{j\omega\tau_1}\right|^2} \tag{3-23}$$

Similarly, we may show that:

$$\mathrm{Var}[\hat{S}_2] = E[(\hat{S}_2 - S_2)^2] \tag{3-24}$$

$$= \mathrm{Var}[\hat{S}_1] \tag{3-25}$$

From Chapter II, we know that the phase angle estimate depends on the signal-to-noise ratio. It is interesting to compare the performance of the signal phase estimate of the resolved path method with that of the single hydrophone method. The expressions for the signal-to-noise ratios of these two methods are shown below.

Resolved path (MLE) : $$\mathrm{SNR} = \frac{a_i^2\left|e^{j\omega\tau_2} - e^{j\omega\tau_1}\right|^2}{2\sigma_n^2} \quad \text{for } i=1,2 \tag{3-26}$$

$$\text{Single hydrophone:} \quad \text{SNR} = \frac{\left|a_1 e^{j\theta_1} + a_2 e^{j\theta_2}\right|^2}{\sigma_n^2} \tag{3-27}$$

where a_i is the signal amplitude of the ith signal path,

and θ_i is the signal phase of the ith signal path.

In the single hydrophone case, the signal-to-noise ratio goes to zero even for multipath signals with large amplitudes if the signal phases, θ_1 and θ_2, are 180° out of phase and the signal amplitudes are identical. This signal-to-noise degradation may be minimized by employing the spatial discriminating capability of a vertical array. As shown in equation (3-26) the signal-to-noise ratio of the resolved path maximum likelihood estimate is a function of time delays τ_1 and τ_2, where the time delays are proportional to the array element spacing. Since both τ_1 and τ_2 depend on the separation of array elements, proper control of the separation of the array elements will increase the signal-to-noise ratio to its maximum at $2\, a_i^2/\sigma_n^2$. For a K-element array the maximum signal-to-noise ratio may reach $K\, a_i^2/\sigma_n^2$. From the discussion above we observe that the signal-to-noise ratio of the resolved path estimate depends on the spatial resolving power of the array and the signal-to-noise ratio can be increased by increasing the array aperture. If the "noise like" fluctuation of the signal amplitude, as shown in the single hydrophone case [4], is truly due to multipath signal cancellation, then the resolved path signal estimate should be stable enough to provide additional signal amplitude information for studying the channel characteristics.

On the other hand, equation (3-27) shows that the signal-to-noise ratio of the single hydrophone estimate depends highly on the relative phases of signals from different paths. As shown in Tolstoy and Clay [1], the variation of signal phase due to the variation of the channel temperature profile is

different from path to path. This implies that the summed signal phase may fluctuate significantly. Due to the potential signal cancellation, the signal-to-noise ratio and the confidence interval of the phase estimate may vary dramatically in the single hydrophone case. Since the fluctuation of τ_1 and τ_2, which depends on the incident angles of planewave arrivals are relative stable compared to that of summed signal phases, we may conclude that the resolved path method should provide additional information for studying both the signal amplitude and phase.

CHAPTER IV

ESTIMATION AND DETECTION OF RANDOM MULTIPATH SIGNALS USING A VERTICAL ARRAY

The maximum a posteriori probability estimate (MAP) for each individual signal path is presented in this chapter. The relationship between the maximum likelihood estimate and the maximum a posteriori probability estimate is also investigated. The optimal array signal detector which uses the likelihood ratio test will be shown to have a beamformer structure and cross-correlator terms. Only the structure of the detector will be discussed in this chapter. The performance of the detector will be presented in Chapter V.

4.1 Maximum A Posteriori Probability Estimate (MAP)

Suppose the multipath signals are uncorrelated zero-mean Gaussian random processes. Then we may find the maximum a posteriori probability estimate (MAP) for the random multipath signals. Assuming we know the covariance matrix of the received multipath signal vector $\underline{S}$, the MAP estimate can be obtained by maximizing the probability of $\underline{S}$ given $\underline{R}$. The expression for $p(\underline{S}|\underline{R})$ is shown below.

$$p(\underline{S}|\underline{R}) = \frac{p(\underline{S},\underline{R})}{p(\underline{R})} \tag{4-1}$$

$$= \frac{p(\underline{R}|\underline{S})p(\underline{S})}{p(\underline{R})} \tag{4-2}$$

where

$$p(\underline{R}|\underline{S})p(\underline{S}) = C_1 \exp[-(\underline{R}-\underline{A}\ \underline{S})^* \underline{Q}_n^{-1}(\underline{R}-\underline{A}\ \underline{S}) - \underline{S}^* \underline{Q}_s^{-1}\underline{S}]$$

and $\underline{Q}_s$, $\underline{Q}_n$ are the covariance matrices of received multipath signals and received noises respectively.

Schweppe [21] has derived the maximum a posteriori probability estimate for Gaussian signals in uncorrelated Gaussian noise. The maximum a posteriori probability estimate of the signal, $\hat{\underline{S}}_{MAP}$, is expressed in equation (4-4). Unlike the maximum likelihood estimate, $\hat{\underline{S}}_{MAP}$ does not have a $K \geqq M$ restriction.

$$\hat{\underline{S}}_{MAP} = [\underline{A}^*\underline{A} + \sigma_n^2 \underline{Q}_s^{-1}]^{-1}\underline{A}^*\underline{R} \quad K \gtreqless M \qquad (4\text{-}4)$$

Although the number of array elements, K, is assumed no less than the number of paths, M, in this chapter, the expression above is valid even for $K < M$. We recall that in the expression for the maximum likelihood estimate, the matrix $\underline{A}^*\underline{A}$ cannot be inverted if $K < M$. But, in the expression for the MAP estimate the inverse of the matrix $[\underline{A}^*\underline{A} + \sigma_n^2 \underline{Q}_s^{-1}]$ does exist even for $K < M$, because the rank of the matrix is equal to $\max(K,M)$. This is due to the introduction of a priori knowledge, $\underline{Q}_s$, into the processor. So, even when we do not have enough array elements to resolve every path, we can combine the a priori knowledge with the observed data to do a MAP estimate for the Gaussian signal for each path.

For the cases where $K \geq M$, there is a relationship between the MLE and the MAP estimator. The expression for $\hat{\underline{S}}_{MAP}$ can be rewritten as:

$$\hat{\underline{S}}_{MAP} = [\underline{I} + \sigma_n^2(\underline{A}^*\underline{A})^{-1}\underline{Q}_s]^{-1}(\underline{A}^*\underline{A})^{-1}\underline{A}^*\underline{R} \quad \text{for } K \geq M \qquad (4\text{-}5)$$

$$= [\underline{I} + \sigma_n^2(\underline{A}^*\underline{A})^{-1}\underline{Q}_s]^{-1}\hat{\underline{S}}_{MLE} \qquad (4\text{-}6)$$

This expression shows clearly how to bring in the a priori knowledge into the MAP estimator. Since all matrix operations are linear, we may derive $\hat{\underline{S}}_{MAP}$ from $\hat{\underline{S}}_{MLE}$ by a linear transformation for K>M.

4.2 Structure of the Optimal Array Processor for Detecting Multipath Gaussian Signals in Gaussian Noises

The optimal array detector can be formulated by implementing the likelihood ratio $\Lambda(\underline{R})$ which is defined as $\Lambda(\underline{R}) = \frac{p(\underline{R}|H_1)}{p(\underline{R}|H_0)}$ [20]. The probability of $\underline{R}$, which is a complex random variable given the signal is present, can be expressed as [22]:

$$p(\underline{R}|H_1) = \pi^{-K}\{\det \underline{Q}_1\}^{-1} \exp[-\underline{R}^* \underline{Q}_1^{-1} \underline{R}] \tag{4-7}$$

where $$\underline{Q}_1 = E[\underline{R}\,\underline{R}^*|H_1] = \underline{A}\,E[\underline{S}\,\underline{S}^*]\underline{A}^* + E[\underline{n}\,\underline{n}] \tag{4-8}$$

Similarly, the probability of $\underline{R}$ given the signal is absent is:

$$p(\underline{R}|H_0) = \pi^{-K}\{\det \underline{Q}_0\}^{-1} \exp[-\underline{R}^* \underline{Q}_0^{-1} \underline{R}] \tag{4-9}$$

where $$\underline{Q}_0 = E[\underline{R}\,\underline{R}^*|H_0] = E[\underline{n}\,\underline{n}^*] \tag{4-10}$$

The likelihood ratio of $\underline{R}$ is the ratio between equations (4-7) and (4-9).

$$\Lambda(\underline{R}) = \frac{\det \underline{Q}_0}{\det \underline{Q}_1} \exp[-\underline{R}^* \underline{Q}_1^{-1} \underline{R} + \underline{R}^* \underline{Q}_0^{-1} \underline{R}] \tag{4-11}$$

A sufficient statistic, y, which is a monotonic function of $\Lambda(\underline{R})$, is shown in the next equation.

$$y = \underline{R}^* [\underline{Q}_0^{-1} - \underline{Q}_1^{-1}] \underline{R} \tag{4-12}$$

To simplify the detector structure, we assume that the multipath random signals are independent from path to path.

Then,

$$\underline{Q}_1 = \underline{Q}_0 + E[\underline{A}\,\underline{S}\,\underline{S}^*\underline{A}^*] \tag{4-13}$$

$$= \underline{Q}_0 + \underline{A}\, E[\underline{S}\,\underline{S}^*]\underline{A}^* \tag{4-14}$$

$$= \underline{Q}_0 + [\underline{v}_1, \underline{v}_2, \cdots, \underline{v}_M] \begin{bmatrix} \sigma_{s_1}^2 & & & \\ & \sigma_{s_2}^2 & & \\ & & \ddots & \\ & & & \sigma_{s_M}^2 \end{bmatrix} \begin{bmatrix} \underline{v}_1^* \\ \underline{v}_2^* \\ \vdots \\ \underline{v}_M^* \end{bmatrix} \tag{4-15}$$

$$= \underline{Q}_0 + \sum_{m=1}^{M} \sigma_{s_m}^2 \, \underline{v}_m \, \underline{v}_m^* \tag{4-16}$$

where $$\underline{A} = [\underline{v}_1, \underline{v}_2, \cdots, \underline{v}_M] \tag{4-17}$$

and $\sigma^2_{s_m}$ is the variance of signal from the mth path.

From the structure of $\underline{Q}_1$ as shown in equation (4-16), we may apply the well-known matrix inversion lemma M times to find $\underline{Q}_1^{-1}$. The lemma [23] is stated in the following equation.

$$[\underline{B} + \underline{u}\,\underline{u}^*]^{-1} = \underline{B}^{-1} - \frac{1}{(1 + \underline{u}^*\underline{B}^{-1}\underline{u})}\,\underline{B}^{-1}\underline{u}\,\underline{u}^*\underline{B}^{-1} \tag{4-18}$$

where $\underline{u}$ is a vector and $\underline{B}$ is a square matrix.

A M=2 example is formulated to give more insight into the detector structure. In the example we assume that the noises are independent from element to element, so

$$\underline{Q}_1 = \sigma^2_n\,\underline{I} + \sigma^2_{s_1}\,\underline{v}_1\underline{v}_1^* + \sigma^2_{s_2}\,\underline{v}_2\underline{v}_2^* \tag{4-19}$$

We let the first two terms in the equation shown above be $\underline{B}_1$, such that $\underline{B}_1 = \sigma^2_n\,\underline{I} + \sigma^2_{s_1}\,\underline{v}_1\underline{v}_1^*$. Then,

$$\underline{B}_1^{-1} = [\sigma^2_n\,\underline{I} + \sigma^2_{s_1}\,\underline{v}_1\underline{v}_1^*]^{-1} = \frac{1}{\sigma^2_n}\,\underline{I} - \frac{\sigma^2_{s_1}/\sigma^4_n}{1 + K\frac{\sigma^2_{s_1}}{\sigma^2_n}}\,\underline{v}_1\underline{v}_1^* \tag{4-20}$$

and

$$\underline{Q}_1^{-1} = [\sigma_n^2 \underline{I} + \sigma_{s_1}^2 \underline{v}_1\underline{v}_1^* + \sigma_{s_2}^2 \underline{v}_2\underline{v}_2^*]^{-1} \tag{4-21}$$

$$= [\underline{B}_1 + \sigma_{s_2}^2 \underline{v}_2\underline{v}_2^*]^{-1} \tag{4-22}$$

$$= \underline{B}_1^{-1} - \frac{\sigma_{s_2}^2}{1 + \sigma_{s_2}^2 \underline{v}_2^* \underline{B}_1^{-1} \underline{v}_2} \underline{B}^{-1}\underline{v}_2\underline{v}_2^*\underline{B}_1^{-1} \tag{4-23}$$

After some manipulations, we find:

$$\underline{Q}_1^{-1} = \frac{1}{\sigma_n^2} \underline{I} - c_1\underline{v}_1\underline{v}_1^* - c_2\underline{v}_2\underline{v}_2^* + c_3[(\underline{v}_2^*\underline{v}_1)\underline{v}_2\underline{v}_1^* + (\underline{v}_1^*\underline{v}_2)\underline{v}_1\underline{v}_2^*] \tag{4-24}$$

where $$c_1 = \frac{\frac{\sigma_{s_1}^2}{\sigma_n^4}\left(1 + \frac{K\sigma_{s_2}^2}{\sigma_n^2}\right)}{\left(1 + \frac{K\sigma_{s_2}^2}{\sigma_n^2}\right)\left(1 + \frac{K\sigma_{s_1}^2}{\sigma_n^2}\right) - \frac{\sigma_{s_1}^2 \sigma_{s_2}^2}{\sigma_n^4}\left|\underline{v}_2^*\underline{v}_1\right|^2}, \tag{4-25}$$

$$c_2 = \frac{\frac{\sigma_{s_2}^2}{\sigma_n^4}\left(1 + \frac{K\sigma_{s_1}^2}{\sigma_n^2}\right)}{\left(1 + \frac{K\sigma_{s_2}^2}{\sigma_n^2}\right)\left(1 + \frac{K\sigma_{s_1}^2}{\sigma_n^2}\right) - \frac{\sigma_{s_1}^2 \sigma_{s_2}^2}{\sigma_n^4}\left|\underline{v}_2^* \underline{v}_1\right|^2} \quad , \qquad (4\text{-}26)$$

and

$$c_3 = \frac{\frac{\sigma_{s_1}^2 \sigma_{s_2}^2}{\sigma_n^6}}{\left(1 + \frac{K\sigma_{s_2}^2}{\sigma_n^2}\right)\left(1 + \frac{K\sigma_{s_1}^2}{\sigma_n^2}\right) - \frac{\sigma_{s_1}^2 \sigma_{s_2}^2}{\sigma_n^4}\left|\underline{v}_2^* \underline{v}_1\right|^2} \quad . \qquad (4\text{-}27)$$

So,

$$\underline{Q}_0^{-1} - \underline{Q}_1^{-1} = \frac{1}{\sigma_n^2}\underline{I} - \underline{Q}_1^{-1} \qquad (4\text{-}28)$$

$$= c_1 \underline{v}_1 \underline{v}_1^* + c_2 \underline{v}_2 \underline{v}_2^* - c_3[(\underline{v}_2^* \underline{v}_1)\underline{v}_2 \underline{v}_1^* + (\underline{v}_1^* \underline{v}_2)\underline{v}_1 \underline{v}_2^*] \qquad (4\text{-}29)$$

Consequently, the sufficient statistic $y = \underline{R}^*(\underline{Q}_0^{-1} - \underline{Q}_1^{-1})\underline{R}$ can be expressed as:

$$y = c_1(\underline{R}^* \underline{v}_1)(\underline{v}_1^* \underline{R}) + c_2(\underline{R}^* \underline{v}_2)(\underline{v}_2^* \underline{R}) - c_3[(\underline{v}_2^* \underline{v}_1)(\underline{R}^* \underline{v}_2)(\underline{v}_1^* \underline{R}) + (\underline{v}_1^* \underline{v}_2)(\underline{R}^* \underline{v}_1)(\underline{v}_2^* \underline{R})] \qquad (4\text{-}30)$$

We may call $\underline{v}_1^* \underline{R}$ a beamformer pointing in the direction of the first path. Similarly, $\underline{v}_2^* \underline{R}$ is a beamformer pointing in the direction of the second path. The term $(\underline{R}^* \underline{v}_1)(\underline{v}_1^* \underline{R}) = |\underline{v}_1^* \underline{R}|^2$ can be physically realized as a beamformer pointing in the direction of $\underline{v}_1$ followed by an envelope detector. The structure of the optimal array detector is shown in Figure 4.1 as a combination of beamformers, envelope detectors and cross correlators. The first and second terms in equation (4-30) measure the output power of beamformers. The third term is a correction term which correlates the output of two beamformers. The effect of the third term on the detection performance will be discussed in Chapter V.

Although we only dealt with a single frequency case in this part, it is not difficult to extend this result to broadband signals. The difference between the single frequency and broadband signals cases is that one uses time delays instead of phase shifts for the broadband signals.

CHAPTER V

PERFORMANCE OF DETECTING MULTIPATH GAUSSIAN SIGNALS IN GAUSSIAN NOISE WITH A LINEAR ARRAY

A general method called the "Eigenvalue Method" for evaluating performance of array detectors will be introduced in this chapter. The method is general enough to cover all detectors which employ the quadratic sufficient statistic (i.e. $y=\underline{R}^* \underline{Q}\, \underline{R}$, where $\underline{Q}$ is a hermitian matrix.) The performance of the optimal detector will be evaluated and compared with that of conventional suboptimal detectors such as the single beamformer and multibeamformer.

5.1 The "Eigenvalue Method"

Suppose the array signal detector has a quadratic sufficient statistic $y = \underline{R}^* \underline{Q}\, \underline{R}$ where $\underline{Q}$ is hermitian (i.e. $\underline{Q}^* = \underline{Q}$). Then, we may find the characteristic function of y using the following equations.

$$\phi_y(i\Phi) = E_y[\exp(i\Phi y)] \tag{5-1}$$

$$= E_{\underline{R}}\{\exp[i\Phi \underline{R}^* \underline{Q}\, \underline{R}]\} \tag{5-2}$$

$$= \int_{\underline{R}} [\exp(i\Phi \underline{R}^* \underline{Q}\, \underline{R})] p(\underline{R}) d\underline{R} \tag{5-4}$$

where $$p(\underline{R}) = \pi^{-k}\{\det \underline{V}\}^{-1} \exp[-\underline{R}^* \underline{V}^{-1} \underline{R}] , \tag{5-4}$$

$$\underline{V} = \mathrm{cov}[\underline{R}] ,$$

and $\phi_y(i\Phi)$ is the characteristic function of y.

Then, $$\phi_y(i\phi) = \int_{\underline{R}} \pi^{-k}\{\det \underline{V}\}^{-1}\exp[-\underline{R}^*\underline{V}^{-1}\underline{R} + i\phi\underline{R}^*\underline{Q}\,\underline{R}]d\,\underline{R} \qquad (5\text{-}5)$$

$$= \int_{\underline{R}} \pi^{-K}\{\det \underline{V}\}^{-1}\exp[-\underline{R}^*\underline{V}^{-1}\{\underline{I} - i\phi\underline{V}\,\underline{Q}\}\underline{R}]d\underline{R} \qquad (5\text{-}6)$$

$$= \{\det[\underline{I} - i\phi\,\underline{V}\,\underline{Q}]\}^{-1} \qquad (5\text{-}7)$$

To simplify the notation, we let $\underline{G} = \underline{V}\,\underline{Q}$, where $\underline{G}$ is a square matrix with dimension K. Any square matrix $\underline{G}$ is similar to either a diagonal matrix or a triangular matrix. We may find matrices $\underline{P}^{-1}$ and $\underline{P}$ such that $\underline{P}^{-1}\underline{G}\,\underline{P} = \underline{B}$ where $\underline{B}$ is either a diagonal matrix or triangular matrix with all the eigenvalues of $\underline{G}$ on the main diagonal. Then, $\det[\underline{I} - i\phi\underline{G}]$ can be expressed as:

$$\det[I - i\Phi\,\underline{G}] = \det\{\underline{P}^{-1}\}\det[\underline{I} - i\Phi\,\underline{G}]\det\{\underline{P}\} \qquad (5\text{-}8)$$

$$= \det[\underline{I} - i\Phi\,\underline{P}^{-1}\underline{Q}\,\underline{P}] \qquad (5\text{-}9)$$

$$= \det[\underline{I} - i\Phi\,\underline{B}] \qquad (5\text{-}10)$$

$$= \prod_{\ell=1}^{K}(1 - i\phi\lambda_\ell) \qquad (5\text{-}11)$$

where λ_ℓ is the eigenvalue of matrix $\underline{G}$.

Hence, the characteristic function of y becomes

$$\phi_y(i\Phi) = \prod_{\ell=1}^{K}(1 - i\Phi\lambda_\ell)^{-1} \qquad (5\text{-}12)$$

The density function of y can be obtained directly by taking the inverse transform of the characteristic function, $\phi_y(i\Phi)$ of y. Dyer [26] used this technique to derive the expressions for the density functions of y as:

(1) All λ_ℓ's are equal to λ.

$$p(y) = \begin{cases} \frac{1}{\lambda^K \Gamma(K)} y^{K-1} \exp(-y/\lambda) & \text{for } y \geq 0 \\ 0 & \text{for } y < 0 \end{cases} \qquad (5\text{-}13)$$

(2) Each λ_ℓ has a distinct value

$$p(y) = \begin{cases} \sum_{\ell=1}^{K} \lambda_\ell^{-1} h_\ell^{-1} \exp(-y/\lambda_\ell) & \text{for } y \geq 0 \\ 0 & \text{for } y < 0 \end{cases} \qquad (5\text{-}14)$$

$$\text{where } h_\ell = \prod_{j \neq \ell}^{K} \left(1 - \frac{\lambda_j}{\lambda_\ell}\right) \qquad (5\text{-}15)$$

(3) m groups of eigenvalues, each group has M_ℓ identical eigenvalues.

$$p(y) = \prod_{\ell=1}^{m} \frac{(-i)^{1-M_\ell}}{\lambda_\ell^{M_\ell}} \sum_{n=1}^{m} \frac{1}{\Gamma(M_n)} \frac{\partial^{M_n-1}}{\partial k^{M_n-1}} x$$

$$\left[\frac{\exp(-i\,k\,y)}{\prod_{j\neq n}^{m}(k + i\lambda_j^{-1})^{M_j}}\right]_{k\,=\,-i\lambda_n^{-1}} \tag{5-16}$$

The above equations are derived using calculus of residues. The first two equations are very useful, but the last equation does not give us any idea of the functional form of p(y). Hence, another approach is taken in this report as will now be shown.

We recognize that the probability density function corresponding to the characteristic function $(1 - i\Phi\lambda_\ell)^{-1}$ is exponentially distributed. In other words, if $\phi_x(i\Phi) = (1 - i\Phi\lambda_\ell)^{-1}$ then,

$$p(x) = \begin{cases} \frac{1}{\lambda_\ell}\exp(-x/\lambda_\ell) & \text{for } x \geq 0 \\ 0 & \text{for } x < 0 \end{cases} \tag{5-17}$$

We can view the random variable y as a sum of independent random variables, x_i , because the characteristic function of y can be factored as $\phi_y(i\Phi) = \phi_{x_1}(i\Phi)\cdot\phi_{x_2}(i\Phi)\cdots\phi_{x_k}(i\Phi)$. Since the probability of x_i is exponentially distributed as described in equation (5-17), the probability density function of y is the convolution of exponentially distributed probability densities. The resultant function p(y), obtained from the convolution, will

take one of the following three functional forms.

(1) All λ_ℓ are equal to λ.

$$p(y) = \begin{cases} \frac{1}{\lambda^K \Gamma(K)} y^{K-1} \exp(-y/\lambda) & \text{for } y \geq 0 \\ 0 & \text{for } y < 0 \end{cases} \tag{5-18}$$

(2) Each λ_ℓ has a distinct value.

$$p(y) = \begin{cases} \sum_{\ell=1}^{K} C_\ell \exp(-y/\lambda_\ell) & \text{for } y \geq 0 \\ 0 & \text{for } y < 0 \end{cases} \tag{5-19}$$

where $$C_\ell = \frac{\lambda_\ell^{K-2}}{\prod_{j \neq \ell}^{K} (\lambda_\ell - \lambda_j)}$$

(3) m groups of eigenvalues, each group has M_ℓ identical eigenvalues.

$$p(y) = \begin{cases} \sum_{\ell=1}^{m} \left[\sum_{r=0}^{M_\ell - 1} d_{r\ell} \, y^{(M_\ell - 1 - r)} \exp(-y/\lambda_\ell) \right] & \text{for } y \geq 0 \\ 0 & \text{for } y < 0 \end{cases} \tag{5-20}$$

where M_ℓ is the number of elements in the ℓth group,

$$\sum_{\ell=1}^{m} M_\ell = K,$$

and $d_{r\ell}$ depends on the eigenvalues, but is not a function of y. From equations (5-18), (5-19), and (5-20), we can see that p(y) is a finite sum of functions with form $y^m e^{ay}$. This functional form will give us closed form expressions for the probability of detection (P_D) and the probability of false alarm (P_F). By definition, P_D and P_F can be written as:

$$P_D = \int_\eta^\infty p(y|H_1)dy \tag{5-21}$$

$$P_F = \int_\eta^\infty p(y|H_0)dy \tag{5-22}$$

If we perform these integrals, we will have expressions like $\int_\eta^\infty y^m e^{ay}dy$, which can be found in an integral table as:

$$\int_\eta^\infty y^m e^{ay}dy = e^{ay} \sum_{r=0}^{m} (-1)^r \frac{m!\, y^{m-r}}{(m-r)!\, a^{r+1}} \Bigg|_\eta^\infty$$

$$= e^{a\eta} \sum_{r=0}^{m} (-1)^{r+1} \frac{m!\, \eta^{m-r}}{(m-r)!\, a^{r+1}} \tag{5-23}$$

Eventually, we will not have any integral left in the expressions for P_D and P_F. In the next two sections, we will find the eigenvalues of $\underline{G}$ along with the expressions for P_D and P_F analytically, for some special cases. In general, the eigenvalues of the $\underline{G}$ matrix can be calculated using numerical methods. There are computer programs developed at Argonne National Laboratory and currently available at many computing centers [24] for solving eigenvalues of any complex matrix. After solving for the eigenvalues of matrices $\underline{G}_0$ and $\underline{G}_1$, equations (5-18), (5-19), (5-20), (5-21), and (5-22) can be used to calculate P_D and P_F. This method which is called the "Eigenvalue Method" can be used to calculate the exact values of P_D and P_F at any point on the ROC curve with the aid of a computer.

5.2 Optimal Performance Evaluation for Array Detectors

In this section, we will investigate some special properties of the eigenvalue λ_ℓ in the optimal detector cases. We will also derive eigenvalues analytically for some special cases. Performances of the detectors are compared to see the effect of adding hydrophones to the array receivers.

First, we would like to derive a general formula for performance evaluation. From Chapter IV, we saw that a sufficient statistic for likelihood ratio, y, can be expressed as:

$$y = \underline{R}^*(\underline{Q}_0^{-1} - \underline{Q}_1^{-1})\underline{R} \qquad (5\text{-}24)$$

where $\underline{Q}_0$ is $\mathrm{cov}[\underline{R}|H_0]$

and $\underline{Q}_1$ is $\mathrm{cov}[\underline{R}|H_1]$.

$$\phi_y(i\Phi) = E_y[\exp(i\Phi y)]$$

$$= E_{\underline{R}}\{\exp[\, i\Phi \underline{R}^* (\underline{Q}_0^{-1} - \underline{Q}_1^{-1})\underline{R}]\} \tag{5-25}$$

$$= \int_{\underline{R}} \pi^{-K}\{\det \underline{V}\}^{-1} \exp[\, -\underline{R}^* \underline{V}^{-1} \underline{R} + i\Phi \underline{R}^* (\underline{Q}_0^{-1} - \underline{Q}_1^{-1})\underline{R}]\, d\underline{R} \tag{5-26}$$

$$= \int_{\underline{R}} \pi^{-K}\{\det \underline{V}\}^{-1} \exp[\, -\underline{R}^* \underline{V}^{-1} \{\underline{I} - i\Phi \underline{V}(\underline{Q}_0^{-1} - \underline{Q}_1^{-1})\}\underline{R}]\, d\underline{R} \tag{5-27}$$

$$= \{\det[\, \underline{I} - i\Phi \underline{V}(\underline{Q}_0^{-1} - \underline{Q}_1^{-1})]\}^{-1} \tag{5-28}$$

where $\underline{V} = \text{cov}[\underline{R}]$ (5-29)

We let $\underline{G} = \underline{V}\,(\underline{Q}_0^{-1} - \underline{Q}_1^{-1})$ to simplify the notation. The matrix $\underline{G}$ under both H_0 and H_1 can be further expressed as:

$$H_0: \quad \text{cov}[\underline{R}|H_0] = \underline{Q}_0 \tag{5-30}$$

$$\underline{G}_0 = \underline{Q}_0(\underline{Q}_0^{-1} - \underline{Q}_1^{-1}) \tag{5-31}$$

$$= \underline{I} - \underline{Q}_0\, \underline{Q}_1^{-1} \tag{5-32}$$

$$= \underline{I} - (\underline{Q}_1\, \underline{Q}_0^{-1})^{-1} \tag{5-33}$$

$$H_1: \text{cov}[\underline{R}|H_1] = \underline{Q}_1 \tag{5-34}$$

$$\underline{G}_1 = \underline{Q}_1(\underline{Q}_0^{-1} - \underline{Q}_1^{-1}) \tag{5-35}$$

$$= \underline{Q}_1\, \underline{Q}_0^{-1} - \underline{I} \tag{5-36}$$

From equations (5-33) and (5-36), we may find the relationship between the eigenvalues of $\underline{G}$ and that of $\underline{Q}_1 \underline{Q}_0^{-1}$ as:

$$\lambda_{G_0} = 1 - \frac{1}{\lambda_{Q_1 Q_0^{-1}}} \tag{5-37}$$

$$\lambda_{G_1} = \lambda_{Q_1 Q_0^{-1}} - 1 \tag{5-38}$$

These two equations show that we need only to solve for the eigenvalues of $\underline{Q}_1 \underline{Q}_0^{-1}$ and then use equations (5-37) and (5-38) to calculate λ_{G_0} and λ_{G_1}. Furthermore, we may derive the relationship between λ_{G_0} and λ_{G_1}.

$$\lambda_{G_1} = \frac{1}{1-\lambda_{G_0}} - 1 \tag{5-39}$$

$$= \frac{\lambda_{G_0}}{1-\lambda_{G_0}} \tag{5-40}$$

$$\lambda_{G_0} = 1 - \frac{1}{1+\lambda_{G_1}} \tag{5-41}$$

$$= \frac{\lambda_{G_1}}{1+\lambda_{G_1}} \tag{5-42}$$

This implies that once we know λ_{G_0} we can find λ_{G_1} very easily.

There are special cases in which analytical expressions for the eigenvalues of $\underline{G}$ can be obtained. These special cases will be shown as examples. To simplify the derivation, we further assume that $\underline{Q}_0 = \sigma_n^2 \underline{I}$, which means the noises at the receiving array elements are independent from element to element and have equal power.

Example 1: Single Path Signal

If we have only one path, then the covariance matrix $\underline{Q}_1$ can be written as:

$$\underline{Q}_1 = \sigma_n^2 \underline{I} + \sigma_{s_1}^2 \underline{v}_1 \underline{v}_1^* \tag{5-43}$$

The matrices $\underline{G}_0$ and $\underline{G}_1$ become:

$$\underline{G}_0 = \underline{I} - \sigma_n^2 \underline{Q}_1^{-1} \tag{5-44}$$

$$= \underline{I} - \sigma_n^2 (\sigma_n^2 \underline{I} + \sigma_{s_1}^2 \underline{v}_1 \underline{v}_1^*)^{-1} \tag{5-45}$$

$$\underline{G}_1 = (\sigma_n^2 \underline{Q}_1^{-1})^{-1} - \underline{I} \tag{5-46}$$

$$= \frac{1}{\sigma_n^2} \underline{Q}_1 - \underline{I} \tag{5-47}$$

$$= \frac{1}{\sigma_n^2} (\sigma_n^2 \underline{I} + \sigma_{s_1}^2 \underline{v}_1 \underline{v}_1^*) - \underline{I} \tag{5-48}$$

$$= \frac{\sigma_{s_1}^2}{\sigma_n^2} \underline{v}_1 \underline{v}_1^* \tag{5-49}$$

From equations (5-45) and (5-49), we know that it is easier to find λ_{G_1} than to find λ_{G_0}. λ_{G_1} can be found using the following equation.

$$\underline{G}_1 \underline{v}_1 = \frac{\sigma_{s_1}^2}{\sigma_n^2} \underline{v}_1 (\underline{v}_1^* \underline{v}_1) \tag{5-50}$$

$$= \frac{K\sigma_{s_1}^2}{\sigma_n^2} \underline{v}_1 \tag{5-51}$$

$$= \lambda_{G_1} \underline{v}_1 \tag{5-52}$$

Equation (5-52) shows the eigenvalue $\lambda_{G_1} = \frac{k\sigma_{s_1}^2}{\sigma_n^2}$ and the eigenvector $\underline{v}_1$ of $\underline{G}_1$. Once we find λ_{G_1}, we may substitute λ_{G_1} into equation (5-42) to find λ_{G_0}.

$$\lambda_{G_0} = \frac{\lambda_{G_1}}{1 + \lambda_{G_1}} \tag{5-53}$$

$$= \frac{k\sigma_{s_1}^2}{K\sigma_{s_1}^2 + \sigma_n^2} \tag{5-54}$$

From equation (5-49), we observed that the rank of $\underline{G}_1$ is one. By using equations (5-40) and (5-42), we know that a zero eigenvalue of either $\underline{G}_0$ or $\underline{G}_1$ will imply a zero eigenvalue of the other. So, the rank of $\underline{G}_0$ is also one. Hence, the density functions of y under both hypotheses are exponentially distributed as:

$$p(y|H_0) = \begin{cases} \frac{1}{\lambda_{G_0}} \exp(-y/\lambda_{G_0}) & \text{for } y \geq 0 \\ 0 & \text{for } y < 0 \end{cases} \tag{5-55}$$

$$p(y|H_1) = \begin{cases} \frac{1}{\lambda_{G_1}} \exp(-y/\lambda_{G_1}) & \text{for } y \geq 0 \\ 0 & \text{for } y < 0 \end{cases} \tag{5-56}$$

Then, P_D and P_F become:

$$P_D = \int_{\eta}^{\infty} p(y|H_1)dy \tag{5-57}$$

$$= \exp(-\eta/\lambda_{G_1}) \tag{5-58}$$

$$P_F = \int_{\eta}^{\infty} p(y|H_0)dy \tag{5-59}$$

$$= \exp(-\eta/\lambda_{G_0}) \tag{5-60}$$

The corresponding ROC curve has been identified as a power type ROC curve by Birdsall [25].

$$P_F = (P_D)^A \tag{5-61}$$

$$= (P_D)^{\left(\frac{\lambda_{G_1}}{\lambda_{G_0}}\right)} \tag{5-62}$$

$$= P_D^{\left(1 + \frac{K\sigma_{s_1}^2}{\sigma_n^2}\right)} \tag{5-63}$$

The ROC curves can be calculated from equation (5-63) as long as the total signal-to-noise ratio, $\frac{K\sigma_{s_1}^2}{\sigma_n^2}$, is specified. A set of ROC curves with different A values are shown in Figure 5.1. The slope of the curves in Figure 5.1 decreases as the A value increases. As shown in Figure 5.1 the slope of the power type ROC curves is always less than the slope of the ROC curve of the known-waveform signal case [20]. From equations (5-61) and (5-63), the parameter A can be identified as the total signal-to-noise ratio plus one. By using this relation, we may look at Figure 5.1 again and find that the performance improvement measured on normal-normal paper is not linearly proportional to the signal-to-noise ratio. In the high P_D and low P_F region, the performance improvement is less than that in the low P_D and low P_F region for the same signal-to-noise ratio improvement. These observations show the shortcomings of using detectability

index as a performance measure for the Gaussian signal case.

Example 2: Two Path Signals Detected by a Two-Element Array

In this example we assume two signal paths (M=2) and two elements (K=2) and use the characteristic equation $\det[\underline{Q}_1 - \lambda\underline{I}] = 0$ to solve for λ. Since $\underline{Q}_0 = \sigma_n^2 \underline{I}$, the matrix $\underline{Q}_1\underline{Q}_0^{-1}$ is equal to $\frac{1}{\sigma_n^2}\underline{Q}_1$. From equation (5-36), we find the relationship between λ_{G_1} and λ_{Q_1} as follows:

$$\lambda_{G_1} = \frac{1}{\sigma_n^2}\lambda_{Q_1} - 1 \tag{5-64}$$

Substituting equation (5-64) into equation (5-40) we have:

$$\lambda_{G_0} = 1 - \frac{\sigma_n^2}{\lambda_{Q_1}} \tag{5-65}$$

The key to obtaining λ_{G_1} and λ_{G_0} is to solve λ_{Q_1} from the characteristic equation, $\det[\underline{Q}_1 - \lambda\underline{I}] = 0$.

$$\underline{Q}_1 - \lambda\underline{I} = \sigma_n^2\underline{I} + \sigma_{s_1}^2 \underline{v}_1 \underline{v}_1^* + \sigma_{s_2}^2 \underline{v}_2 \underline{v}_2^* - \lambda\underline{I} \tag{5-66}$$

$$= \begin{bmatrix} \sigma_n^2 - \lambda & 0 \\ 0 & \sigma_n^2 - \lambda \end{bmatrix} + \sigma_{s_1}^2 \begin{bmatrix} 1 & e^{j\omega\tau_1} \\ e^{-j\omega\tau_1} & 1 \end{bmatrix} + \sigma_{s_2}^2 \begin{bmatrix} 1 & e^{j\omega\tau_2} \\ e^{-j\omega\tau_2} & 1 \end{bmatrix} \tag{5-67}$$

$$\det[\underline{Q}_1 - \lambda\underline{I}] = (\sigma_{s_1}^2 + \sigma_{s_2}^2 + \sigma_n^2 - \lambda)^2 - \left|\sigma_{s_1}^2 e^{j\omega\tau_1} + \sigma_{s_2}^2 e^{j\omega\tau_2}\right|^2 \tag{5-68}$$

The eigenvalues of $\underline{Q}_1$ can be solved very easily from equation (5-68).

$$\lambda_{Q_1} = \sigma_{s_1}^2 + \sigma_{s_2}^2 + \sigma_n^2 \pm \left| \sigma_{s_1}^2 e^{j\omega\tau_1} + \sigma_{s_2}^2 e^{j\omega\tau_2} \right| \tag{5-69}$$

The eigenvalues of $\underline{G}_1$ and $\underline{G}_0$ become:

$$\lambda_{G_1} = \frac{\lambda_{Q_1}}{\sigma_n^2} - 1 \tag{5-70}$$

$$= \frac{\sigma_{s_1}^2 + \sigma_{s_2}^2 \pm \left| \sigma_{s_1}^2 e^{j\omega\tau_1} + \sigma_{s_2}^2 e^{j\omega\tau_2} \right|}{\sigma_n^2} \tag{5-71}$$

$$\lambda_{G_0} = 1 - \frac{\sigma_n^2}{\lambda_{Q_1}} \tag{5-72}$$

$$= \frac{\sigma_{s_1}^2 + \sigma_{s_2}^2 \pm \left| \sigma_{s_1}^2 e^{j\omega\tau_1} + \sigma_{s_2}^2 e^{j\omega\tau_2} \right|}{\sigma_n^2 + \sigma_{s_1}^2 + \sigma_{s_2}^2 \pm \left| \sigma_{s_1}^2 e^{j\omega\tau_1} + \sigma_{s_2}^2 e^{j\omega\tau_2} \right|} \tag{5-73}$$

The two non-zero eigenvalues of $\underline{G}_1$ and $\underline{G}_0$ are distinct except for the rare case that $\left| \sigma_{s_1}^2 e^{j\omega\tau_1} + \sigma_{s_2}^2 e^{j\omega\tau_2} \right| = 0$. The density function of y takes the form of equation (5-7). The probability of detection (P_D) and the probability of false alarm (P_F) become:

$$P_D = \frac{\lambda_{G_{1,1}}}{\lambda_{G_{1,1}} - \lambda_{G_{1,2}}} \exp\left(-\frac{\eta}{\lambda_{G_{1,1}}}\right) + \frac{\lambda_{G_{1,2}}}{\lambda_{G_{1,2}} - \lambda_{G_{1,1}}} \exp\left(-\frac{\eta}{\lambda_{G_{1,2}}}\right) \tag{5-74}$$

$$P_F = \frac{\lambda_{G_{0,1}}}{\lambda_{G_{0,1}} - \lambda_{G_{0,2}}} \exp\left(-\frac{\eta}{\lambda_{G_{0,1}}}\right) + \frac{\lambda_{G_{0,2}}}{\lambda_{G_{0,2}} - \lambda_{G_{0,1}}} \exp\left(-\frac{\eta}{\lambda_{G_{0,2}}}\right) \tag{5-75}$$

where $\lambda_{G_{0,1}}$ and $\lambda_{G_{1,1}}$ are expressed in equation (5-73) and (5-71) with positive sign and $\lambda_{G_{0,2}}$ and $\lambda_{G_{1,2}}$ with negative sign.

In order to examine the character of the ROC curves, we considered a specific case and plotted the ROC curves in Figures 5.2 and 5.3. In Figure 5.2 the optimal performance of a 2-element array for detecting 2-path signals are plotted for different total signal-to-noise ratios. The signal incident angles are assumed to be $\pm 15°$ from the horizontal axis and the signal strengths from both paths are assumed equal. The ROC curves are similar to the power type ROC curves shown in Figure 5.1. We would also like to examine the ROC curves for 2 path signals with different signal strengths. The ratios of signal strength are assumed to be 1:1, 2:1 and 10:1. In Figure 5.3, three sets of curves are drawn on normal-normal paper. By comparing these curves we conclude that the performances are almost equal for low signal-to-noise ratios. However, for high signal-to-noise

ratios, the case in which each path has equal signal strength gives the highest performance among the three.

Example 3 M Signal Paths Detected by a Two-element array

The extension of the two-path results in example 2 to the M-path case is straight forward. For the M-path signal case, $\underline{Q}_1$ becomes:

$$\underline{Q}_1 = \sigma_n^2 \underline{I} + \sigma_{s_1}^2 \underline{v}_1 \underline{v}_1^* + \cdots + \sigma_{s_M}^2 \underline{v}_M \underline{v}_M^* \tag{5-76}$$

Consequently, the characteristic equation is:

$$\det[\underline{Q}_1 - \lambda \underline{I}] = (\sigma_{s_1}^2 + \cdots + \sigma_{s_M}^2 + \sigma_n^2 - \lambda)^2 - \left| \sum_{i=1}^{M} \sigma_{s_i}^2 e^{j\omega\tau_i} \right|^2 \tag{5-77}$$

and the eigenvalues of λ_{Q_1} are

$$\lambda_{Q_1} = \sum_{i=1}^{M} \sigma_{s_i}^2 + \sigma_n^2 \pm \left| \sum_{i=1}^{M} \sigma_{s_i}^2 e^{j\omega\tau_i} \right| \tag{5-78}$$

The eigenvalues of $\underline{G}_0$ and $\underline{G}_1$ can be expressed as:

$$\lambda_{G_1} = \frac{\sum_{i=1}^{M} \sigma_{s_1}^2 \pm \left| \sum_{i=1}^{M} \sigma_{s_i}^2 e^{j\omega\tau_i} \right|}{\sigma_n^2} \tag{5-79}$$

$$\lambda_{G_0} = \frac{\sum_{i=1}^{M} \sigma_{s_i}^2 \pm \left| \sum_{i=1}^{M} \sigma_{s_i}^2 \, e^{j\omega\tau_i} \right|}{\sigma_n^2 + \sum_{i=1}^{M} \sigma_{s_i}^2 \pm \left| \sum_{i=1}^{M} \sigma_{s_i}^2 \, e^{j\omega\tau_i} \right|} \qquad (5\text{-}80)$$

By substituting equations (5-79) and (5-80) into equations (5-73) and (5-74), we may find P_D and P_F for the M signal path case.

Ten signal paths with equal spatial angular separations are assumed to be within the range of $\pm 15°$ from the horizontal axis. The signal strength of all paths is assumed equal. The ROC curves of the 2-element array detector are plotted in Figure 5.4. The general shape of the curve is similar to the curves in Figure 5.1. This may be explained by the fact that there are only two non-zero eigenvalues and one of them is dominant under hypothesis H_1. Hence, the density function of y under H_1 is very similar to an expontial curve and the resulting ROC curves are similar to the power type ROC curves. The results shown in this example also demonstrate that it is not sufficient to characterize the ROC curves by using only the mean and variance of the sufficient statistic y. In this case, there are only two non-zero eigenvalues in spite of the number of signal paths. The density function of y under both hypotheses is very much different from the Gaussian distribution and cannot be characterized completely by only the mean and the variance of y. Besides, one of the two non-zero eigenvalues of $\underline{G}_1$ is much larger than another. This is why the ROC curves for this case, as shown in Figure 5.4, are very similar to the power type ROC curves.

For any matrix, the eigenvalues can be evaluated by solving the equation $\det[\underline{Q} - \lambda\underline{I}] = 0$. However, if the dimension of the matrix is larger than 4, the eigenvalue cannot be solved for analytically. Even for a (3x3) matrix case, obtaining the eigenvalues can be quite tricky. Example 4 will show a case with two signal paths and a 3-element array.

Example 4 Two Signal Paths Detected by a Three-element Array

We assume M=2 and K=3 in this example, where M is the number of paths and K is the number of array elements. The covariance matrix $\underline{Q}_1$ becomes:

$$\underline{Q}_1 = \sigma_n^2 \underline{I} + \sigma_{s_1}^2 \underline{v}_1 \underline{v}_1^* + \sigma_{s_2}^2 \underline{v}_2 \underline{v}_2^* \qquad (5\text{-}81)$$

Then,

$$\underline{Q}_1 - \lambda\underline{I} = (\sigma_n^2 - \lambda)\underline{I} + \sigma_{s_1}^2 \underline{v}_1 \underline{v}_1^* + \sigma_{s_2}^2 \underline{v}_2 \underline{v}_2^* \qquad (5\text{-}82)$$

$$= \begin{bmatrix} \sigma_n^2 - \lambda & 0 & 0 \\ 0 & \sigma_n^2 - \lambda & 0 \\ 0 & 0 & \sigma_n^2 - \lambda \end{bmatrix} + \sigma_{s_1}^2 \begin{bmatrix} 1 & e^{j\omega\tau_1} & e^{2j\omega\tau_1} \\ e^{-j\omega\tau_1} & 1 & e^{j\omega\tau_1} \\ e^{-j\omega\tau_1 2} & e^{-j\omega\tau_1} & 1 \end{bmatrix}$$

$$+ \sigma_{s_2}^2 \begin{bmatrix} 1 & e^{j\omega\tau_2} & e^{2j\omega\tau_2} \\ e^{-j\omega\tau_2} & 1 & e^{j\omega\tau_2} \\ e^{-2j\omega\tau_2} & e^{-j\omega\tau_2} & 1 \end{bmatrix} \tag{5-83}$$

and,

$$\det[\underline{Q}_1 - \lambda \underline{I}] = (\sigma_{s_1}^2 + \sigma_{s_2}^2 + \sigma_n^2 - \lambda)^3 + (A_1^*)^2 A_2 + A_1^2 A_2^* - (\sigma_{s_1}^2 + \sigma_{s_1}^2 + \sigma_n^2 - \lambda)(A_2 A_2^* + 2A_1 A_1^*) \tag{5-84}$$

where $$A_1 = \sigma_{s_1}^2 e^{j\omega\tau_1} + \sigma_{s_2}^2 e^{j\omega\tau_2} \tag{5-85}$$

and $$A_2 = \sigma_{s_1}^2 e^{2j\omega\tau_1} + \sigma_{s_2}^2 e^{2j\omega\tau_2} \tag{5-86}$$

From equation (4-29) we know that the matrix

$$\underline{Q}_0^{-1} - \underline{Q}_1^{-1} = c_1 \underline{v}_1 \underline{v}_1^* + c_2 \underline{v}_2 \underline{v}_2^* - c_3[(\underline{v}_2^* \underline{v}_1)\underline{v}_2 \underline{v}_1^* + (\underline{v}_1^* \underline{v}_2)\underline{v}_1 \underline{v}_2^*] \tag{5-87}$$

has rank 2. We also know that both $\underline{G}_0 = \underline{Q}_0 (\underline{Q}_0^{-1} - \underline{Q}_1^{-1})$ and $\underline{G}_1 = \underline{Q}_1 (\underline{Q}_0^{-1} - \underline{Q}_1^{-1})$ have rank 2. This implies that one of the solutions

to the characteristic equation of $\underline{G}_0$ and $\underline{G}_1$ has to be zero. In other words, one of the eigenvalues of $\underline{Q}_1$ should satisfy the following two equations.

$$\lambda_{G_0} = 1 - \frac{\sigma_n^2}{\lambda_{Q_1}} = 0 \tag{5-88}$$

$$\lambda_{G_1} = \frac{\lambda_{Q_1}}{\sigma_n^2} - 1 = 0 \tag{5-89}$$

We found that λ_{Q_1} should be equal to σ_n^2 to satisfy both equation (5-88) and equation (5-89). This eigenvalue, $\lambda_{Q_1} = \sigma_n^2$, will be verified with the following equations.

$$\det[\underline{Q}_1 - \lambda_{Q_1}\underline{I}] = \det[\underline{Q}_1 - \sigma_n^2\,\underline{I}] \tag{5-90}$$

$$= \det[\sigma_{s_1}^2\,\underline{v}_1\underline{v}_1^* + \sigma_{s_2}^2\,\underline{v}_2\underline{v}_2^*] \tag{5-91}$$

Since the rank of $\sigma_{s_1}^2\,\underline{v}_1\underline{v}_1^* + \sigma_{s_2}^2\,\underline{v}_2\underline{v}_2^*$ is two and the dimension of the matrix $\underline{Q}_1$ is three, we can easily see that $\det[\underline{Q}_1 - \sigma_n^2\,\underline{I}] = 0$. This shows that $\lambda_{Q_1} = \sigma_n^2$ is indeed a solution to the characteristic equation of $\underline{Q}_1$. The next step is to reduce the 3rd order equation by dividing $\det[\underline{Q}_1 - \lambda\underline{I}]$ by $(\sigma_n^2 - \lambda)$. After some manipulations we obtained a simple second degree equation in λ.

$$\frac{\det[\underline{Q}_1 - \lambda \underline{I}]}{\sigma_n^2 - \lambda} = 3(\sigma_{s_1}^2 + \sigma_{s_2}^2)^2 + 3(\sigma_{s_1}^2 + \sigma_{s_2}^2)(\sigma_n^2 - \lambda) + (\sigma_n^2 - \lambda)^2$$

$$-[A_2 A_2^* + 2A_1 A_1^*] = 0 \qquad (5\text{-}92)$$

where A_1 and A_2 are defined in equations (5-85) and (5-86).

We may solve the second degree equation to get λ_{Q_1}.

$$(\sigma_n^2 - \lambda) = \frac{-3(\sigma_{s_1}^2 + \sigma_{s_2}^2) \pm \sqrt{-3(\sigma_{s_1}^2 + \sigma_{s_2}^2)^2 + 4(A_2 A_2^* + 2A_1 A_1^*)}}{2} \qquad (5\text{-}93)$$

so,

$$\lambda_{Q_1} = \sigma_n^2 + \frac{3(\sigma_{s_1}^2 + \sigma_{s_2}^2)}{2} \pm \frac{1}{2}\sqrt{-3(\sigma_{s_1}^2 + \sigma_{s_2}^2)^2 + 4(A_2 A_2^* + 2A_1 A_1^*)} \qquad (5\text{-}94)$$

where $-3\left(\sigma_{s_1}^2 + \sigma_{s_2}^2\right)^2 + 4\left(A_2 A_2^* + 2A_1 A_1^*\right) = 9\,\sigma_{s_1}^4 + 9\,\sigma_{s_2}^4 - 6\,\sigma_{s_2}^2\,\sigma_{s_1}^2\Big[$

$$\left(e^{-j2\omega\tau_1 + j2\omega\tau_2} + e^{-j2\omega\tau_2 + j2\omega\tau_1}\right) + 2\left(e^{-j\omega\tau_1 + j\omega\tau_2} + e^{j\omega\tau_1 - j\omega\tau_2}\right)\Big]$$

Substituting equation (5-94) into equations (5-70) and (5-72), we can get λ_{G_0} and λ_{G_1}.

To show the detection performance of the 3-element array, we use the same two signal paths as in example 3. The optimal ROC curves for several signal-to-noise ratios are shown in Figure 5.5 for a 3-element array. We notice that there are only 2 non-zero eigenvalues because there are only two paths. In general, the number of non-zero eigenvalues is no larger than min(K,M), where K is the number of array elements and M is the number of signal paths. In Figure 5.5, the shape of the ROC curves for a 3-element array is similar to that in Figure 5.2, and is apparently not like normal ROC curves which would be the result for the case with Gaussian distributed sufficient statistics under both hypothesis. By using the equation A = 1 + K·SNR, we also recognize that the slope of the ROC curves in this example is slightly higher than that for the power type ROC curves shown in Figure 5.1.

In order to see the performance improvement by adding hydrophones to the array receiver, we make the performances comparison among arrays with different numbers of elements in the next section.

5.3 Performance Comparison between Optimal Array Processors with Different Numbers of Elements

In the previous section, we have derived performance evaluation methods analytically for some special cases. However, we will not solve

every problem by using the analytical method because it is too tedious and error prone. A numerical method for finding the eigenvalues of a complex matrix is shown in Appendix A. By employing the software subroutine package EISPACK, a computer program for evaluating the detection performance numerically has been developed to find the performance of arrays with more than 3 elements. To make sure of the correctness of the computer program, we have checked the numerical results with the ROC curves obtained from the analytical method for several cases.

We use the case with two signal paths coming in at $\pm 15°$ from the horizontal axis as an example to show the detection performance improvement due to adding hydrophones to the array. In Figure 5.6 and Figure 5.7, performances of arrays with one, two, and three elements are plotted for different values of signal-to-noise ratio per element, $\text{SNR} = \frac{\sigma_{s_1}^2 + \sigma_{s_2}^2}{\sigma_n^2}$, where $\sigma_{s_1}^2$ and $\sigma_{s_2}^2$ are signal power of path 1 and path 2 respectively. The ROC curve has a slope less than tan 45° on the normal-normal paper. In general, the slope of the ROC curves is smaller for high signal-to-noise ratios than for low signal-to-noise ratios. We also notice that the performance improvement obtained by adding one hydrophone to a 2-element array is less than that obtained by adding one hydrophone to a single-element array for SNR=10. However, for low signal-to-noise ratios such as SNR of 1 and 2, improvements from adding one hydrophone to a 2-element or a 3-element array are nearly the same. This phenomenon can also be seen by comparing the solid lines in Figures 5.8 and 5.9. In Figure 5.8, the ROC curves for SNR=1

and K=1, 2, 3 and 4 are parallel with equal spacing. On the other hand, the ROC curves in Figure 5.9 for SNR=10 and K=1, 2, 3 and 4 have unequal spacing. Apparently, the performance improvement due to adding one hydrophone to an array depends on the array factor as well as the signal-to-noise ratio per element. In general, the performance improvement is less for high SNR than that for low SNR. This shows a difference between the performance of detecting multipath Gaussian signals and that of detecting multipath known waveform signals [28] in which the performance improvement due to adding hydrophones is independent of signal-to-noise ratio.

It is also interesting to compare the performance characteristics of array detectors with that of a single phone detector. We look into the question of how much performance improvement an array can gain over the signal phone. To answer this we compare the performance of a single hydrophone detector with the performance of the array detector with K elements. In Figure 5.8 we compare the performance of a single hydrophone detector with K times the signal-to-noise ratio with the performance of K-element array detectors for K=1, 2, 3, 4 and 10, and SNR=1. We observe that the performances of these two cases are nearly the same for small (K·SNR) values. But, for large (K·SNR) values the performance of an array detector is better than that of the single hydrophone case. In Figure 5.9 we make a similar comparison for SNR=10. The curves in Figure 5.9 show dramatic performance improvement for the array detectors. By referring to the structure of the optimum array detector in which signals from each path are spatially separated from other paths by beamforming action, we may conclude that the array detectors not only receive a total output signal-to-noise ratio K times

higher than that of the single phone, but also provide the capability of separating multipath signals spatially. The spatial discriminating capability of the array detector does improve the performance considerably for high signal-to-noise ratio cases.

By inspecting the slopes of the curves in Figure 5.8 and 5.9, we notice the difference in shape between the array and single hydrophone ROC curves. This can be explained by looking at the density function of y. As discussed before, we know that for a single hydrophone the density function of y is exponentially distributed. On the other hand, the density function of y for the array detector depends on two non-zero eigenvalues for various K values and signal-to-noise ratio as is shown in Table I. From the table we observe that in some cases two eigenvalues are almost identical and in other cases one eigenvalue is larger than the other. For the K=2 cases, there exists a dominant eigenvalue which is due to the fact that the size of the array is too small to discriminate two signal paths. Hence, the resulting ROC curves have shapes similar to that of the power type ROC curves, which is the character of the ROC curves for a single hydrophone detector. For the K=4 cases, the width of the mainlobe of a 4-element array is about 60° which is about two times the angular separation between the two signal paths. In other words, the 4-element array may point a beam to one path and null out the other path simultaneously. As a result, the eigenvalues for this case are almost identical. Consequently, the distribution of y is the χ^2 distribution with 4 degrees of freedom. The noticeable difference on ROC curves between the exponential distribution and the χ^2 distribution with 4 degrees of freedom is the slope of the ROC

curves. The curves of the former case have smaller slopes than that of the latter case.

By investigating the beam pattern of a K-element array [27], we found that the main beam width is approximately equal to 180°/(K-1). For K=2 and K=3 cases, both signal paths are in the mainlobe of the beam pattern, and for K=4 and K=10 cases, one path is in the mainlobe and the other is in the sidelobe. Consequently, the eigenvalues of $\underline{G}_1$ for the K=4 and K=10 cases are close to each other while the λ_{G_1}'s for K=2 and K=3 are far apart. The dependency of the eigenvalues on the array beam pattern will be discussed further in the next section in which we will investigate the performance of suboptimal processors such as single and double beamformers.

TABLE I

M = 2, K = 2, 3, 4, 10 $\phi' = 75°$, $\phi' = 105$

		K = 2		K = 3		K = 4		K = 10	
SNR=1	λ_{G_1}	1.6872	0.3218	1.9446	1.05538	2.0761	1.9238	5.662	4.3374
	λ_{G_0}	0.6279	0.2382	0.6604	0.5134	0.6749	0.6580	0.8498	0.812662
SNR=2	λ_{G_1}	3.3745	0.6255	3.8892	2.11078	4.15226	3.84774	11.3241	3.84774
	λ_{G_0}	0.7714	0.3848	0.79547	0.67854	0.805911	0.79372	0.805911	0.793718
SNR=10	λ_{G_1}	16.8724	3.1276	19.446	10.5539	20.7613	19.2387	56.62	43.379
	λ_{G_0}	0.944	0.7577	0.95109	0.91345	0.954047	0.95059	0.982645	0.977467

5.4 Detection Performance of Suboptimal Array Beamformers

A. Single Beamformer

A single beamformer which points to one of the M signal paths and a double beamformer which points to two signal paths are investigated in this section. The trade-off between the complexity of the processor structure and the detection performance will be evaluated.

A single beamformer is a suboptimal array which ignores the existence of the multipath structure and points a beam to the direct path. The simplicity of the processor structure makes it popular in practical applications. The sufficient statistic y of the single beamformer may be expressed by

$$y = \underline{R}^* \, \underline{u} \, \underline{u}^* \, \underline{R} \tag{5-95}$$

where $\underline{u}$ is the pointing vector of the single beamformer.
Then, by definition,

$$\underline{G}_0 = \underline{Q}_0 \, (\underline{u} \, \underline{u}^*) \tag{5-96}$$

$$= \sigma_n^2 \, \underline{u} \, \underline{u}^* \tag{5-97}$$

and

$$\underline{G}_1 = \underline{Q}_1 \, (\underline{u} \, \underline{u}^*) \tag{5-98}$$

$$= \sigma_n^2 \, \underline{u} \, \underline{u}^* + \sigma_{s_1}^2 \underline{v}_1 (\underline{v}_1 \underline{u}^*) \underline{u}^* + \cdots + \sigma_{s_M}^2 \underline{v}_M (\underline{v}_M^* \underline{u}) \underline{u}^* \tag{5-99}$$

where

$$\underline{Q}_1 = \sigma_n^2 \underline{I} + \sigma_{s_1}^2 \underline{v}_1 \underline{v}_1^* + \cdots + \sigma_{s_M}^2 \underline{v}_M \underline{v}_M^* \tag{5-100}$$

It is quite easy to find the eigenvalue of $\underline{G}_0$ from the next equation.

$$\underline{G}_0 \, \underline{u} = \sigma_n^2 \, \underline{u} \, (\underline{u}^* \underline{u}) \tag{5-101}$$

$$= K\sigma_n^2 \, \underline{u} \tag{5-102}$$

To find the eigenvalues of $\underline{G}_1$ is not obvious. We should use the matrix theorem that "the eigenvalue of $\underline{G}_1$ is equal to that of $\underline{G}_1^T$". By observation, we found the eigenvector and eigenvalue of $\underline{G}_1^T$ from the following equations.

$$\underline{G}_1^T \underline{u}^{*T} = \sigma_n^2 \, \underline{u}^{*T} (\underline{u}^T \underline{u}^{*T}) + \sum_{i=1}^{M} \sigma_{s_i}^2 (\underline{v}_i^* \underline{u}) \underline{u}^{*T} (\underline{v}_i^T \underline{u}^{*T}) \tag{5-103}$$

$$= \sigma_n^2 \, K \, \underline{u}^{*T} + \sum_{i=1}^{M} \sigma_{s_i}^2 \left| \underline{v}_i^* \underline{u} \right|^2 \underline{u}^{*T} \tag{5-104}$$

Hence,

$$\lambda_{G_1} = \sigma_n^2 \, K + \sum_{i=1}^{M} \sigma_{s_i}^2 \left| \underline{v}_i^* \underline{u} \right|^2 \tag{5-105}$$

The ROC curve for this case is apparently a power type ROC curve and can be expressed by

$$P_F = (P_D)^A \tag{5-106}$$

where
$$A = \frac{\lambda_{G_1}}{\lambda_{G_0}} \tag{5-107}$$

$$= 1 + \frac{\sum_{i=1}^{M} \sigma_{s_i}^2 \left| \underline{v}_i^* \underline{u} \right|^2}{K\sigma_n^2} \tag{5-108}$$

The second term in equation (5-108) is the summation of signal energy weighted by the beam pattern.

In order to compare the single beamformer performance with the optimal processor performance, two signal paths are chosen coming at $\pm 15°$ from the horizontal axis. The values of A for K = 2, 3, 4 and 10 are 2.4723, 2.6313, 3.0029, 6.1121 respectively in the $\sigma_{s_1}^2 = \sigma_{s_2}^2 = \frac{1}{2}\sigma_n^2$ cases. We notice that the value of A can be approximated by $A = 1 + \frac{K\sigma_{s_1}^2}{\sigma_n^2}$ when $K \geq 4$. This is due to the fact that the beamwidth of the mainlobe for $K \geq 4$ is less than 60°. Hence, the second signal is in the sidelobe of the beam pattern and does not contribute too much signal energy. In other words, the single beamformer array nulls out the second signal source when the size of the array is large. Consequently, it has the same performance as that of the single path case in which the ROC curves are characterized by $A = 1 + \frac{K\sigma_s^2}{\sigma_n^2}$.

The ROC curves of the single beamformer are plotted in Figure 5.10 and Figure 5.11 for different signal-to-noise ratios. By comparing these ROC curves with that of the optimal detectors, we conclude that the performance loss due to not taking account of the second path increases as the number of array elements increases. This indicates that the larger the array size, the more important the knowledge about the spatial structure of the signal.

B. Double Beamformer

If we want to retain the beamforming structure and improve the performance, then the double beamformer is our next choice for detecting two path signals. The sufficient statistic y is described in equation (5-109).

$$y = \underline{R}^*(\sigma_{s_1}^2 \ \underline{v}_1\underline{v}_1^* + \sigma_{s_2}^2 \ \underline{v}_2\underline{v}_2^*)\underline{R} \tag{5-109}$$

$$\underline{G}_0 = \underline{Q}_0(\sigma_{s_1}^2 \ \underline{v}_1\underline{v}_1^* + \sigma_{s_2}^2 \ \underline{v}_2\underline{v}_2^*) \tag{5-110}$$

$$= \sigma_n^2(\sigma_{s_1}^2 \ \underline{v}_1\underline{v}_1^* + \sigma_{s_2}^2 \ \underline{v}_2\underline{v}_2^*) \tag{5-111}$$

$$\underline{G}_1 = \underline{Q}_1(\sigma_{s_1}^2 \ \underline{v}_1\underline{v}_1^* + \sigma_{s_2}^2 \ \underline{v}_2\underline{v}_2^*) \tag{5-112}$$

$$= \sigma_n^2(\sigma_{s_1}^2 \ \underline{v}_1\underline{v}_1^* + \sigma_{s_2}^2 \ \underline{v}_2\underline{v}_2^*)+(\sigma_{s_1}^2 \ \underline{v}_1\underline{v}_1^*+\sigma_{s_2}^2 \ \underline{v}_2\underline{v}_2^*)^2 \tag{5-113}$$

From equation (5-111) and (5-113), we know that we need only to find the

eigenvalues, λ_{DB}, of matrix $(\sigma_{s_1}^2 \underline{v}_1\underline{v}_1^* + \sigma_{s_2}^2 \underline{v}_2\underline{v}_2^*)$, because λ_{G_0} and λ_{G_1} may be expressed in terms of λ_{DB} as shown in the following equations.

$$\lambda_{G_0} = \sigma_n^2 \lambda_{DB} \tag{5-114}$$

$$\lambda_{G_1} = \sigma_n^2 \lambda_{DB} + \lambda_{DB}^2 \tag{5-115}$$

Eigenvalue λ_{DB} may be evaluated by both analytical and numerical methods. A simple two-element case will be shown as an example for the analytical method.

$$\sigma_{s_1}^2 \underline{v}_1\underline{v}_1^* + \sigma_{s_2}^2 \underline{v}_2\underline{v}_2^*$$

$$= \sigma_{s_1}^2 \begin{bmatrix} 1 & e^{j\omega\tau_1} \\ e^{-j\omega\tau_1} & 1 \end{bmatrix} + \sigma_{s_2}^2 \begin{bmatrix} 1 & e^{j\omega\tau_2} \\ e^{-j\omega\tau_2} & 1 \end{bmatrix} \tag{5-116}$$

$$\det[\sigma_{s_1}^2 \underline{v}_1 \underline{v}_1^* + \sigma_{s_2}^2 \underline{v}_2 \underline{v}_2^* - \lambda \underline{I}]$$

$$= (\sigma_{s_1}^2 + \sigma_{s_2}^2 - \lambda)^2 - \left|\sigma_{s_1}^2 e^{j\omega\tau_1} + \sigma_{s_2}^2 e^{j\omega\tau_2}\right|^2 \qquad (5\text{-}117)$$

$$\lambda_{DB} = \sigma_{s_1}^2 + \sigma_{s_2}^2 \pm \left|\sigma_{s_1}^2 e^{j\omega\tau_1} + \sigma_{s_2}^2 e^{j\omega\tau_2}\right| \qquad (5\text{-}118)$$

Substituting equation (5-118) into equations (5-114) and (5-115), we may find λ_{G_0} and λ_{G_1}. The rest of the performance evaluation procedure is similar to that of the examples in the previous sections.

The structure of the double beamformer can be realized as two beamformers followed by envelope detectors as shown in Figure 5.12. Comparing Figure 5.12 with Figure 4.1, the only difference is that the cross correlated terms are missing in Figure 5.12. The performance degradation due to the lack of the correlated terms is the main topic in this subsection.

The performance of the double beamformer has been calculated by using numerical programs for two, three, four, and ten element arrays. The ROC curves are shown as the dashed lines in Figure 5.13 and Figure 5.14. On the same Figures the ROC curves of the optimal detectors are also shown. It is interesting to see that the performance of the double beamformer is very close to optimum for $K \geq 4$. This can be explained by the fact that one of the two signal paths is in the sidelobe of the beam pattern and consequently the cross correlated terms in the optimal array are small compared to the beamformer output power. Hence, the cross correlated terms may be ignored when the array size is large enough such that the main beam width is less

than two times the angular separation of the two signal paths. In Figure 5.13 we observe that the performance of the double beamformer is very close to optimum for K = 2, 3, 4 and 10 at a signal-to-noise ratio of 1. But, in Figure 5.14 the performance degradation is severe at K = 2 at a signal-to-noise ratio of 10. This indicates that the cross correlated term plays an important role only for cases with high signal-to-noise ratio and small array sizes.

CHAPTER VI SUMMARY

This report has proposed vertical arrays for estimating parameters of multipath signals and for detecting multipath Gaussian signals. The spatial discriminating capability of vertical array processors can be used to isolate individual signal paths in an underwater acoustic channel. The amplitude and phase estimates of signals from each individual path are obtained and compared to that for a single hydrophone case. The signal-to-noise ratio of each individual path is shown to be independent of the relative signal phases of other paths. This suggests that the vertical array processor may be useful in the deep fading problem for minimizing multipath signal cancellation. Two approaches are taken to estimate the signal parameters. In Chapter III, the signal parameters are assumed non-random and the maximum likelihood estimates (MLE) and their performances are shown. It is clear that if the number of array elements is less than the number of signal paths, then the maximum likelihood ratio estimate is not unique. In Chapter IV, the signal parameters are assumed to be Gaussian random variables with covariance matrix $\underline{Q}_s$, and the maximum a posteriori probability estimates (MAP) of multipath signal parameters are employed. With the a priori knowledge about the signal in terms of the covariance matrix $\underline{Q}_s$, the MAP estimate has a unique value even for the case where the number of array elements is less than the number of signal paths. The linear relationship between MAP and MLE estimates is presented to show the incorporation of the a priori knowledge of the signal parameters.

The second part of this report is devoted to the detection of multipath Gaussian signals in Gaussian noise. Like most Gaussian signal detectors the optimal array detector has a quadratic structure. A two-path signal example shows that the optimal array not only points two beams in both signal directions but also correlates both beams to form a cross correlation term, even when multipath random signals are assumed independent from path to path. In Chapter V, the significance of the two-beamformer structure and the cross correlation term are investigated in terms of detection performance. An analytical method called the "Eigenvalue method" is developed for evaluating the performance of any array signal detector which has a quadratic sufficient statistic. The eigenvalue method starts with the characteristic function of the sufficient statistic under both hypotheses and then transforms the characteristic function to the probability density function. The probability of false alarm and probability of detection may be calculated analytically once the eigenvalues of the covariance matrices of the observed data under both hypotheses are calculated. Although we may find the eigenvalues of any matrix with dimension less than four by an analytical method, the calculation of eigenvalues is performed mostly by a numerical method in Chapter IV. For matrices with dimensionality less than three, both methods are demonstrated.

Performance comparisons were made between optimal arrays with different number of elements. By use of the two-path signal case as an example, we found that the performance improvement obtained by adding one hydrophone to a 2-element array is less than that of adding one hydrophone to a

single-element array for high signal-to-noise ratios around SNR = 10. But, for low signal-to-noise ratios such as one, two and four the performance improvement for both cases are nearly the same. This shows the difference between the performance of detecting Gaussian signals and the performance of detecting known waveform signals. It is well-known that in the latter case the detectability index is the product of two functions, one depends on the signal-to-noise ratio, another depends on the array factor. In other words, the performance improvement in terms of detectability index by adding one hydrophone to an array is independent of the signal-to-noise ratio. The phenomena of the former case may be explained by the property of power type ROC curves which are the type ROC curves that result in the Gaussian signal detection problem. The family of power type ROC curves shows that the performance improvement due to the increase in signal-to-noise ratio starts to decrease after the parameter A becomes larger than about 21. During the process of comparing the ROC curves for the Gaussian signal array detectors with the power type ROC curves, we observed the difference in the slopes of ROC curves. This led to a comparison between the performance of a k-element array with that of a single phone detector with k times the signal-to-noise ratio. For low total output signal-to-noise ratios in the range of one to four the difference in performance between these two cases is insignificant. However, for high signal-to-noise ratios, (i.e. $(k \cdot SNR) \geq 10$), the array detector is better than the single phone detector, for the same total signal-to-noise ratio. This may be attributed to the spatial discriminating capability of the array.

The trade-off between the processor complexity and performance is also shown in Chapter V by comparing the performance of an optimal array detector with that of conventional beamformers. Again, the two-path case is used to demonstrate the performance difference between optimal, single beamformer and double beamformer arrays. A single beamformer array which points a beam in one of the two signal directions performs poorly compared to the optimal array. Although the structure of the single beamformer is only one branch of the optimal processor, the performance of a 10-element single beamformer array is equivalent to that of the optimal array with only 4 elements at SNR = 1.

Another suboptimal array processor which points two beams to two signal paths and sums up the envelope detector outputs is also investigated. The performance comparison shows that if the aperture of the array is large enough such that the second signal direction is not in the mainlobe or any significant sidelobe of the array pattern, the difference between the suboptimal array and optimal array in performance is very small for all signal-to-noise ratios. For high signal-to-noise ratios and small arrays the performance difference between the suboptimal and optimal arrays is noticeable. This finding implies that the cross correlation term in the optimal processor is not very significant if the array aperture is large enough to isolate signal paths or the signal-to-noise ratio is low.

The eigenvalue method, introduced in this report, is a powerful tool for evaluating performance of array detectors. Since the detection performance and the processor complexity are two major factors to consider in the implementation of array detectors, the trade-off of these factors,

as shown in this report, gives insight into the problem of detecting multipath Gaussian signals in Gaussian noise.

REFERENCES

[1] I. Tolstoy, and C. S. Clay, Ocean Acoustics, Theory and Experiment in Underwater Sound, McGraw-Hill Book Company, 1966.

[2] R. J. Urick, Principles of Underwater Sound for Engineer, McGraw-Hill Book Company, New York, 1967.

[3] R. P. Flanagen, N. L. Weinberg and J. G. Clark, "Coherent Analysis of Ray Propagation with Moving Source and Fixed Receiver," JASA, Vol. 56, No. 6, December 1964, pp. 1673-1680.

[4] J. C. Steinberg and T. G. Birdsall, "Underwater Sound Propagation in the Straits of Florida," JASA, Vol. 39, No. 2, 1966, pp. 301-315.

[5] H. A. Deferrari and R. Leung, "Spectrum of Phase Fluctuations Caused by Multipath Interference," JASA, pp. 604-607.

[6] J. G. Clark and M. Kronengold, "Long Period Fluctuations of CW Signals in Deep and Shallow Water," JASA, Vol. 56, 1974, Oct.-Dec.

[7] R. N. Baer and M. J. Jacobson, "Sound Transmission in a Channel with Bilinear Sound Speed and Environmental Variations, JASA, Vol. 54, No. 1, 1973, pp. 80-89.

[8] I. Dyer, "Statistics of Sound Propagation in the Ocean," JASA, Vol. 48, No. 1 (Part 2), 1970, pp. 337-345.

[9] S. L. Adams, "Dispersive Properties of the Underwater Acoustic Channel," presented at IEEE Signal Processing Group Conference, 1976.

[10] W. J. Jobst, "An Application of Poisson Process Models to Multipath Sound Propagation of Sinusoidal Signals," JASA, Vol. 57, No. 6, Part II, June 1975.

[11] R. E. Williams, H. F. Battestin, "Time Coherence of Acoustic Signals Transmitted Over Resolved Paths in Deep Ocean," JASA, Feb. 1976, Vol. 59, No. 2.

[12] R. J. Urick, "Measurements of the Vertical Coherence of the Sound From a Near-Surface Source in the Sea and the Effect on the Gain of an Additive Vertical Array," JASA, Vol. 54, No. 1, 1973.

[13] W. J. Jobst, private communication at Institute for Acoustical Research, Miami, Fla.

[14] M. J. Hinich, "Maximum-Likelihood Signal Processing for a Vertical Array," JASA, Vol. 54, No. 2, 1973, pp. 499-503.

[15] H. P. Bucker, "Use of Calculated Sound Fields and Matched Field Detection to Locate Sound Sources in Shallow Water," JASA, Vol. 59, No. 2, February, 1976.

[16] S. M. Flatte, F. D. Tappert, "Calculation of the Effect of Internal Waves on Oceanic Sound Transmission," JASA, Vol. 58, No. 6, December, 1975, pp. 1151-1159.

[17] J. B. Thomas, An Introduction to Statistical Communication Theory, pp. 165-167, 1969, John Wiley & Sons, Inc.

[18] G. N. Cederquist, "The Use of Computer-Generated Pictures to Extract Information from Underwater Acoustic Transfer Function Data." Appendix E. Technical Report No. 227, Cooley Electronics Laboratory, The University of Michigan, Ann Arbor, Michigan, April 1975.

[19] A. M. Mood, Introduction to the Theory of Statistics, McGraw-Hill Book Company, 1950.

[20] H. L. Van Trees, Detection, Estimation, and Modulation Theory, Part I, John Wiley & Sons, Inc., 1968.

[21] F. C. Schweppe, "Sensor-Array Data Processing for Multiple Signal Sources," IEEE Transaction on Information Theory, March, 1968, pp. 294-305.

[22] N. R. Goodman, "Statistical Analysis Based on a Certain Multivariate Complex Gaussian Distribution (An Introduction)," Annals of Math. Statistics, Vol. 34, pp. 152-157.

[23] M. S. Bartlett, "An Inverse Matrix Adjustment Arising in Discriminant Analysis," Annals of Math. Statistics, Vol. 22, pp. 107-111, 1951.

[24] Subroutine package EISPACK, which is developed by Argonne National Lab, can be used to calculate the eigenvalues of any complex matrix. Information about EISPACK can be found in the book "Lecture Notes in Computer Science, Volumn 6, Matrix Eigensystem Routines-EISPACK Guide," by Smith, Boyle, Garbow, Ikebe, Klema, Moler; Springer-Verlag, 1976.

[25] T. G. Birdsall, "The Theory of Signal Detectability: ROC Curves and Their Character." Technical Report No. 177, Cooley Electronic Laboratory, The University of Michigan, Ann Arbor, Mich. 1973.

[26] I. Dyer, "Statistics of Distant Shipping Noise," JASA, Vol. 53, No. 2, pp. 564-570, 1973.

[27] C. S. Liu, "Adaptive Optimum Array Tracking Detectors." Technical Report 11, Adaptive Signal Detection Laboratory, Duke University, Durham, N. C., August 1975.

[28] C. S. Liu, "Adaptive Optimal Array Detectors for the Two Path Channel." Master degree thesis, Department of Electrical Engineering, Duke University, Durham, N. C., 1972.

APPENDIX A

COMPUTER PROGRAMS

The computer programs for evaluating eigenvalues of matrices $\underline{G}_0$ and $\underline{G}_1$, and for calculating P_D and P_F are shown in this appendix. The subroutine calling sequences are shown in the block diagrams. There are two types of methods for evaluating the eigenvalues of a complex matrix. One is the analytical method which is limited by the dimensionality of the matrix. It is not trivial to find the performance of array detectors with more than three elements by the analytical method. Another method is a numerical one which can be used for arrays with any number of elements.

(1) Analytical Method

A typical calling sequence for the analytical method is shown below.

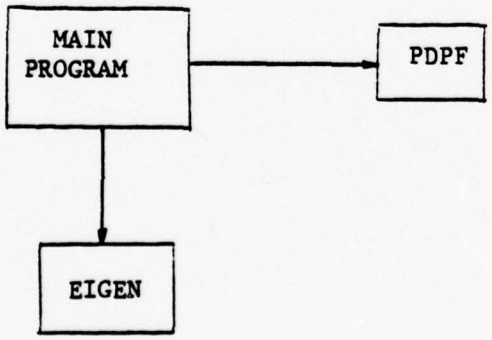

Subroutine "EIGEN" calculates the eigenvalues of matrices $\underline{G}_0$ and $\underline{G}_1$, and subroutine "PDPF" calculates the probability of detection (P_D) and the probability of false alarm (P_F). The analytical algorithms used in

subroutine "EIGEN" depend upon the number of array elements, the number of signal paths, and the sufficient statistic. The mathematical descriptions of these algorithms are described in the main text. In the following computer program listings, a complete program for optimal array detectors for K = 2 and M = 2, several "EIGEN" subroutines, and a complete program for optimal array detectors for M = 10 and K = 2 are included.

```
C THIS IS THE MAIN PGM FOR CALCULATING PDPF BY ANALITICAL METHOD.
    C THIS PGM WILL CALL SUBROUTINE EIGEN WHICH WILL CALCUATE EIGENVALUES
C OF G0,G1. THE MAIN ALSO CALL SUBROUTINE PDPF TO GET PD AND PF
C WE ASSSUME D=.5 WAVELENGTH
      DIMENSION ELTA(10),PD(10),PF(10)
      WRITE (6,101)
      READ(5,100) APHI,APHIP
      PHI=APHI*3.1416/180.
      PHIP=APHIP*3.1416/180.
      WRITE(6,102)
      READ(5,100) VARS1,VARS2,VARN
      WRITE(6,103)
      READ(5,100) (ELTA(I),I=1,10)
  100 FORMAT(F14.0)
  101 FORMAT(1X,24HTYPE IN APHI,APHIP,F14.0)
  103 FORMAT(1X,26HTYPE IN 10 THRESHOLD VALUE)
  102 FORMAT(1X,30HTYPE IN VARS1,VARS2,VARN,F14.0)
      CALL EIGEN(PHI,PHIP,VARS1,VARS2,VARN,G11,G12,G01,G02)
      CALL PDPF(ELTA,G11,G12,G01,G02,PD,PF)
      WRITE(6,200) G11,G12,G01,G02
      WRITE(6,300) (PD(J),PF(J),J=1,10)
  300 FORMAT(2X,2F12.6)
  200 FORMAT(2X,2F10.4)
      STOP
      END
      SUBROUTINE PDPF(ELTA,G11,G12,G01,G02,PD,PF)
      DIMENSION ELTA(10),PD(10),PF(10)
      DO 10 K=1,10
      PD(K)=G11*EXP(-ELTA(K)/G11)/(G11-G12)+G12*EXP(-ELTA(K)/
     1 G12)/(G12-G11)
      PF(K)=G01*EXP(-ELTA(K)/G01)/(G01-G02)+G02*EXP(-ELTA(K)/
     1 G02)/(G02-G01)
   10 CONTINUE
      RETURN
      END
      SUBROUTINE EIGEN(PHI,PHIP,VARS1,VARS2,VARN,G11,G12,G01,G02)
C THIS IS FOR K=2,M=2     OPTIMAL CASE (ANALITICAL METHOD).
C WE ASSSUME D=.5 WAVELENGTH
      CC1=3.1416*COS(PHI)
      CC2=3.1416*COS(PHIP)
      COMPLEX A1,A2,C1,C2
      C1=CMPLX(0.,CC1)
      C2=CMPLX(0.,CC2)
      A1=CEXP(C1)
      A2=CEXP(C2)
      R=CABS(VARS1*A1+VARS2*A2)
      G11=(VARS1+VARS2+R)/VARN
      G12=(VARS1+VARS2-R)/VARN
      G01=(VARS1+VARS2+R)/(VARS1+VARS2+VARN+R)
      G02=(VARS1+VARS2-R)/(VARS1+VARS2+VARN-R)
      RETURN
      END
```

THIS PAGE IS BEST QUALITY PRACTICABLE
FROM COPY FURNISHED TO DDC

```
C THIS IS SUBROUTINE EIGEN FOR DOUBLE BEAMFORMER
C USE THIS WITH MAIN PGM AND SUBROUTINE PDPF
      SUBROUTINE EIGEN(PHI,PHIP,VARS1,VARS2,VARN,G11,G12,G01,G02)
C THIS IS FOR SUBOPTIMAL BEAMFORMER PERFORMANCE K=2,M=2
      COMPLEX C1,C2
      C1=CMPLX(0.,3.1416*COS(PHI))
      C2=CMPLX(0.,3.1416*COS(PHIP))
      DA1=VARS1+VARS2+CABS(VARS1*CEXP(C1)+VARS2*CEXP(C2))
      DA2=2.*(VARS1+VARS2)-DA1
      G01=VARN*DA1
      G02=VARN*DA2
      G11=VARN*DA1+DA1*DA1
      G12=VARN*DA2+DA2*DA2
      RETURN
      END



      SUBROUTINE EIGEN(PHI,PHIP,VARS1,VARS2,VARN,G11,G12,G01,G02)
C THIS IS THE SUBROUTINE EIGEN FOR CALCULATING EIGENVALUES FOR M=2,K=3
C THIS IS FOR K=3,M=2     OPTIMAL CASE (ANALITICAL METHOD).
C USE THIS WITH MAIN PGM AND SUBROUTINE PDPF
      COMPLEX CC1,CC2
      CC2=CMPLX(0.,6.2832*(COS(PHI)-COS(PHIP)))
      CC1=CMPLX(0.,3.1416*(COS(PHI)-COS(PHIP)))
      A=9.*(VARS1**2+VARS2**2)-6.*VARS1*VARS2+4.*VARS1*VARS2*(2.
     1  *REAL(CEXP(CC2))+4.*REAL(CEXP(CC1)))
      Q11=VARN+3.*(VARS1+VARS2)/2.+SQRT(A)/2.
      Q12=VARN+3.*(VARS1+VARS2)/2.-SQRT(A)/2.
      G11=Q11/VARN-1.
      G12=Q12/VARN-1.
      G01=1.-VARN/Q11
      G02=1.-VARN/Q12
      RETURN
      END


C THIS PRG IS FOR M=10 AMD K=2 OPTIMAL CASE
C THIS IS THE PGM TO CALCULATE PD AND PF
      DIMENSION ELTA(10),PD(10),PF(10),PHI(10)
      M=10
      DO 5 KK=1,5
      PHI(KK)=(90.-FLOAT(KK)*3.)*3.1416/180.
      KK1=10-KK+1
      PHI(KK1)=(90.+FLOAT(KK)*3.)*3.1416/180.
5     CONTINUE
      WRITE(6,102)
      READ(5,100)VARN
102   FORMAT(1X,12HTYPE IN VARN)
      WRITE(6,103)
      READ(5,100) (ELTA(I),I=1,10)
100   FORMAT(F14.0)
      VARS=1./FLOAT(M)
103   FORMAT(1X,26HTYPE IN 10 THRESHOLD VALUE)
      CALL EIGEN(M,PHI,VARS,VARN,G11,G12,G01,G02)
      CALL PDPF(ELTA,G11,G12,G01,G02,PD,PF)
      WRITE(6,200) G11,G12,G01,G02
```

THIS PAGE IS BEST QUALITY PRACTICABLE
FROM COPY FURNISHED TO DDC

```
      WRITE(6,300) (PD(J),PF(J),J=1,10)
300   FORMAT(2X,2F12.6)
200   FORMAT(2X,2F10.4)
      STOP
      END
       SUBROUTINE PDPF(ELTA,G11,G12,G01,G02,PD,PF)
        DIMENSION ELTA(10),PD(10),PF(10)
        DO 10 K=1,10
      PD(K)=G11*EXP(-ELTA(K)/G11)/(G11-G12)+G12*EXP(-ELTA(K)/
     1  G12)/(G12-G11)
      PF(K)=G01*EXP(-ELTA(K)/G01)/(G01-G02)+G02*EXP(-ELTA(K)/
     1  G02)/(G02-G01)
10      CONTINUE
         RETURN
          END
      SUBROUTINE EIGEN(M,PHI,VARS,VARN,G11,G12,G01,G02)
      DIMENSION PHI(10),C(10),A(10)
      COMPLEX C,A,B
      B=CMPLX(0.,0.)
      DO 10 I=1,M
       C(I)=CMPLX(0., 3.1416*COS(PHI(I)))
       A(I)=CEXP(C(I))
       B=B+A(I)*VARS
10      CONTINUE
        R=CABS(B)
        AM=FLOAT(M)
        G11=(AM*VARS+R)/VARN
      G12=(AM*VARS-R)/VARN
       G01=(AM*VARS+R)/(VARN+AM*VARS+R)
          G02=(AM*VARS-R)/(VARN+AM*VARS-R)
         RETURN
           END
```

THIS PAGE IS BEST QUALITY PRACTICABLE
FROM COPY FURNISHED TO DDC

(2) Numerical Method

A subroutine package called "EISPACK" [24] is employed in the numerical method. The calling sequence is described in the block diagrams below for both the optimal case and the double-beamformer case.

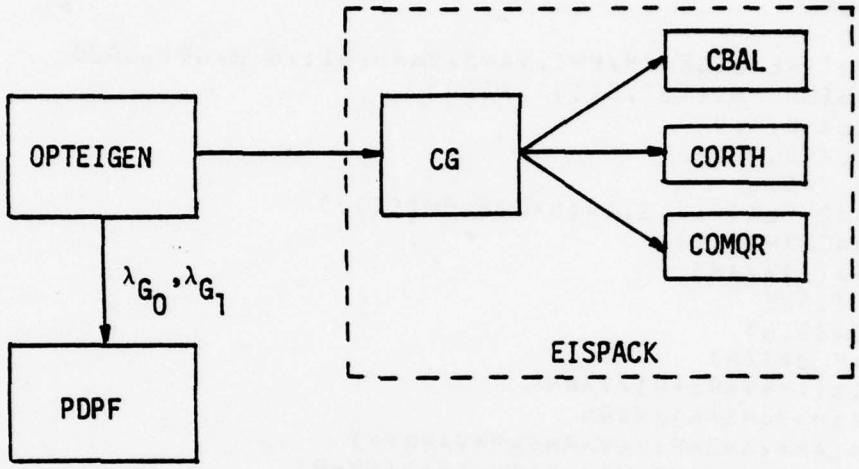

Figure A. 1 Block Diagram for Optimal Case.

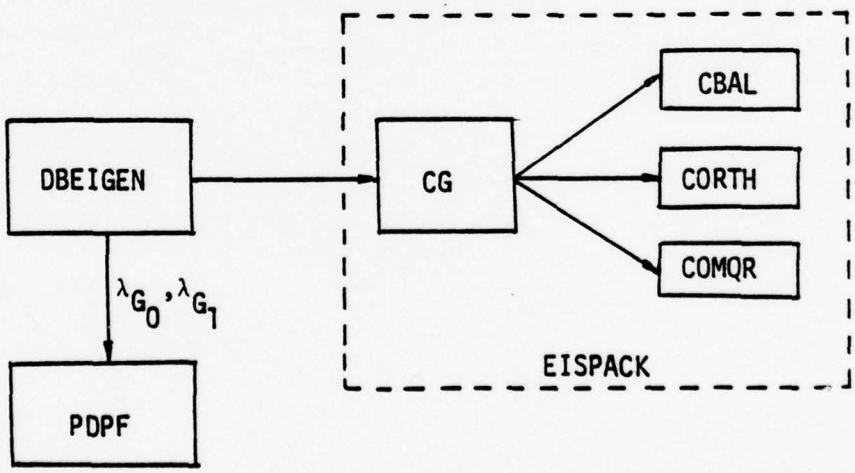

Figure A. 2 Block Daigram for Double Beamformer Case

The following program listing includes the main programs, "OPTEIGEN", "DBEIGEN", and "PDPF". Subroutines in the software package "EISPACK" are excluded in this appendix because of their length. Program listings and documentations are available on request.

```
C THIS IS PGM 'DBEIGEN.
C TO RUN THIS PGM: $RUN -LOAD+NAAS:EISPACK    ON MTS.
C TO RUN THIS PGM: $RUN -LOAD+NAAS:EISPACK ON MTS
C TO RUN THIS PGM IN OTHER UNIV. SUBROUTINE PACKAGE 'EISPACK' IS NEEDED.
C THIS IS THE NUMERICAL METHOD TO GET EIGEN VALUES OF MATRICES DB,G0,G1
      DIMENSION VARS(10),PHI(10),A(10),C(10),G0(10),G1(10)
      REAL*8 AR(10,10),AI(10,10),WR(10),WI(10),ZR(10,10),ZI(10,10),
     1 SV1(10),SV2(10),SV3(10)
      COMPLEX A,C
C START TO GENERAT MATRIX DB FOR DOUBLE BEAMFORMER$$$$$$$$$$$$$$$$$$$$
      WRITE(6,104)
 104   FORMAT(3X,'TYPE IN NO. OF ELEMENTS, I3')
      READ(5,105) K
 105     FORMAT(I3)
       WRITE(6,223)
 223   FORMAT(3X,'TYPE IN NO. OF PATHS,M,I3')
       READ(5,105)M
      WRITE(6,101)
 101    FORMAT(1X,'TYPE IN PHI(1),...PHI(M),F14.0')
      READ(5,100) (PHI(KKM),KKM=1,M)
      WRITE(6,102)
     READ(5,100) (VARS(KKM),KKM=1,M),VARN
 102   FORMAT(1X,'TYPE IN VARS(1),...VARS(M),VARN,F14.0')
 100    FORMAT(F14.0)
        DO 222 KM=1,M
      PHI(KM)=PHI(KM)*3.1416/180.
     C(KM)=CMPLX(0.,3.1416*COS(PHI(KM)))
     A(KM)=CEXP(C(KM))
 222   CONTINUE
C M DENOTE THE NO. OF PATHS, K DENOTE THE NO. OF ELEMENTS
         DO 5 I1=1,K
         DO 6 I2=1,K
      AR(I1,I2)=0.
        AI(I1,I2) =0.
 6        CONTINUE
 5        CONTINUE
        DO 10 I=1,M
        DO 20 I1=1,K
        DO 21 J1=1,K
        AR(I1,J1)=REAL(A(I)**(J1-I1))*VARS(I)+AR(I1,J1)
        AI(I1,J1)=AIMAG(A(I)**(J1-I1))*VARS(I)+AI(I1,J1)
 21      CONTINUE
 20       CONTINUE
 10       CONTINUE
         DO 19 I=1,K
 19       WRITE(6,117) (AR(I,J),J=1,K)
       DO 29 I=1,K
  29       WRITE(6,117) (AI(I,J),J=1,K)
 117      FORMAT(3X,/3020.5)
C  END OF GENERATING MATRIX DB ****************************************
C  REAL(DB) IS AR;  AIMAG(DB) IS AI
      CALL CG(10,K,AR,AI,WR,WI,0,ZR,ZI,SV1,SV2,SV3,IER)
       IF (IER .NE. 0) WRITE (6,179)
 179    FORMAT(3X,'ERROR IN SUB CG')
      WRITE(6,988)
 988   FORMAT(3X,'EIGENVALUES OF DOUBLE BEAMFORMER')
      WRITE(6,113) (WR(I),WI(I),I=1,K)
 113     FORMAT(5X,2020.8)
       DO 90 L=1,K
       G0(L)=VARN*WR(L)
```

THIS PAGE IS BEST QUALITY PRACTICABLE
FROM COPY FURNISHED TO DDC

THIS PAGE IS BEST QUALITY PRACTICABLE
FROM COPY FURNISHED TO DDC

```
      G1(L)=VARN*WR(L)+WR(L)*WR(L)
 90    CONTINUE
       WRITE(6,115) (G1(L1),L1=1,K)
115    FORMAT(5X,'EIGENVALUES OF G1',3E20.8)
       WRITE(6,114) (G0(L1),L1=1,K)
114    FORMAT(5X,'EIGENVALUES OF G0',3E20.8)
       GO TO 99
999     WRITE(6,991)
991    FORMAT(3X,'METHOD FAIL')
99     STOP
      END




C THIS IS PGM 'OPTEIGEN'
C TO RUN THIS PGM: $RUN *LOAD*NAAS:EISPACK    ON MTS.
C TO RUN THIS PGM IN OTHER UNIV. SUBROUTINE PACKAGE 'EISPACK' IS NEEDED.
C THIS IS THE NUMERICAL WAY TO GET THE EIGENVALUES OF Q1 AND G0,G1
      DIMENSION VARS(10),PHI(10),A(10),C(10),G0(10),G1(10)
      REAL*8 AR(10,10),AI(10,10),WR(10),WI(10),ZR(10,10),ZI(10,10)
     1  ,SV1(10),SV2(10),SV3(10)
      COMPLEX A,C
C  START TO GENERATING MATRIX Q0-1Q1. ***********************************
      WRITE(6,104)
104    FORMAT(3X,'TYPE IN NO. OF ELEMENTS K,I3')
       READ(5,105) K
105    FORMAT(I3)
      WRITE(6,223)
223   FORMAT(3X,'TYPE IN NO. OF PATHS,I3')
      READ(5,105) M
      WRITE(6,101)
101    FORMAT(1X,'TYPE IN PHI(1),PHI(2),...,PHI(M),F14.0')
       READ(5,100) (PHI(KKM),KKM=1,M)
      WRITE(6,102)
       READ(5,100) (VARS(KKM),KKM=1,M),VARN
102    FORMAT(2X,'TYPE IN VARS(1),...,VARS(M),VARN,F14.0')
100    FORMAT(F14.0)
      DO 222 KM=1,M
      PHI(KM)=PHI(KM)*3.1416/180.
      C(KM)=CMPLX(0.,3.1416*COS(PHI(KM)))
      A(KM)=CEXP(C(KM))
222   CONTINUE
C M DENOTE THE NO. OF PATHS, K DENOTE THE NO. OF ELEMENTS
        DO 5 I1=1,K
        DO 6 I2=1,K
       IF (I1 .EQ. I2) AR(I1,I2)=VARN
        AI(I1,I2) =0.
*         CONTINUE
5         CONTINUE
       DO 10 I=1,M
       DO 20 I1=1,K
       DO 21 J1=1,K
       AR(I1,J1)=REAL(A(I)**(J1-I1))*VARS(I)+AR(I1,J1)
       AI(I1,J1)=AIMAG(A(I)**(J1-I1))*VARS(I)+AI(I1,J1)
21      CONTINUE
20       CONTINUE
10       CONTINUE
```

```
 117        FORMAT(/,3X,3D20.8)
C    END OF GENERATING G0-G1   $$$$$$$$$$$$$$$$$$$$$$$$$$$$$$$$$$$$$$$$$$$$
C  REAL(Q1) IS AR;  AIMAG(Q1) IS AI
          CALL CG(10,K,AR,AI,WR,WI,0,ZR,ZI,Sv1,Sv2,Sv3,IER)
 115        FORMAT(3X,2D20.8)
            WRITE(6,111) IER
 111       FORMAT(2X,'IER=',I6)
           WRITE(6,112)
 112        FORMAT(2X,'EIGENVALUES OF G1')
            WRITE(6,115) (WR(I),WI(I),I=1,K)
C CALCULATE EIGENVALUES OF G0 AND G1
            DO 90 L=1,K
            G0(L)=1.-VARN/WR(L)
              G1(L)=WR(L)/VARN-1.
 90        CONTINUE
           WRITE(6,115) (G1(L1),L1=1,K)
 114           FORMAT(5X,'EIGENVALUES OF G0',3E20.6)
 115            FORMAT(5X,'EIGENVALUES OF G1',3E20.6)
          WRITE(6,114) (G0(L1),L1=1,K)
            STOP
             END
C THIS IS PGM 'PDPF'. INPUT: EIGENVALUES OF G0,G1; OUTPUT:PD,PF
           DIMENSION ELTA(10),PD(10),PF(10)
          DO 99 III=1,20
           WRITE(6,103)
          READ(5,100) (ELTA(I),I=1,10)
          WRITE(6,104)
 103      FORMAT(2X,'TYPE IN 10 THRESHOLD VALUES')
          READ(5,100) G11,G12,G01,G02
 100       FORMAT(F14.0)
 104      FORMAT(2X,'TYPE IN G11,G12,G01,G02, F14.0')
          CALL PDPF(ELTA,G11,G12,G01,G02,PD,PF)
          WRITE(6,200) G11,G12,G01,G02
          WRITE(6,301)
 301      FORMAT(2X,'THIS IS PD & PF')
          WRITE(6,300) (PD(J),PF(J),J=1,10)
 200       FORMAT(2X,2F18.6)
 300      FORMAT(2X,2F10.5)
           WRITE(6,111)
 111       FORMAT(3X,'STOP? Y: TYPE NONZERO INTEGER; N: TYPE 0')
           READ(5,112) ISTOP
           IF(ISTOP .NE. 0) GO TO  199
 112        FORMAT(I3)
 99         CONTINUE
 199        STOP
              END
           SUBROUTINE PDPF(ELTA,G11,G12,G01,G02,PD,PF)
            DIMENSION ELTA(10),PD(10),PF(10)
            DO 10 K=1,10
          PD(K)=G11*EXP(-ELTA(K)/G11)/(G11-G12)+G12*EXP(-ELTA(K)/
       1  G12)/(G12-G11)
          PF(K)=G01*EXP(-ELTA(K)/G01)/(G01-G02)+G02*EXP(-ELTA(K)/
       1  G02)/(G02-G01)
 10       CONTINUE
            RETURN
             END
```

THIS PAGE IS BEST QUALITY PRACTICABLE
FROM COPY FURNISHED TO DDC

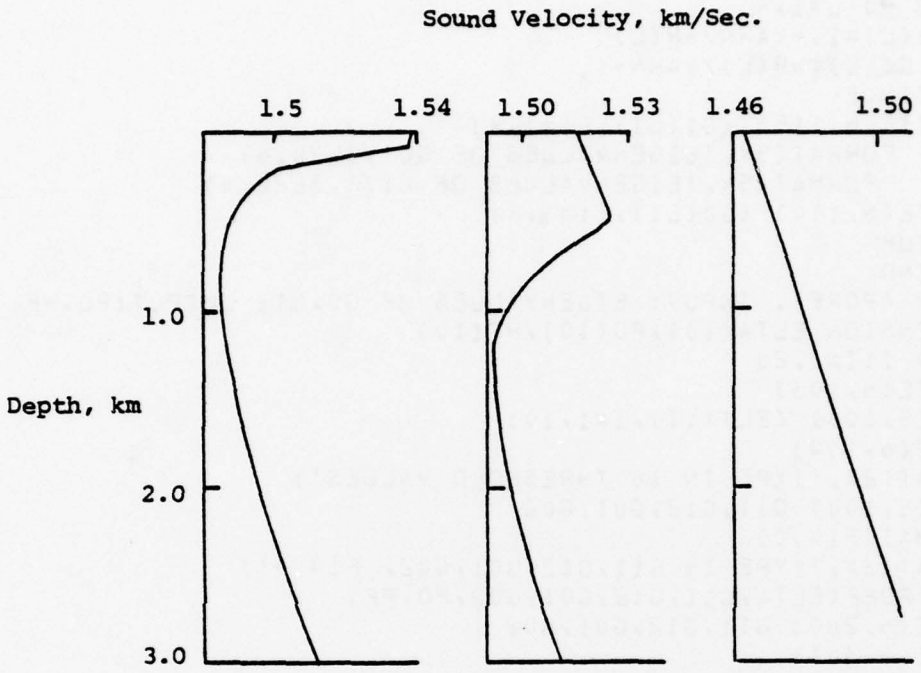

Figure 1.1 Underwater Sound Velocity as a Function of Depth.

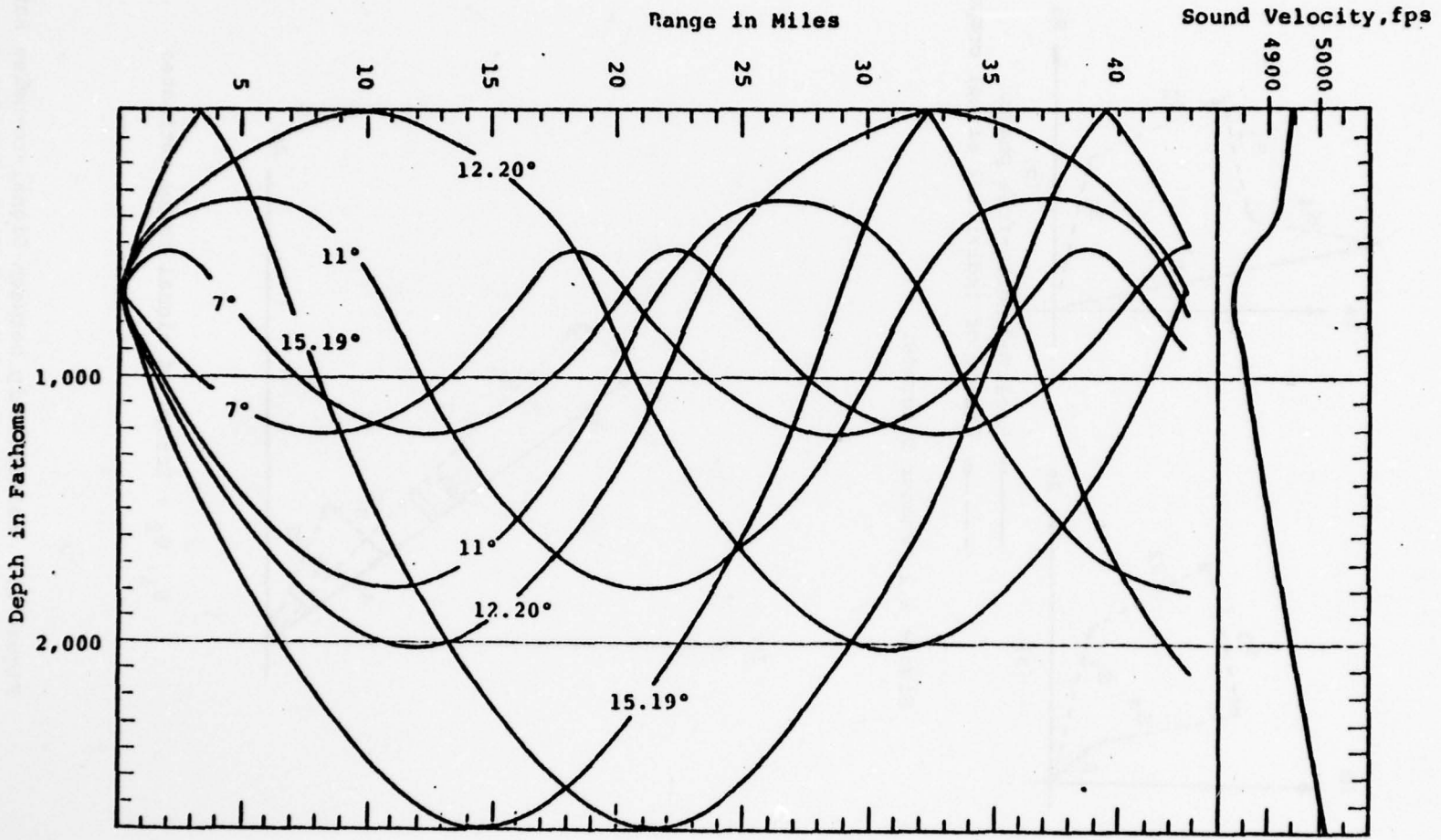

Fig.1.2 Ray diagram of transmission in the deep sound channel for a source on the axis

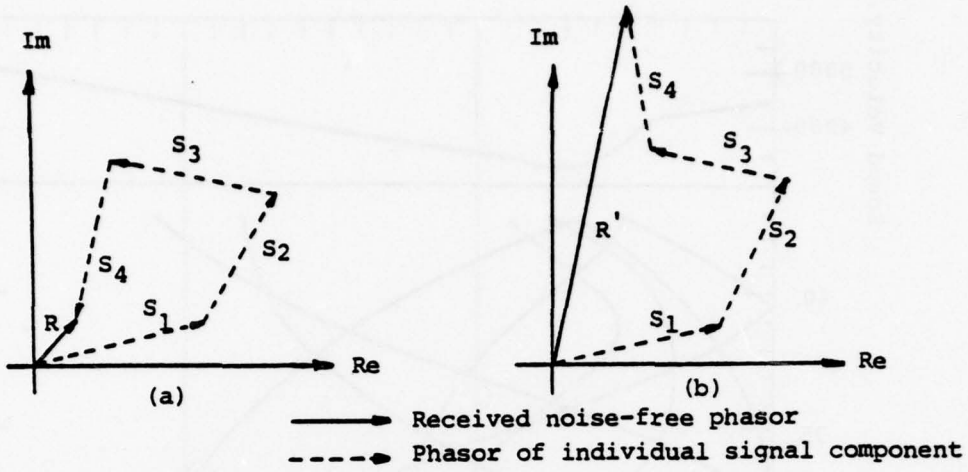

Figure 2.2 Phasor Diagrams.

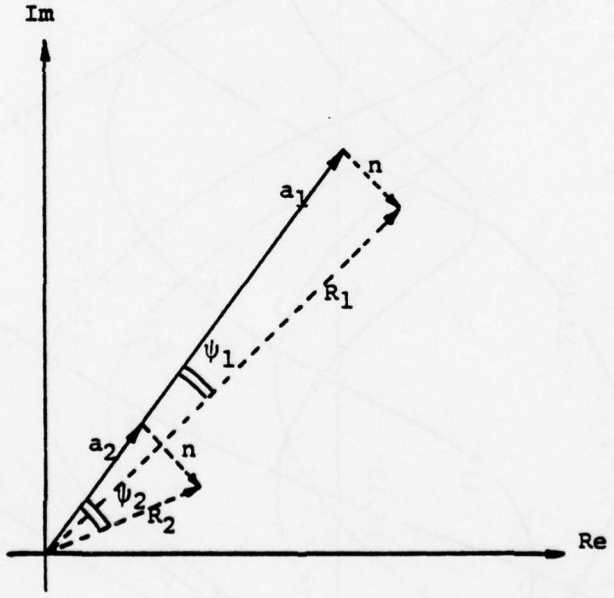

ψ_1, ψ_2 : Errors of signal phase estimates

Figure 2.3 Relationship between Signal-to-noise Ratio and Errors of Signal Phase Estimates.

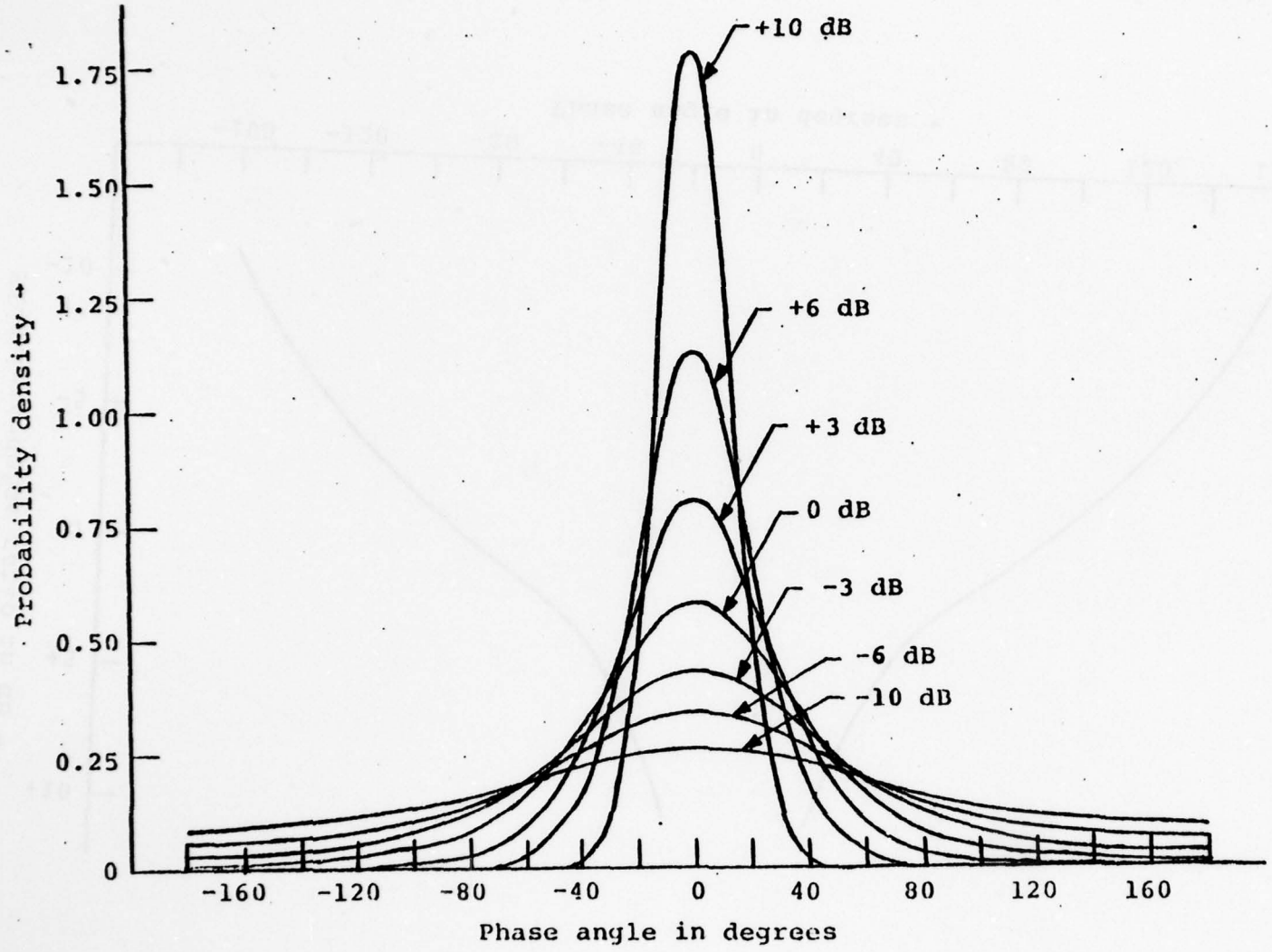

Figure 2.4. The probability density function of phase angle as a function of signal-to-noise ratio in dB

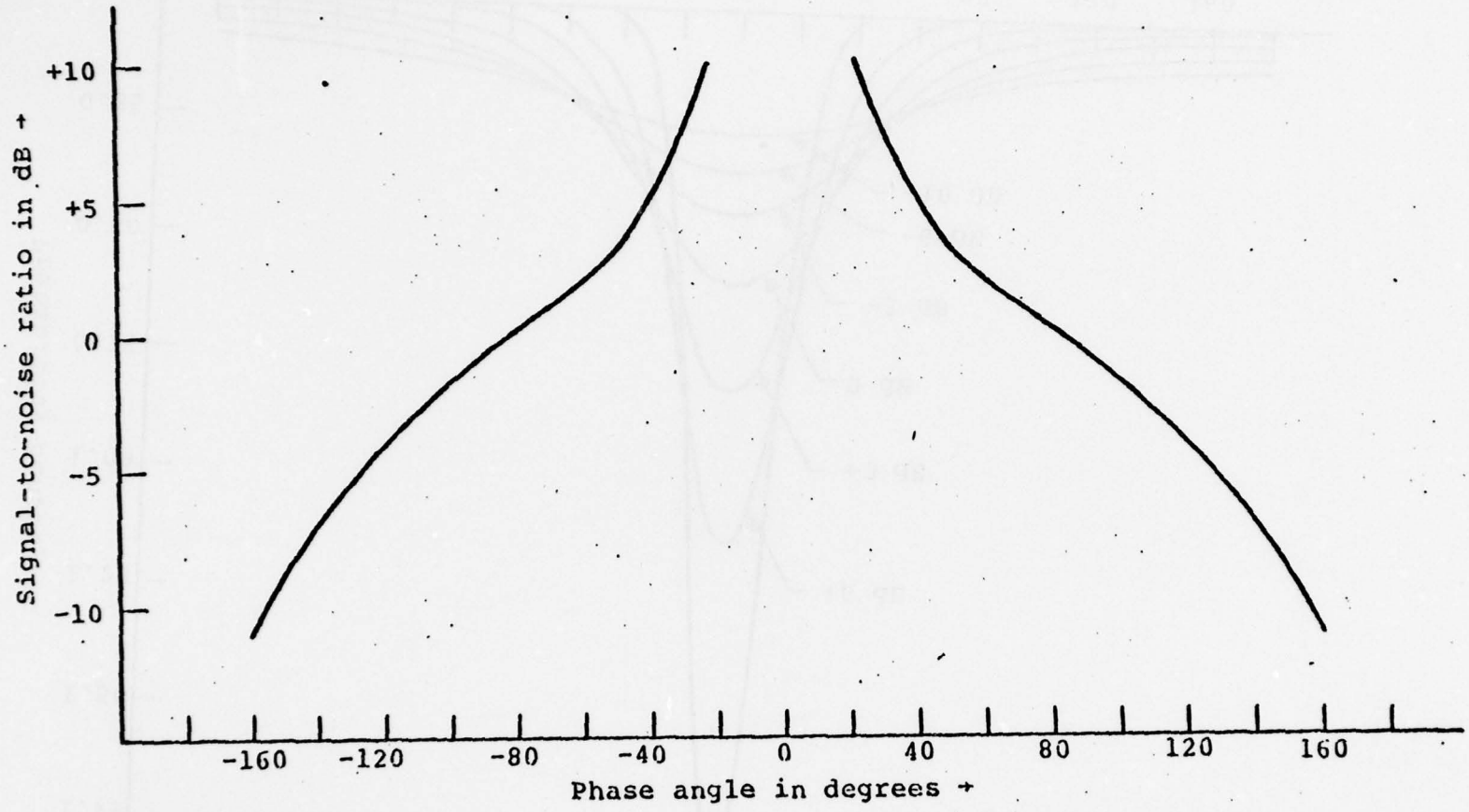

Figure 2.5 90% confidence limits on measured phase as a function of signal-to-noise ratio in dB

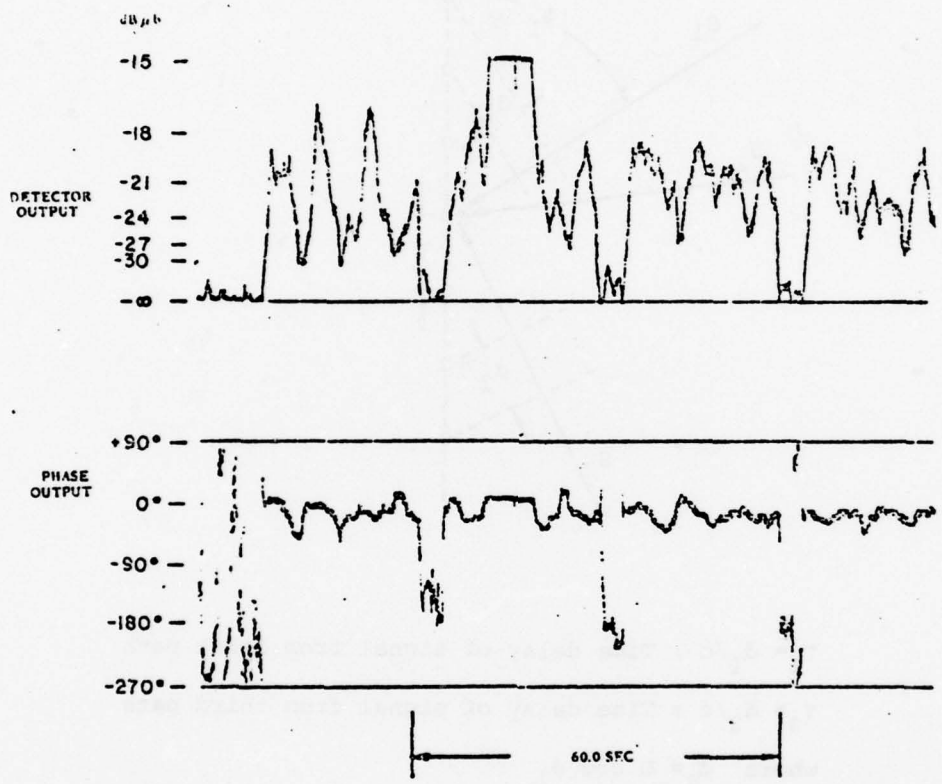

Figure 2.1 Computer-programmed Phase-coherent Demodulation of CW Transmission, 1550 h 3 Feb. 1965. (Figure 16 in Reference [4])

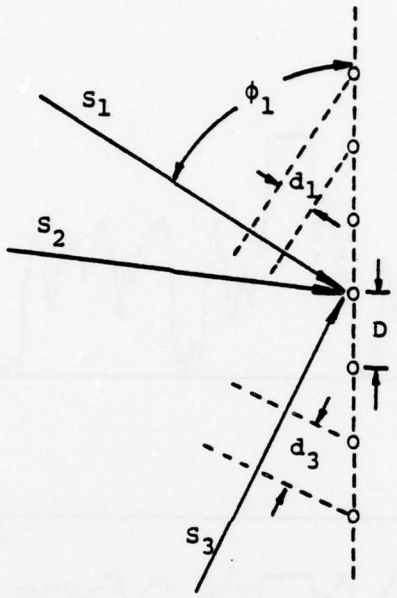

$\tau_1 = d_1/c$: Time delay of signal from first path

$\tau_3 = d_3/c$: Time delay of signal from third path

where $d_1 = D \cos \phi_1$

$d_3 = D \cos \phi_3$

c: sound velocity

Figure 3.1 Multipath Signals Geometry.

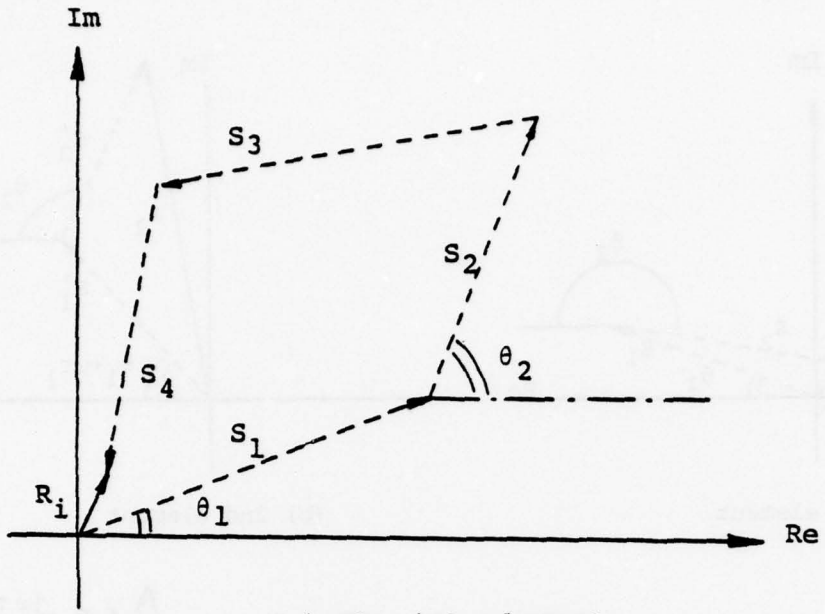

(a) The ith element.

$$S'_m = S_m e^{j\omega\tau_m}$$

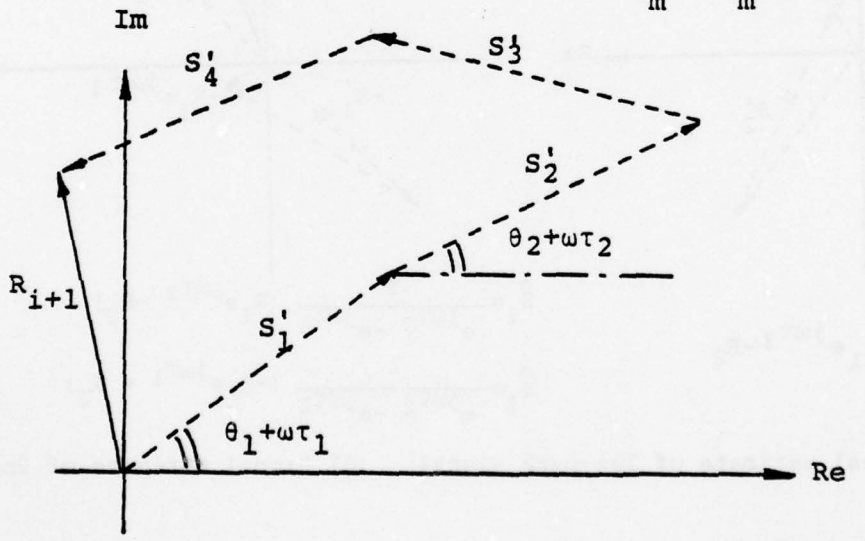

(b) The (i+1)th element.

Figure 3.2 Noise-free Phasors at the ith and (i+1)th Elements.

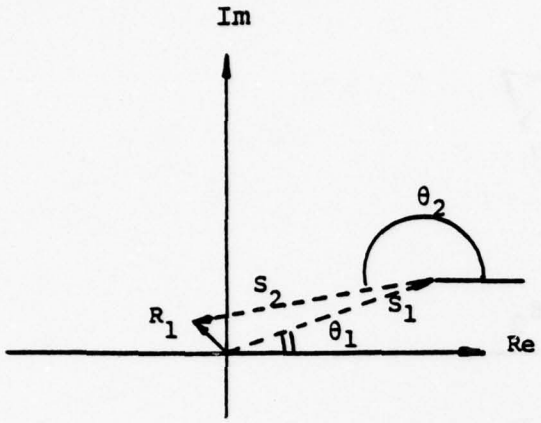

(a) 1st element

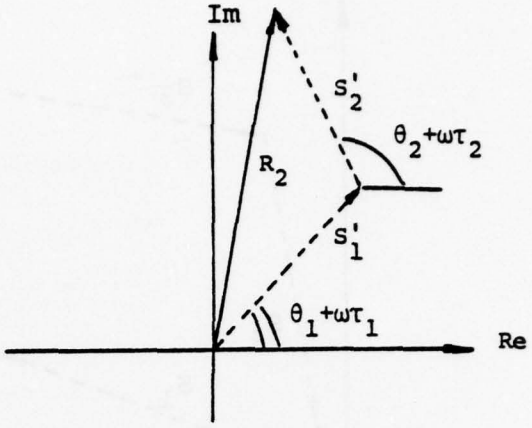

(b) 2nd element

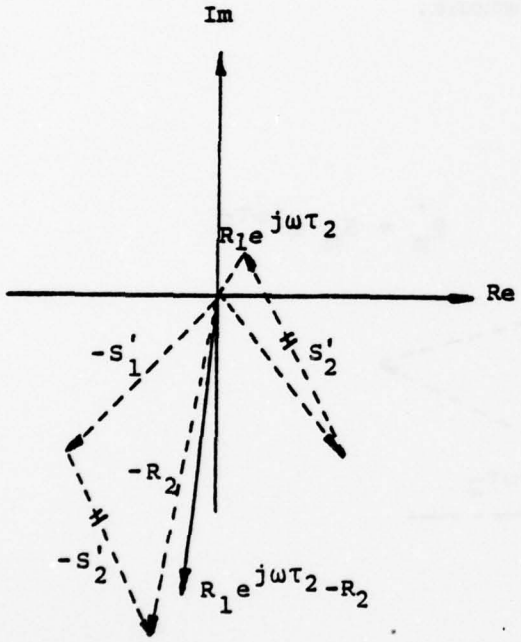

(c) Signal estimate of 1st path signal

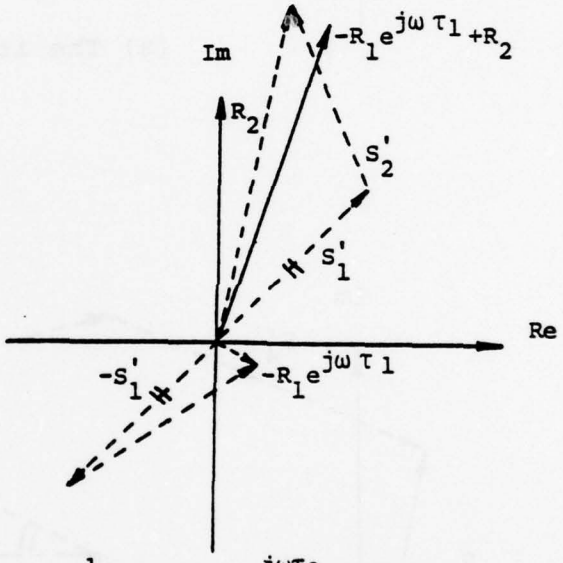

$$\hat{S}_1 = \frac{1}{e^{j\omega\tau_2} - e^{j\omega\tau_1}} (R_1 e^{j\omega\tau_2} - R_2)$$

$$\hat{S}_2 = \frac{1}{e^{j\omega\tau_2} - e^{j\omega\tau_1}} (-R_1 e^{j\omega\tau_1} + R_2)$$

(d) Signal estimate of 2nd path signal

Figure 3.3 (a) Noise-free Data Received at 1st Element.
(b) Noise-free Data Received at 2nd Element.
(c) (d) Phasor Diagrams of Signal Estimates of 1st and 2nd path Signals.

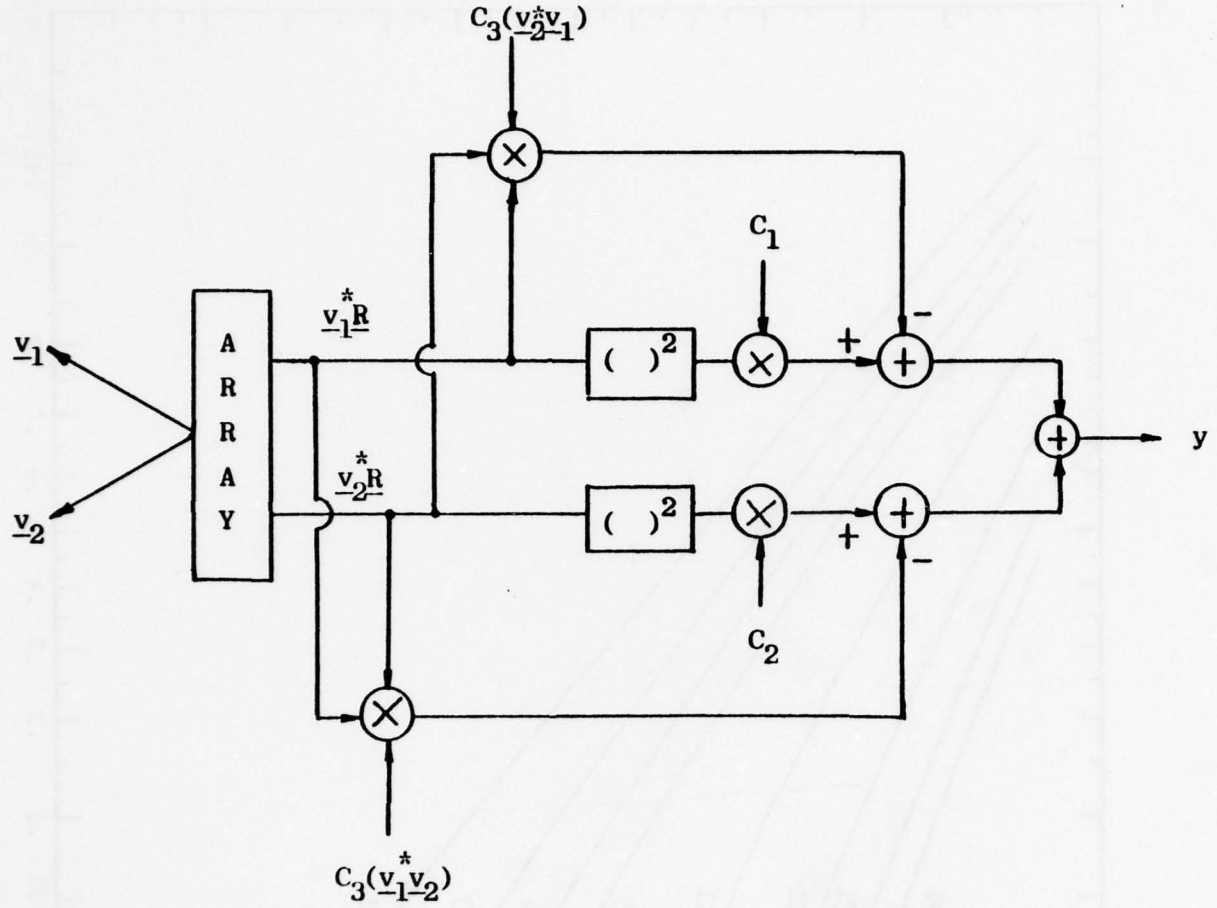

Figure 4.1. Structure of Optimal Array Detector.

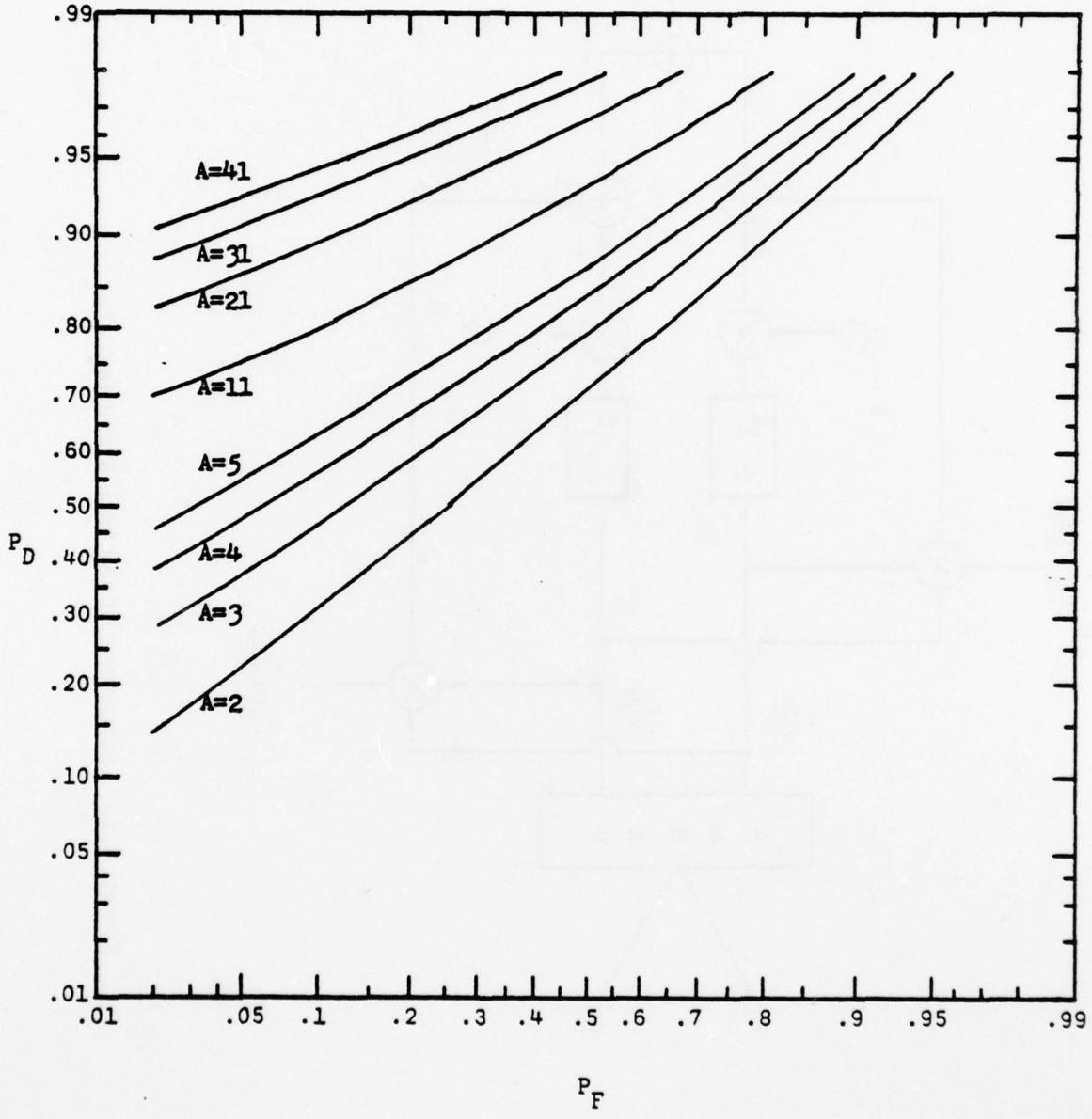

Figure 5.1 Power Type ROC Curves

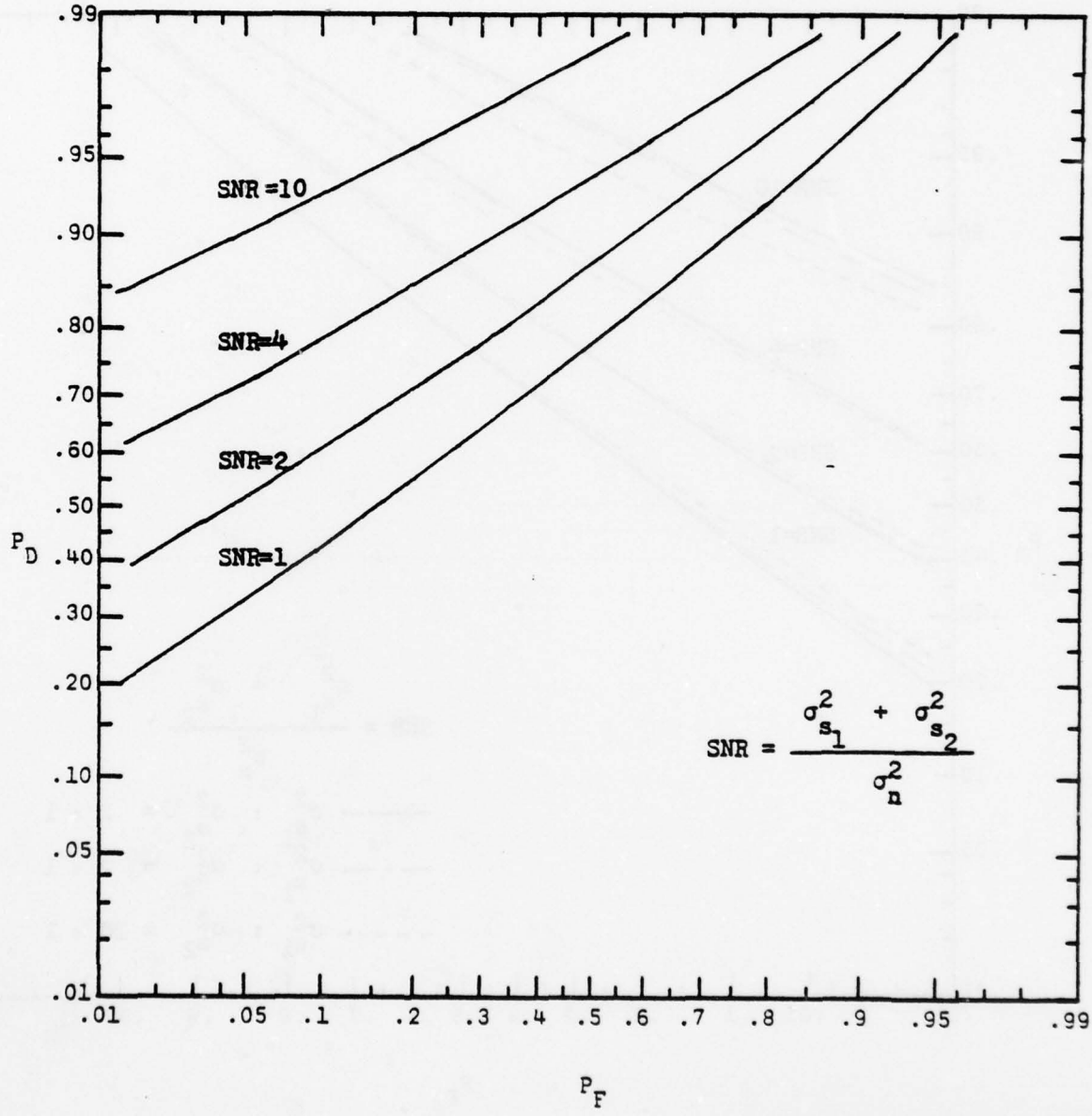

Figure 5.2 Optimal Performance of a 2-element Array for Detecting Two-path Signals from $\pm 15^\circ$ of Horizontal Axis.

AD-A064 969 DUKE UNIV DURHAM N C ADAPTIVE SIGNAL DETECTION LAB F/G 20/1
MULTIPATH SIGNAL PROCESSING USING A VERTICAL ARRAY.(U)
JUL 77 C S LIU N00014-75-C-0191
UNCLASSIFIED TR-13 NL

2 OF 2
AD
A064969

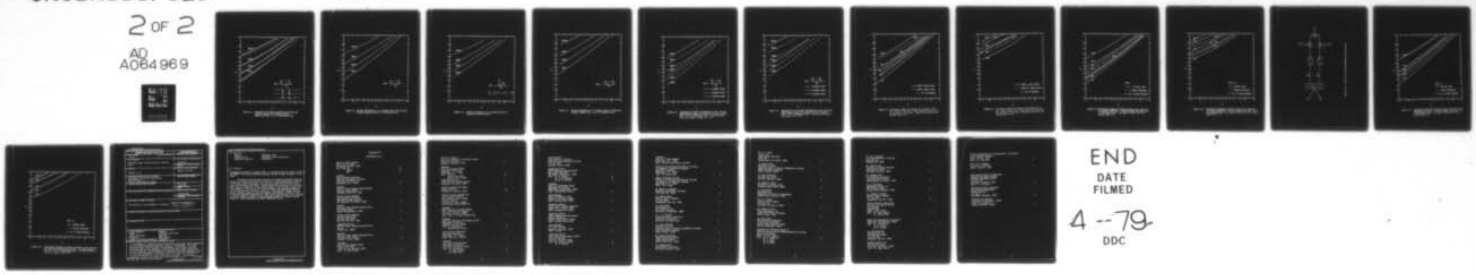

END
DATE
FILMED
4-79
DDC

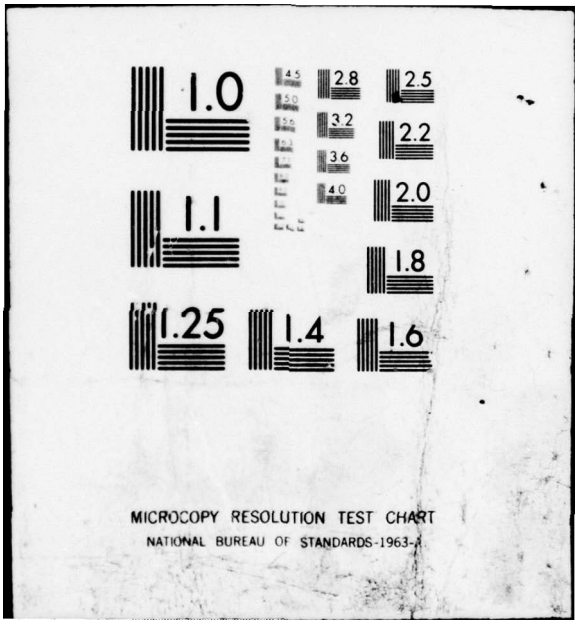
1.0
1.1
1.25
1.4
1.6
1.8
2.0
2.2
2.5
2.8
3.2
3.6
4.0
4.5
5.0
MICROCOPY RESOLUTION TEST CHART
NATIONAL BUREAU OF STANDARDS-1963-A

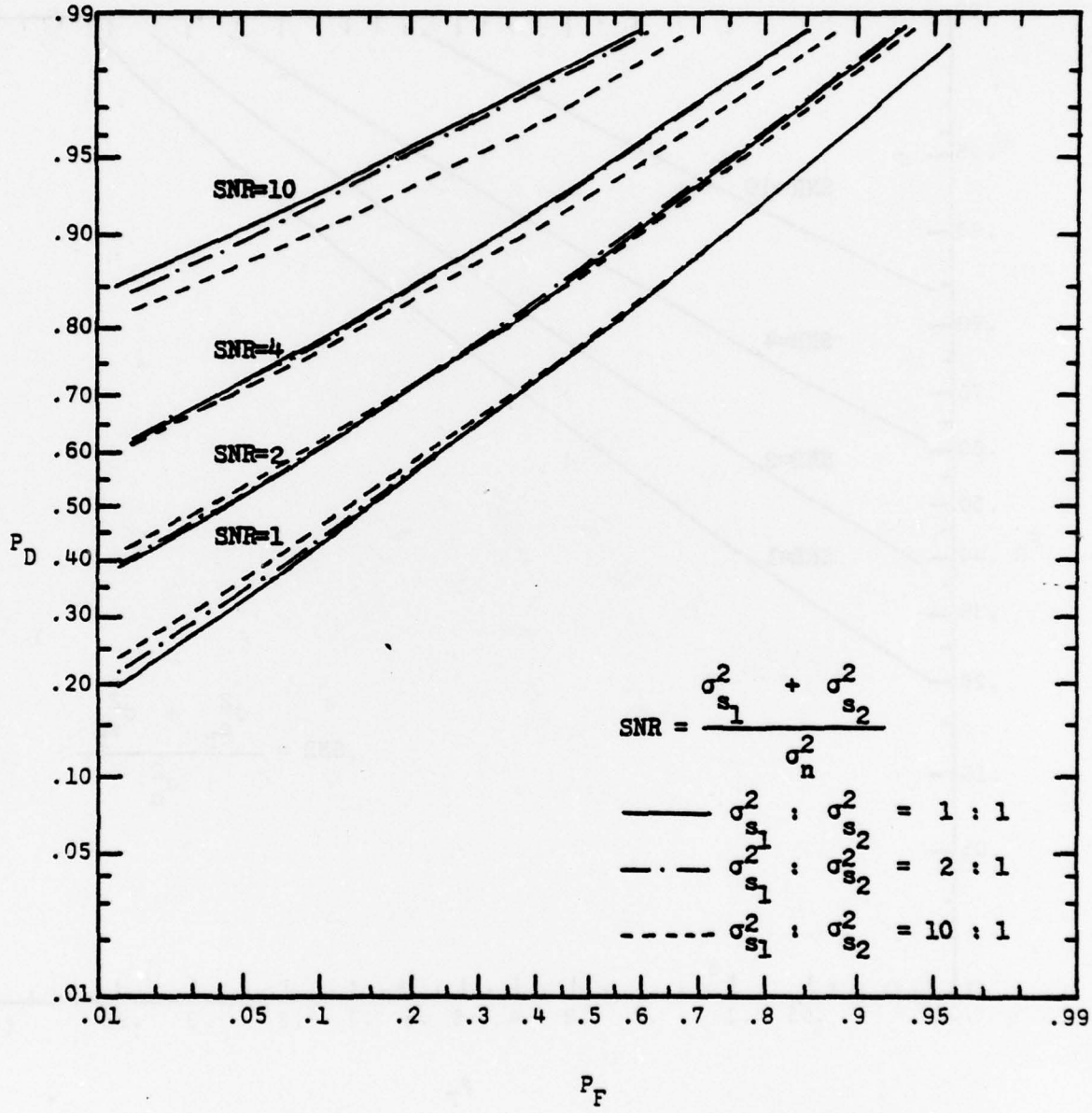

Figure 5.3 Comparison of Optimal performance for Detecting Two-path Signals with Unequal Strength. Signals are from $\pm$ 15° of Horizontal Axis.

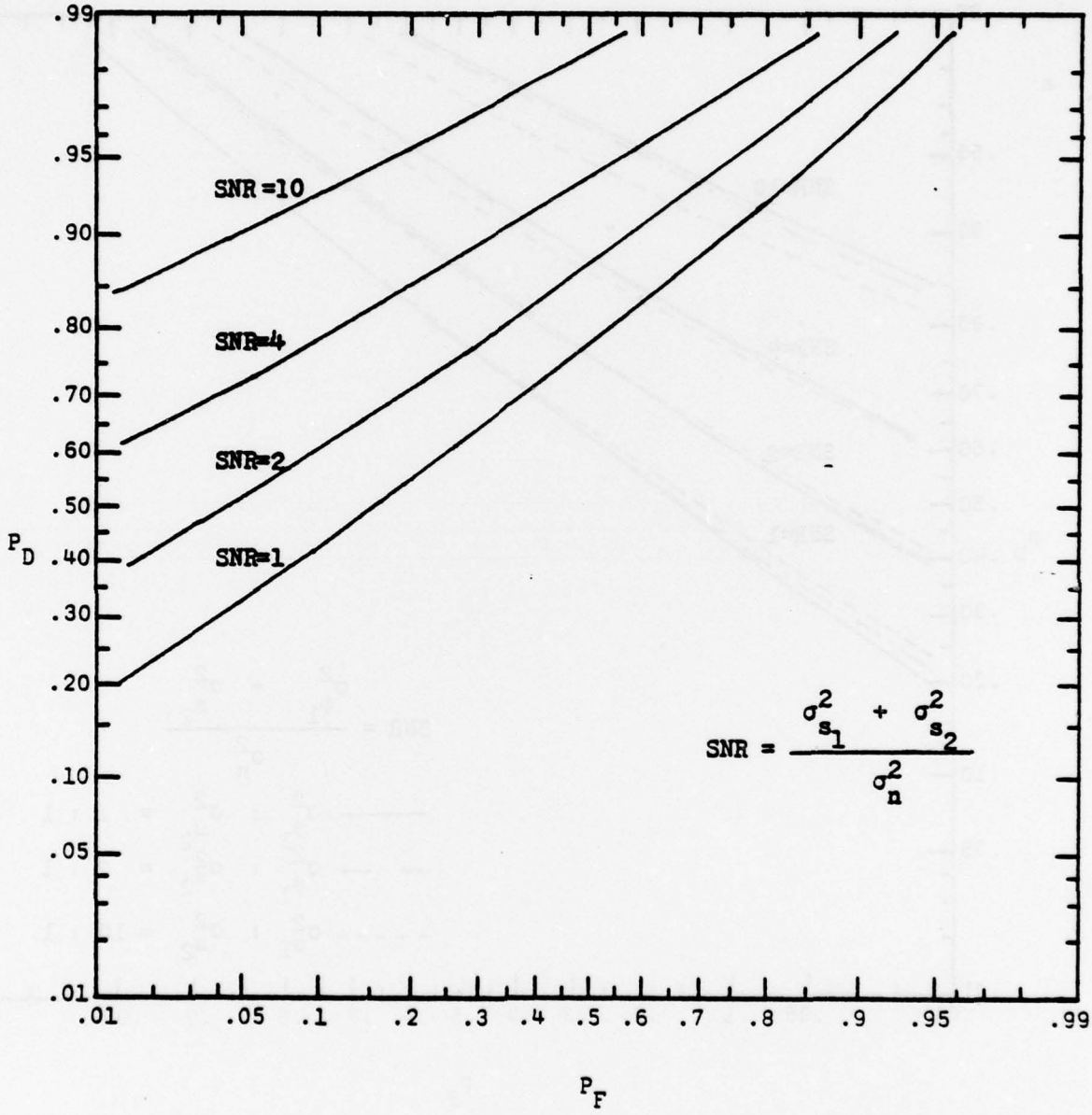

Figure 5.2 Optimal Performance of a 2-element Array for Detecting Two-path Signals from $\pm 15^\circ$ of Horizontal Axis.

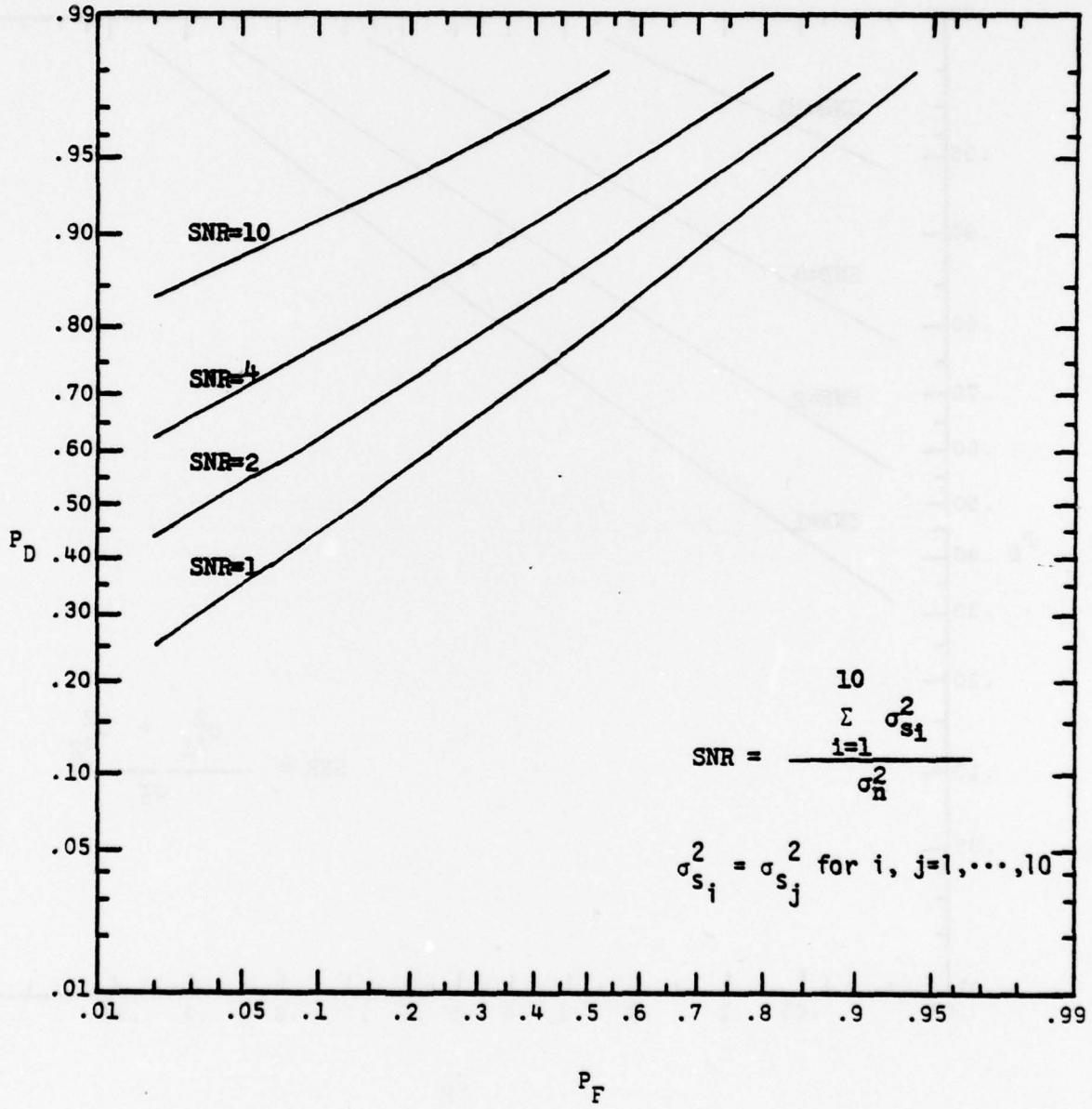

Figure 5.4 Oprimal Performance of a 2-element Array for Detecting 10-path Signals.

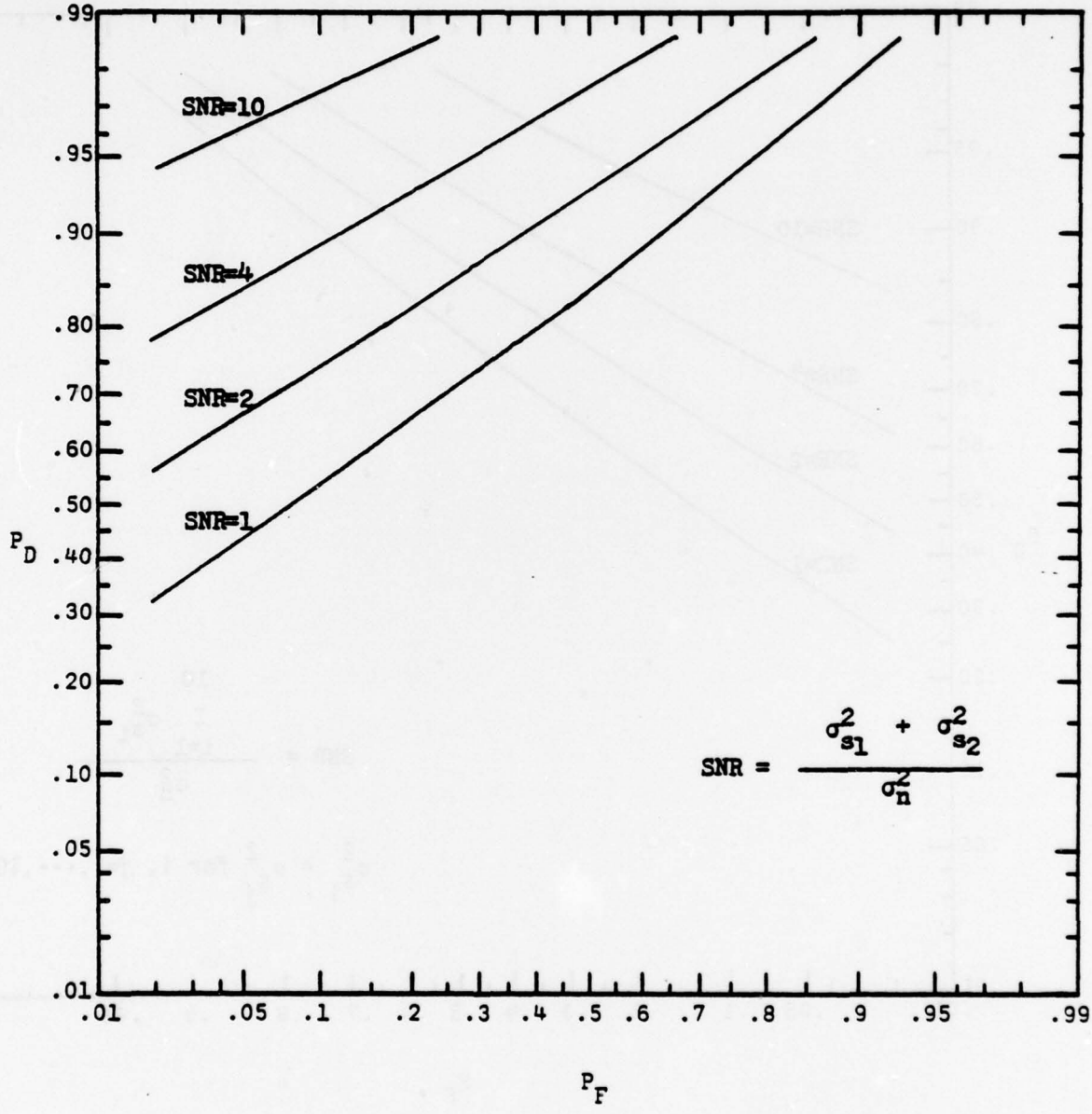

Figure 5.5 Optimal Performance of a 3-element Array for Detecting Two-path Signals from $\pm 15^\circ$ of Horizontal Axis.

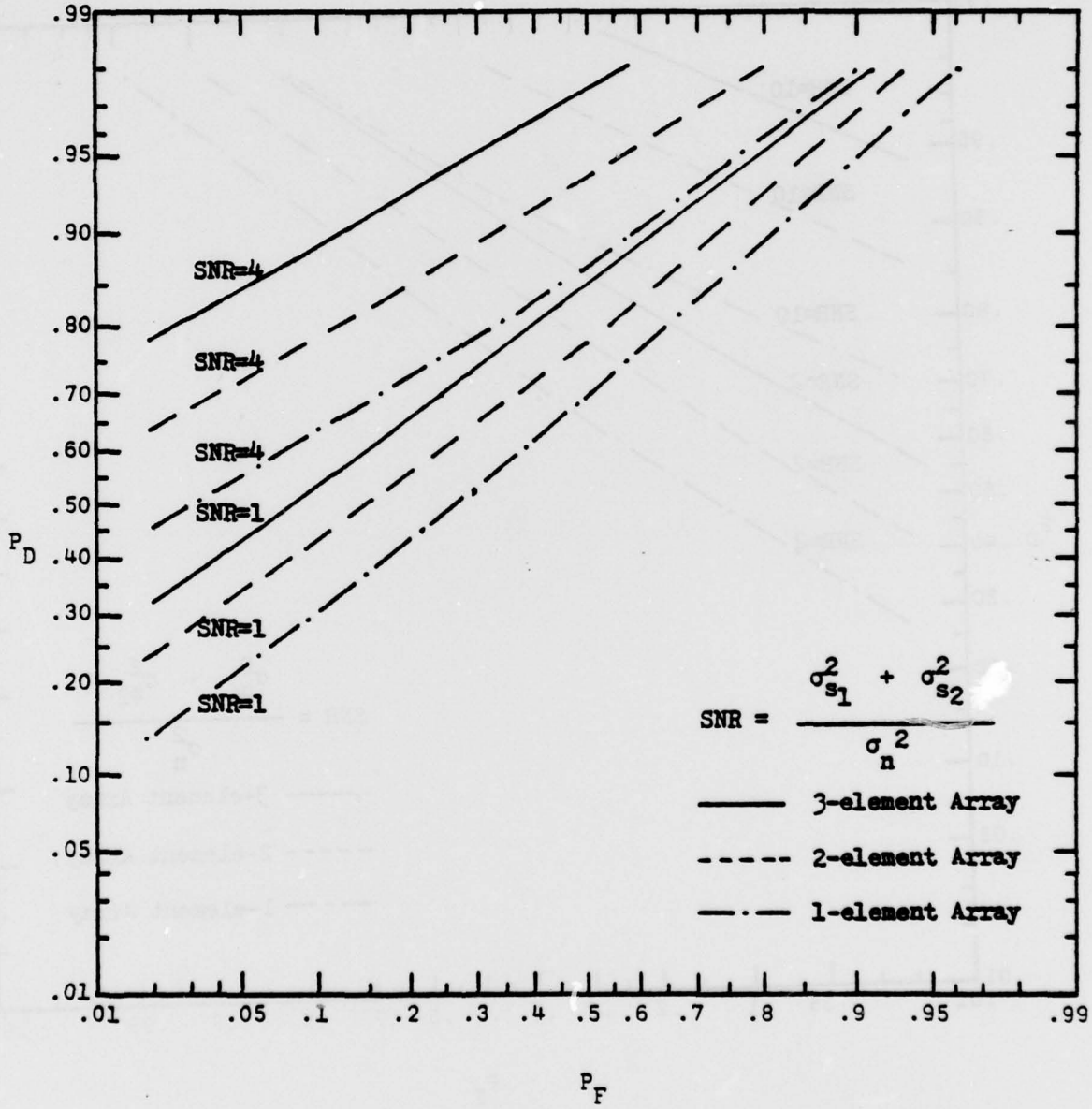

Figure 5.6 Comparison of Optimal Performances of One, Two and Three-Element Arrays for Detecting Two-path Signals from $\pm 15^\circ$ of Horizontal Axis. Signal-to-noise Ratio Per Element Is Equal to 1 or 4.

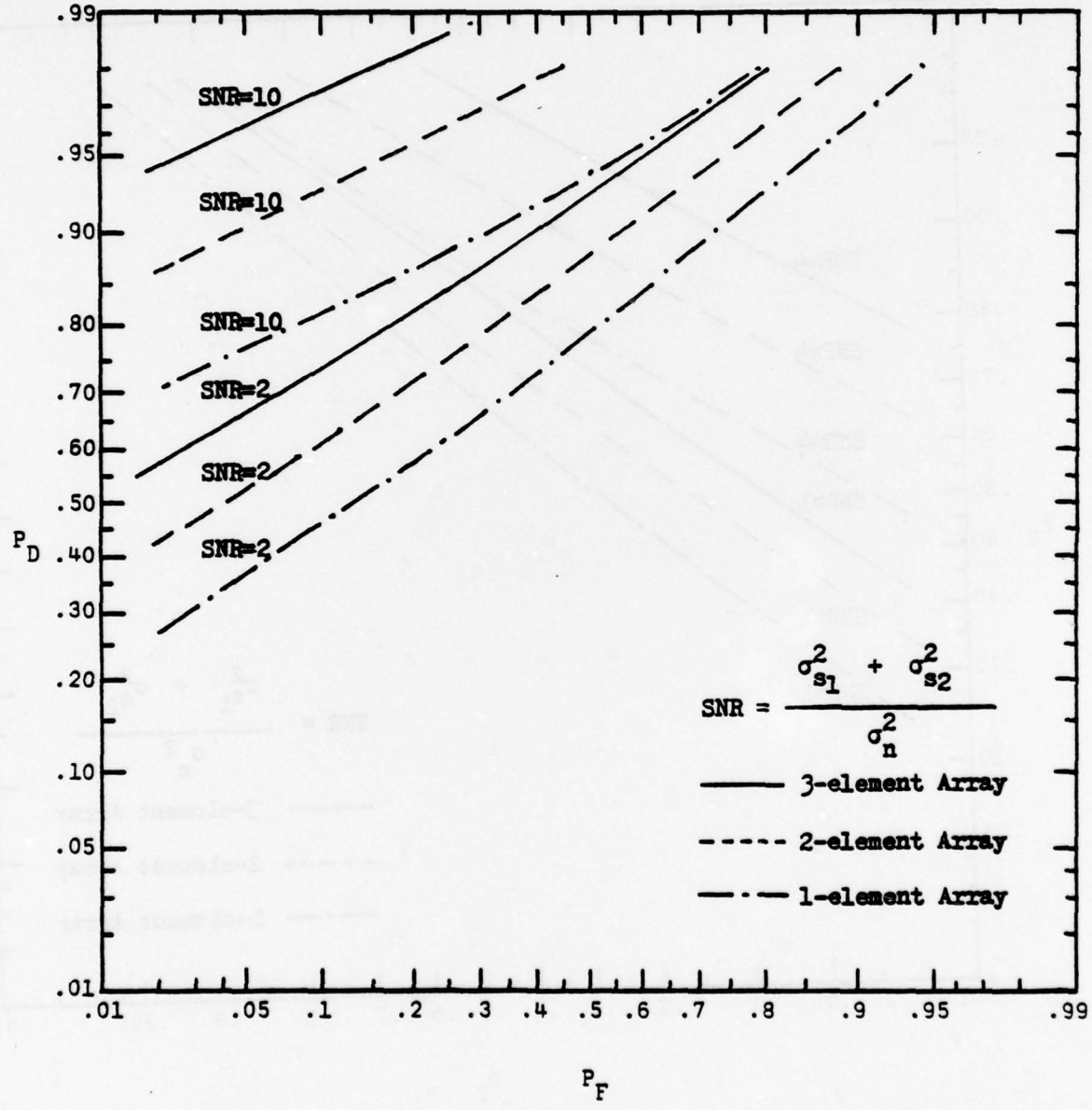

Figure 5.7 Comparison of the Optimal Performances of One, Two, and Three-element Arrays for Detecting Two-path Signals from $\pm 15^\circ$ of Horizontal Axis. Signal-to-noise Ratio Per Element Is 2 or 10.

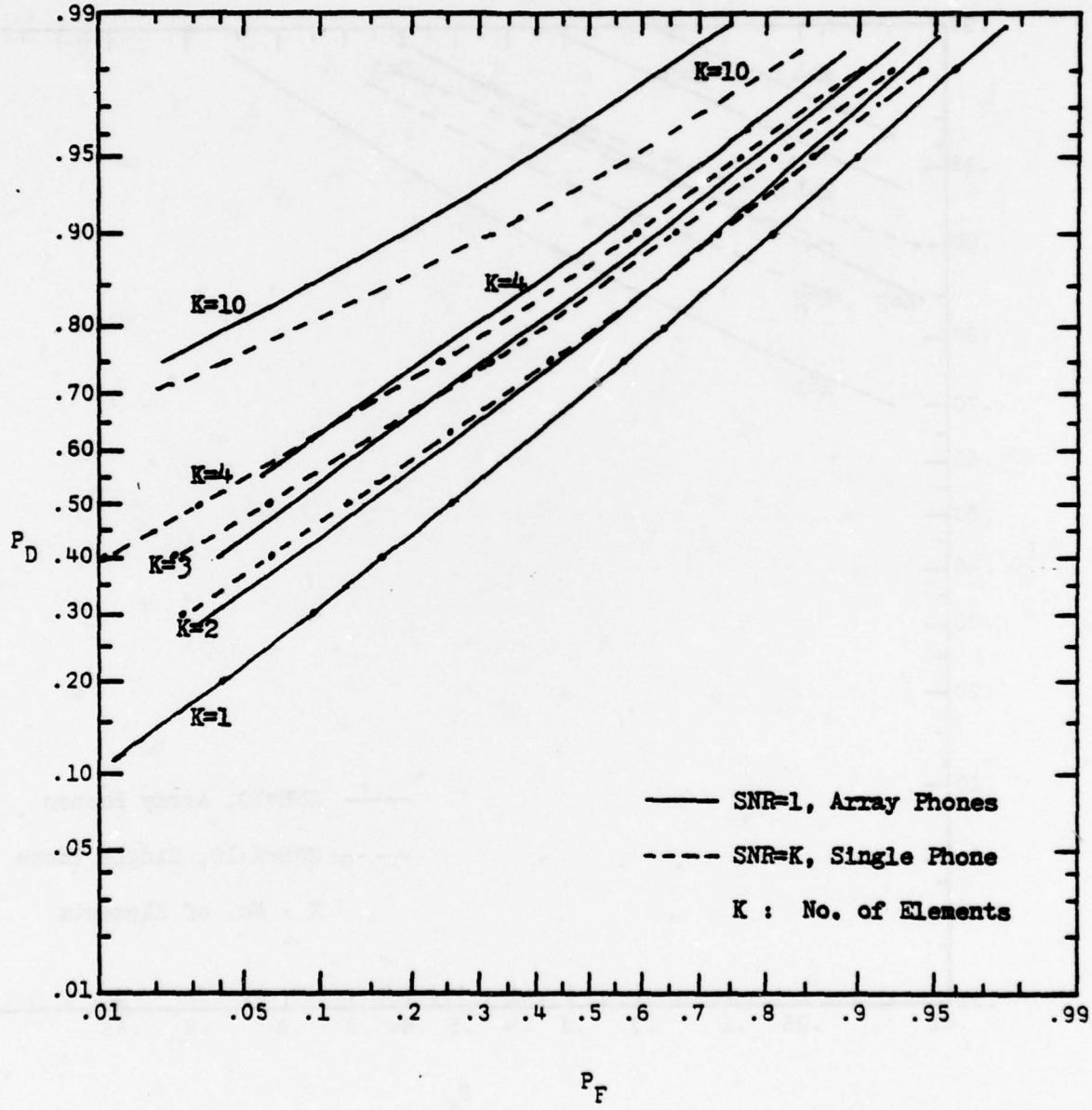

Figure 5.8 Performance Comparison Between the K-element Array and a Single Phone with K Times Signal-to-noise Ratio Per Element of Array Case. Signal-to-noise Ratio Per Element (SNR) Is 1.

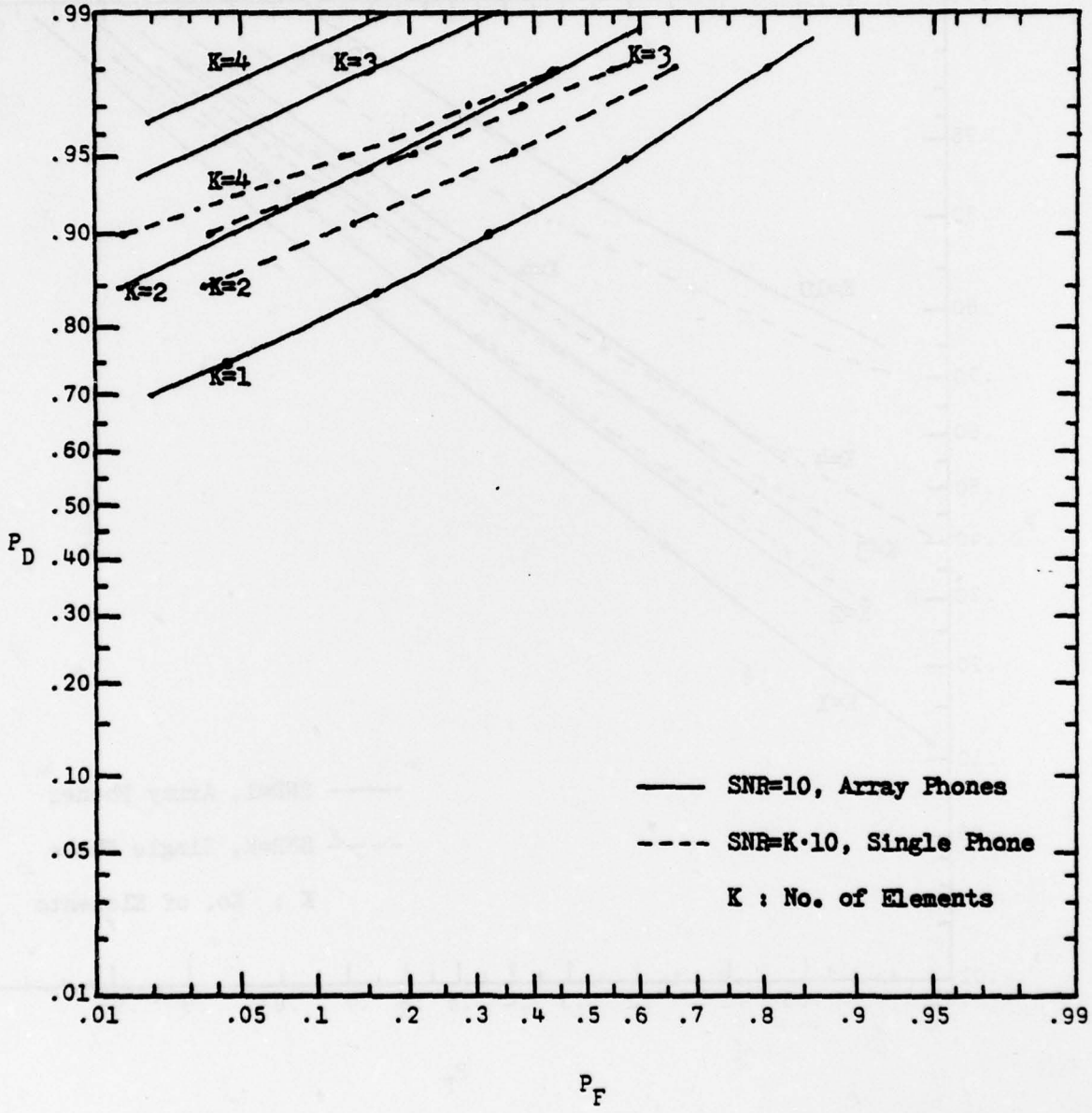

Figure 5.9 Performance Comparison Between the K-element Array and a Single Phone with K Times Signal-to-noise Ratio Per Element of Array Case. Signal-to-noise Ratio Per Element (SNR) is 10.

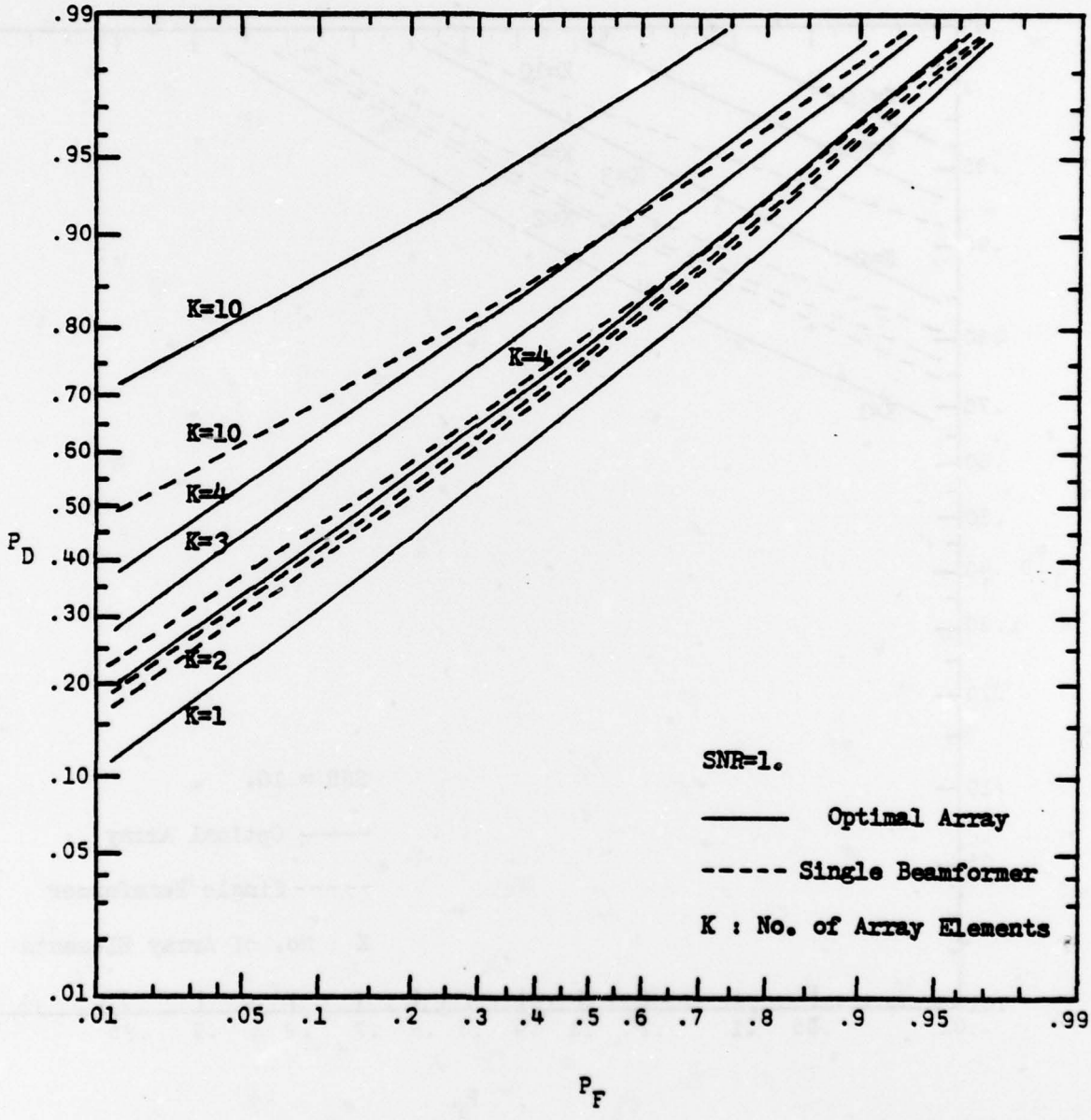

Figure 5.10 Performance Comparison Between Optimal Array Detectors and Single Beamformer. Two-path Signals Are from ± 15° of Horizontal Axis. The Signal-to-noise Ratio Per Element (SNR) Is 1.

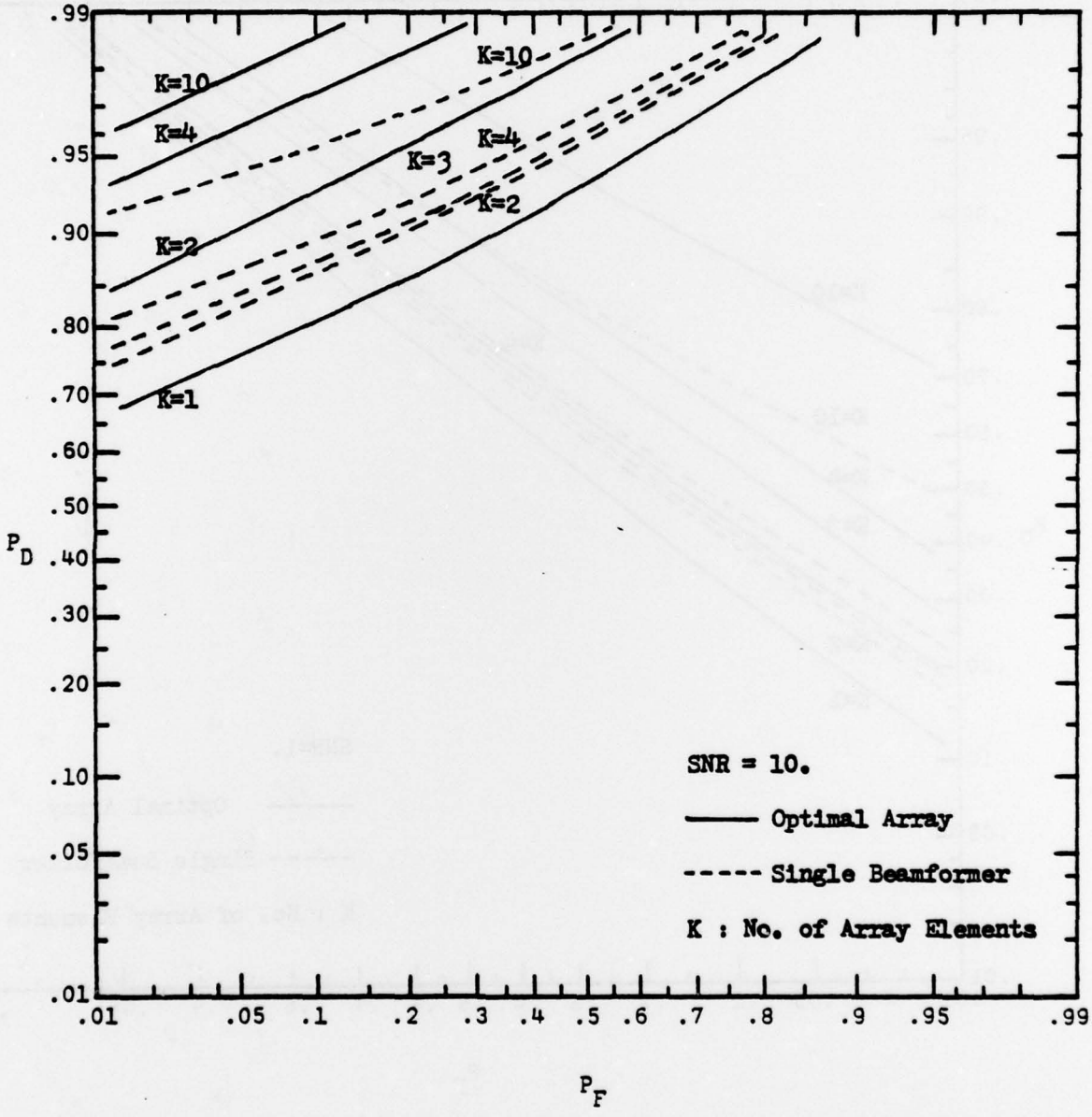

Figure 5.11 **Performance Comparison Between Optimal Array Detectors and Single Beamformer. Two-path Signals Are from ± 15° of Horizontal Axis.** The Signal-to-noise Ratio Per Element (SNR) is 10.

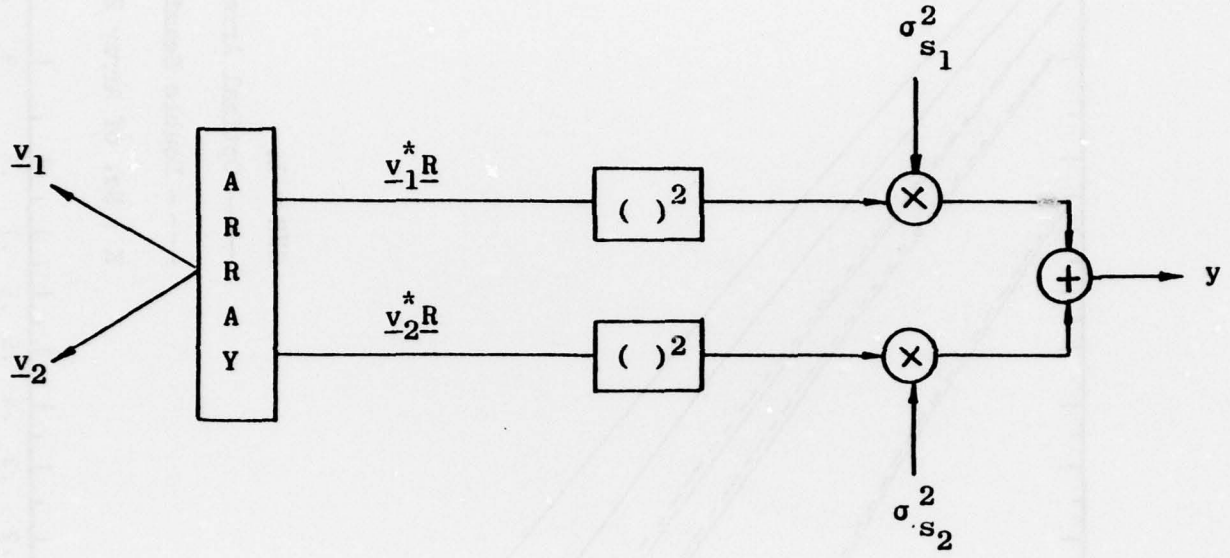

Figure 5.12. Structure of Double Beamformer Array Detector.

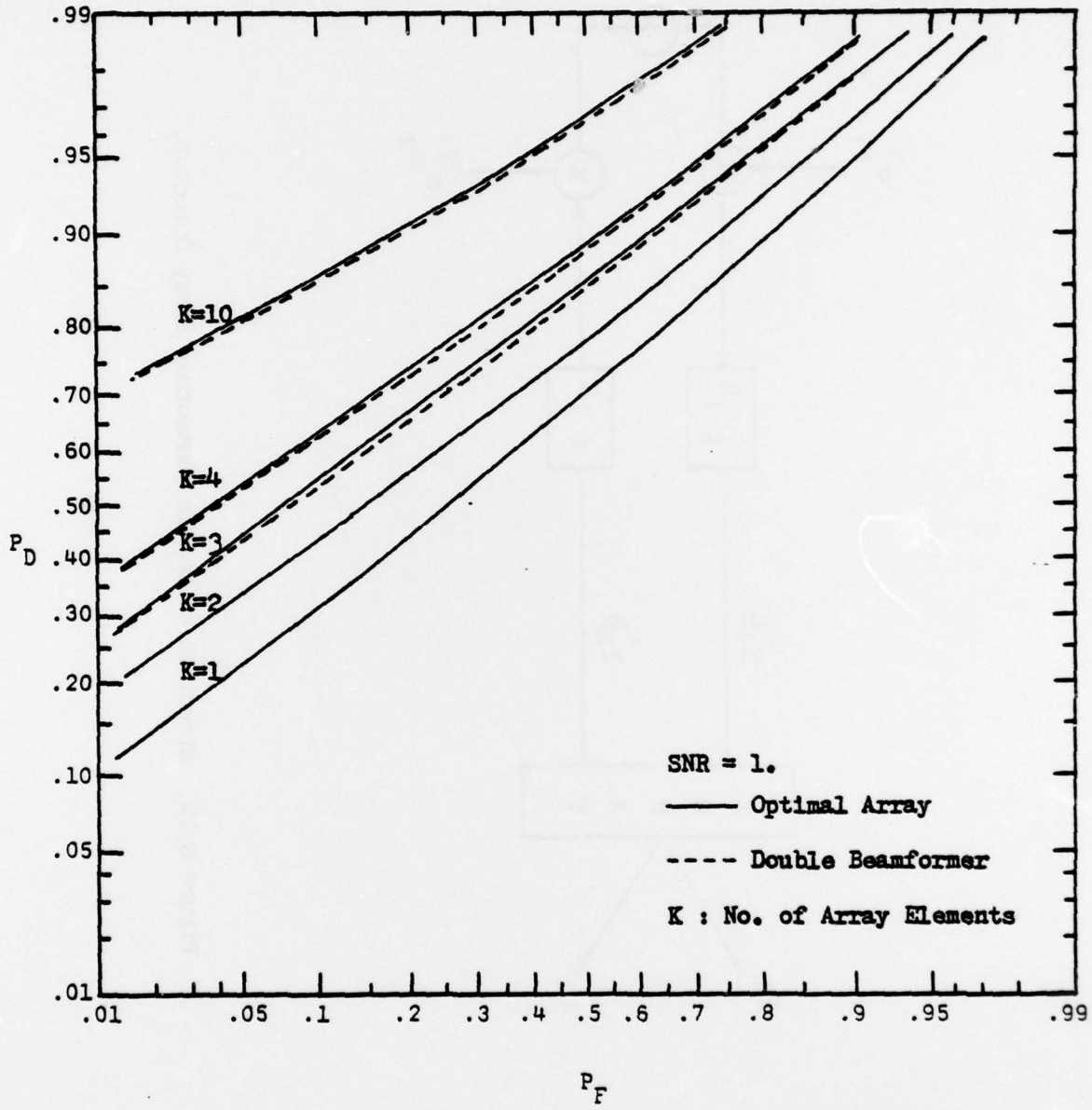

Figure 5.13 Performance Comparison Between Optimal Array and Double Beamformer Detectors. Two-path Signals are from $\pm$ 15° of Horizontal Axis. The Signal-to-noise Ratio Per Element (SNR) Is 1.

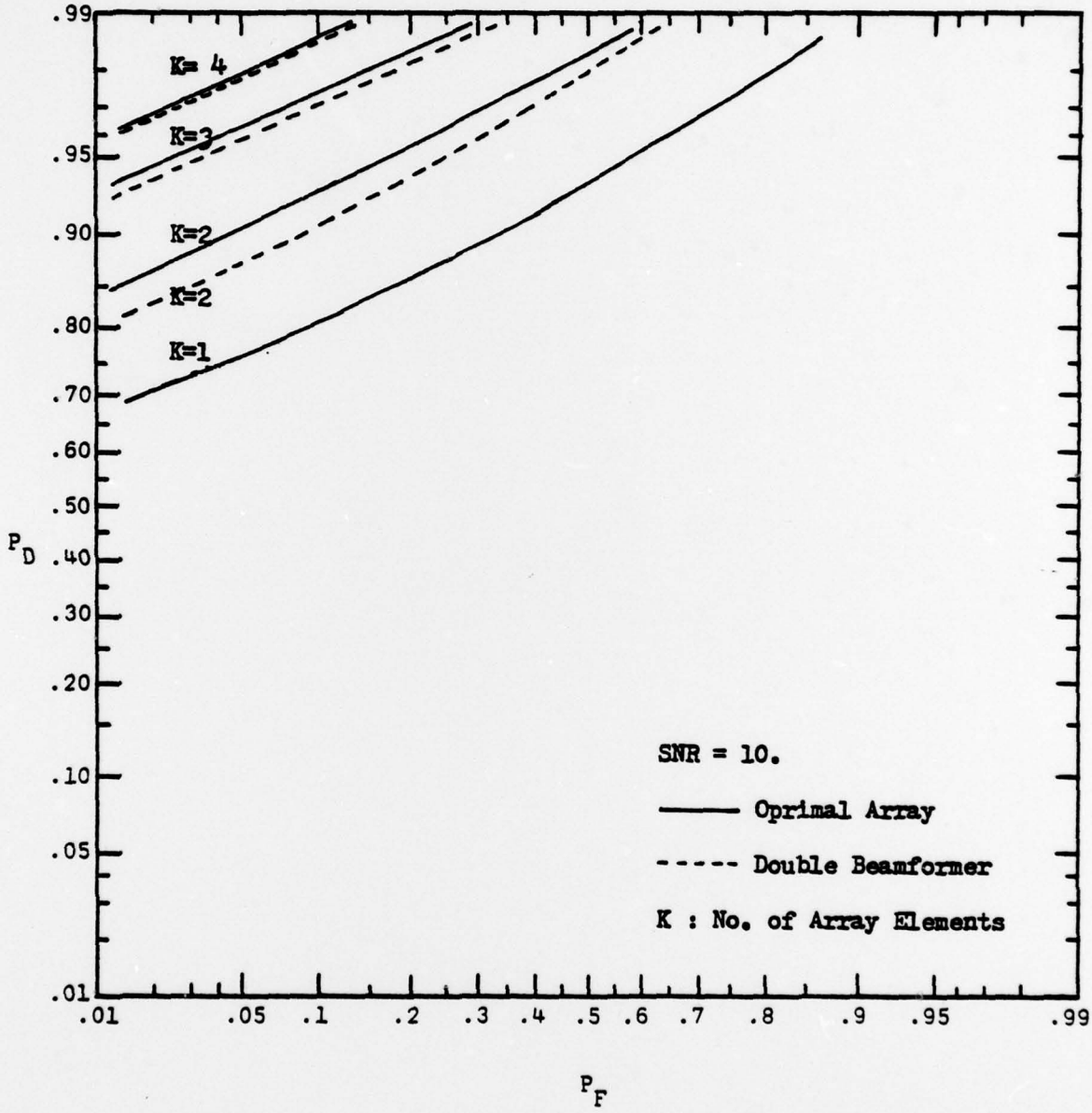

Figure 5.14 Performance Comparison Between the Optimal Array Detectors and the Double Beamformer Detectors. Two-path Signals Are from $\pm 15^{\circ}$ of Horizontal Axis. The Signal-to-noise Ratio Per Element (SNR) is 10.

Unclassified

SECURITY CLASSIFICATION OF THIS PAGE (When Data Entered)

REPORT DOCUMENTATION PAGE		READ INSTRUCTIONS BEFORE COMPLETING FORM
1. REPORT NUMBER TR-13	2. GOVT ACCESSION NO.	3. RECIPIENT'S CATALOG NUMBER
4. TITLE (and Subtitle) Multipath Signal Processing Using a Vertical Array		5. TYPE OF REPORT & PERIOD COVERED Technical 6. PERFORMING ORG. REPORT NUMBER TR-13
7. AUTHOR(s) Charles S. Liu		8. CONTRACT OR GRANT NUMBER(s) N00014-75-C-0191
9. PERFORMING ORGANIZATION NAME AND ADDRESS Department of Electrical Engineering Duke University Durham, North Carolina 27706		10. PROGRAM ELEMENT, PROJECT, TASK AREA & WORK UNIT NUMBERS
11. CONTROLLING OFFICE NAME AND ADDRESS		12. REPORT DATE July 1977 13. NUMBER OF PAGES 84
14. MONITORING AGENCY NAME & ADDRESS(if different from Controlling Office)		15. SECURITY CLASS. (of this report) Unclassified 15a. DECLASSIFICATION/DOWNGRADING SCHEDULE

16. DISTRIBUTION STATEMENT (of this Report)

Distribution of this document is unlimited.

DISTRIBUTION STATEMENT A
Approved for public release;
Distribution Unlimited

17. DISTRIBUTION STATEMENT (of the abstract entered in Block 20, if different from Report)

18. SUPPLEMENTARY NOTES

19. KEY WORDS (Continue on reverse side if necessary and identify by block number)

Signal detection	Bayesian
Arrays	Likelihood ratio test
Signal processing	Gaussian
Estimation	Beam forming
Maximum likelihood estimation	Multipath

20. ABSTRACT (Continue on reverse side if necessary and identify by block number)

Performance of a vertical array for estimating multipath signal parameters and for detecting multipath Gaussian signals is investigated. For known multipath signal direction cases, the parameters of the signal from each individual path may be estimated so that the multipath signal cancellation can be eliminated. The performance of the Maximum Likelihood Estimates (MLE) for the signal parameters of individual paths are shown to be dependent on the angular separation of signal paths and array length. The maximum

next page

DD FORM 1 JAN 73 1473 EDITION OF 1 NOV 65 IS OBSOLETE

Unclassified

SECURITY CLASSIFICATION OF THIS PAGE (When Data Entered)

19. (Cont'd.)

Antenna	Underwater sound
Antenna arrays	Underwater sound transmission
Underwater acoustics	Propagation

20. (Cont'd.)

A Posteriori Probability Estimate (MAP) is considered when the signal statistics are known. The linear relationship between the MLE and MAP estimates is also shown.

The Bayesian optimum array processor for detecting multipath Gaussian signals with known arrival angles not only has multiple beamformers pointing on multipath signal directions, but also has an additional structure which cross-correlates multiple beams. Optimum detection performance of a vertical array can be evaluated by an analytical method if the array has no more than four elements. With the aid of a digital computer the optimum performance can be calculated for an array of any size. The trade-off between the processor structure complexity and the detection performance is shown in terms of receiver operating characteristic (ROC) curves and processor block diagrams. A two-path example is shown for the performance comparison between optimum detector, single beamformer and double beamformer arrays.

UNCLASSIFIED

DISTRIBUTION LIST

Office of Naval Research
800 N. Quincy Street
Arlington, Virginia 22217
Attn: Code 222 — 2
102 OS — 1
480 — 1

Director
Naval Research Laboratory
Technical Information Division
4555 Overlook Avenue S.W.
Washington, D.C. 20375 — 6

Director
Office of Naval Research Branch Office
1030 East Green Street
Pasadena, California 91106 — 1

Office of Naval Research
San Francisco Area Office
760 Market Street Room 447
San Francisco, California 94102 — 1

Director
Office of Naval Research Branch Office
495 Summer Street
Boston, Massachusetts 02210 — 1

Office of Naval Research
New York Area Office
207 West 24th Street
New York, New York 10011 — 1

Commanding Officer
Office of Naval Research Branch Office
Box 39
FPO New York 09510 — 1

Director
Office of Naval Research Branch Office
536 South Clark Street
Chicago, Illinois 60605 — 1

Commander
Naval Surface Weapons Center
Acoustics Division
Silver Spring, Maryland 20910
Attn: Dr. Zaka Slawsky — 1

Officer in Charge
Naval Ship Research & Development Center
Annapolis Laboratory
Annapolis, Maryland 21402 — 1

Commander
Naval Sea Systems Command
Department of the Navy
Washington, D.C. 20362
Attn: SEA 037 — 1
Carey Smith, 06H1 — 1
David F. Bolka, 06H2

Commanding Officer
Fleet Numerical Weather Central
Monterey, California 93940 — 1

Defense Documentation Center
Cameron Station
Alexandria, Virginia 22314 — 12

Director of Navy Laboratories
Chief of Naval Material
2211 Jefferson Davis Highway
Crystal Plaza #5
Arlington, Virginia 20360
Attn Dr. James Probus NAVMAT 03L — 1

Commander
Naval Electronic Systems Command
2511 Jefferson Davis Highway
Arlington, Virginia 20360
Attn: CDR A. R. Miller NAVELEX 320 — 1

Commander
Naval Ship Research & Development Center
Department of the Navy
Bethesda, Maryland 20084
Attn: Mr. Craig Olson — 1
Unclassified Library — 1

Chief of Naval Operations
Room 4D518, Pentagon
Washington, D.C. 20350
Attn: CAPT A. H. Gilmore — 1

Commander
Naval Ocean Systems Center
Department of the Navy
San Diego, California 92132
Attn: Dr. Dan Andrews — 1
Mr. Henry Aurand — 1
Dr. Dean Hanna — 1

Superintendent
Naval Research Laboratory
Underwater Sound Reference Division
P.O. Box 8337
Orlando, Florida 32806 1

Commanding Officer
Naval Underwater Systems Center
New London Laboratory
New London, Connecticut 06320
Attn: Dr. A. Nuttall 1
Mr. A. Ellinthorpe 1
Dr. D. M. Viccione 1

Commander
Naval Air Development Center
Department of the Navy
Warminster, Pennsylvania 18974
Attn: Unclassified Library 1

Superintendent
Naval Postgraduate School
Monterey, California 93940
Attn: Unclassified Library 1

Commanding Officer
Naval Coastal Systems Laboratory
Panama City, Florida 32401
Attn: Unclassified Library 1

Commanding Officer
Naval Underwater Systems Center
Newport Laboratory
Newport, Rhode Island 02840
Attn: Unclassified Library 1

Superintendent
U.S. Naval Academy
Annapolis, Maryland 21402
Attn: Library 1

Commanding Officer
Naval Intelligence Support Center
4301 Suitland Road
Suitland, Maryland 20390
Attn: Dr. Johann Martinek 1
Mr. E. Bissett 1

Commander
Naval Sea Systems Command
Washington, D.C. 20362
Attn: Unclassified Library, SEA 03E 1

Office of the Assistant Secretary of the Navy
for Research, Engineering & Systems
Room 4E732, Pentagon
Washington, D.C. 20350
Attn: Mr. Gerald Cann 1

Special Assistant for ASW
Office of the Assitant Secretary of the Navy
for Research, Engineering & Systems
Washington, D.C. 20350
Attn: Dr. D. Hyde 1

Dr. Melvin J. Jacobson
Rennselaer Polytechnic Institute
Troy, New York 12181 1

Dr. Charles Stutt
General Electric Company
P.O. Box 1088
Schenectady, New York 12301 1

Dr. Alan Winder
MSB Systems, Inc .
25 Sylvan Road South
West Point, Connecticut 06880 1

Dr. T. G. Birdsall
Cooley Electronics Laboratory
University of Michigan
Ann Arbor, Michigan 48105 1

Dr. Harry DeFerrari
University of Miami
Rosentiel School of Marine & Atmospheric Sciences
4600 Rickenbacker Causeway
Miami, Florida 33149 1

Mr. Robert Cunningham
Bendix Electronics Center
15825 Roxford Street
Sylmar, California 91342 1

Dr. Stephen Wolff
Johns Hopkins University
Baltimore, Maryland 21218 1

Dr. M. A. Basin
S.D.P., Inc
15250 Ventura Boulevard
Suite 518
Sherman Oaks, California 91403 — 1

Dr. Walter Duing
University of Miami
Rosentiel School of Marine & Atmospheric Sciences
4600 Rickenbacker Causeway
Miami, Florida 33149 — 1

Dr. David Middleton
127 East 91st Street
New York, New York 10028 — 1

Dr. Donald W. Tufts
University of Rhode Island
Kingston, Rhode Island 02881 — 1

Dr. Loren Nolte
Duke University
Department of Electrical Engineering
Durham, North Carolina 27706 — 1

Mr. S. W. Autrey
Hughes Aircraft Company
P.O. Box 3310
Fullerton, California 92634 — 1

Dr. Thomas W. Ellis
Texas Instruments, Inc
13500 North Central Expressway
Dallas, Texas 75231 — 1

Dr. Terry Ewart
Applied Physics Laboratory
University of Washington
1013 Northeast Fortieth Street
Seattle, Washington 98195 — 1

Institute for Acoustical Research
Miami Division of the Palisades Geophysical Institute
615 S.W. 2nd Avenue
Miami, Florida 33130
Attn: Mr. M. Kronengold
Dr. J. Clark
Dr. W. Jobst
Dr. S. Adams — 2

Mr. Carl Hartdegen
Palisades Geophysical Institute
Sofar Station
FPO New York 09560 — 1

Mr. Charles Loda
Institute for Defense Analyses
400 Army-Navy Drive
Arlington, Virginia 22202 — 1

Mr. Beaumont Buck
Polar Research Laboratory
123 Santa Barbara Avenue
Santa Barbara, California 93101 — 1

Dr. M. Weinstein
Underwater Systems, Inc
8121 Georgia Avenue
Silver Spring, Maryland 20910 — 1

Dr. Thomas G. Kincaid
General Electric Company
P.O. Box 1088
Schenectady, New York 12301 — 1

Applied Research Laboratories
University of Texas at Austin
P.O. Box 8029
10000 FM Road
Austin, Texas 78712
Attn: Dr. Lloyd Hampton
Dr. Charles Wood — 2

Woods Hole Oceanographic Institution
Woods Hole, Massachusetts 02543
Attn: Dr. Paul McElroy
Dr. R. Porter
Dr. R. Spindel — 1

Dr. John Bouyoucos
Hydroacoustics, Inc
321 Northland Avenue
P.O. Box 3818
Rochester, New York 14610 — 1

Systems Control, Inc
260 Sheridan Avenue
Palo Alto, California 94306
Attn: Mr. Robert Baron — 1

Atlantic Oceanographic & Meteorological Laboratories
15 Rickenbacker Causeway
Miami, Florida 33149
Attn: Dr. John Proni — 1

Dr. C. N. K. Mooers
University of Delaware
Newark, Delaware 19711 — 1

Westinghouse Electric Corporation
Advanced Development Program
Marketing Department MS 227
P.O. Box 746
Baltimore, Maryland 21203
Attn: F. J. Frissyn — 1

Oak Ridge National Laboratory
Union Carbide Corporation
Nuclear Division
P.O. Box X
Oak Ridge, Tennessee 37830 — 1

Professor Neil Bershad
University of California, Irvine
School of Engineering
Irvine, California 92664 — 1